UCGE Reports

Number 20132

Department of Geomatics Engineering

Investigations into the Estimation of Residual Tropospheric Delays in a GPS Network

by

JiHong Zhang

November 1999

UNIVERSITY OF
CALGARY

Calgary, Alberta, Canada

THE UNIVERSITY OF CALGARY

Investigations into the Estimation of Residual Tropospheric Delays in a GPS Network

by

JiHong Zhang

A THESIS

SUBMITTED TO THE FACULTY OF GRADUATE STUDIES IN PARTIAL

FULFILMENT OF THE REQUIREMENTS FOR THE

DEGREE OF MASTER OF SCIENCE

DEPARTMENT OF GEOMATICS ENGINEERING

CALGARY, ALBERTA

NOVEMBER, 1999

ABSTRACT

Trop_NetAdjust predicts the residual tropospheric delays on the GPS (Global Positioning System) carrier phase observables using redundant measurements from a network of GPS reference stations. This method not only enhances the effectiveness and reliability of the integer ambiguity resolution process, but it provides a good approach for tropospheric parameter variation forecasting.

The Trop_NetAdjust method is based upon least-squares prediction criteria and enables the prediction of residual tropospheric delays remaining after a standard tropospheric model has been applied to the raw GPS measurements. Two cases are analyzed, namely a first case when the delay is required for an existing satellite at a new point within the network and a second case when the tropospheric delay is required for a new satellite. For both cases, the prediction is based on the double difference carrier phase measurements made on existing satellites at the network reference stations.

Field tests are first conducted using data collected in a network of 11 reference stations covering a 400km x 600km region in southern Norway. The results are analyzed in the measurement domain (double difference ionospheric-free residuals) and show improvements of 20% to 65% RMS errors using Trop_NetAdjust. Similar field tests are also conducted using a 5-receiver network covering a 150km x 400km region in the southern part of Sweden. Improvements of 20% to 66% were obtained for this test network. A comparison between the residual tropospheric delays estimated by the Trop_NetAdjust method and the water vapor radiometer (WVR) measurement shows the limitation of Trop_NetAdjust to estimate absolute tropospheric delays.

ACKNOWLEDGEMENTS

Firstly, I would like to thank my parents, who generously gave everything they had to support and encourage me to go aboard to study for many years. They taught me to respect others, work diligently and devote myself to my country.

Secondly, I would like to acknowledge my supervisor, Dr. Gérard Lachapelle, for his academic support and encouragement during the past two years and for organizing financial support. It was wonderful for us to visit China together last March, including a memorable trip on the Yangtze River. I especially appreciate the time that we spent talking together about my life plan. His guidance and advice are greatly appreciated.

Thirdly, I would like to thank Professors M.E.Cannon, S. Skone, and L.E. Turner, the members of my examining committee. Their efforts in reading through this thesis are greatly appreciated.

Fourthly, I want to take this opportunity to thank all my colleagues who have helped me with this project, especially Huangqi Sun, Luiz Paulo Fortes and Dr. J. Raquet. The assistance of the Norwegian Mapping Authority, Kværner Ship Equipment SA, and Onsala Observatory in providing GPS data is gratefully acknowledged. Dr. J. Raquet and Huangqi Sun have also assisted me with some of the data required for this investigation.

Fifthly, I want to thank all my fellow students in the Positioning and Navigation Lab, especially Mark Petovello, Jayanta Ray, Rakesh Nayak, Samuel Ryan, and Jim Stephen. Their efforts in reviewing and editing the manuscript are greatly appreciated.

Finally, I would like to thank all my fellow Chinese students in the Department, especially my good fiends Luo Ning, and JiunHan Keong. I also want to thank my friends Longmei Li, Huming Wu, Jiayun Zhu, Guang Lu, Chuanyun Fei, Xiangqian Liao,

Zhiling Fei, and Shuxin Yuan. All of their help during the past two years are appreciated. I will cherish their friendship forever.

TBALE OF CONTENTS

LIST OF FIGURES

LIST OF TABLES

NOTATION

List of Symbols

A	Design matrix
B	Double difference matrix
c	Speed of light
C_{ll}	Covariance matrix of the measurement vectors
C_{ss}	Covariance matrix of signal vectors
C_{sl}	Cross-variance matrix of signal and measurement vectors
C_{ee}	Error covariance matrix
dt	Satellite clock error
dT	Receiver clock error
e	Partial pressure of water vapor
H	Kalman filter measurement matrix
I	Identity matrix
K	Kalman filter gain matrix
L1	GPS frequency of 1575.42 MHz
L2	GPS frequency of 1227.60 MHz
n	Refractive index of a medium
N	Carrier phase integer ambiguity
p	Air pressure
P	Observation weight matrix
T	Surface temperature
r	Geometric range from satellite to receiver
dr	Satellite orbit error
dR	Receiver position error
d_{Iono}	Ionospheric delay

d_{Trop}	Tropospheric delay
e_f	Carrier phase measurement noise (receiver noise and multipath)
l	Wavelength of GPS carrier phase
f	GPS frequency (Hz)
d_{Hydro}	Hydrostatic delay
d_{Wet}	Wet delay
e	Satellite elevation
f	Carrier phase
m	Multipath error
v	Receiver noise
w	Kalman processing noise vector
$R(t)$	Autocorrelation function
t_{GM}	Correlation time of first-order Gauss-Markov process
s_{GM}^2	Steady-state variance of first-order Gauss-Markov process
Φ	Kalman filter transition matrix
d	Sum of correlated errors and uncorrelated errors
d_c	Correlated errors (including satellite position, receiver position, tropospheric and ionospheric errors)
d_c	Correlate errors, relative to the reference point p_0
d_u	Uncorrelated errors (including multipath and receiver noise)

List of Acronyms

C/A Code	Coarse/Acquisition Code
DGPS	Differential GPS
DD	Double difference
GPS	Global Positioning System
IF	Ionospheric Free
P Code	Precise Code
PRN	Pseudo-Random Noise code (used to identify the satellites)
RMS	Root Mean Squared value
RTZD	Relative Tropospheric Zenith Delay
SV	Satellite Vehicle
TEC	Total Electron Content
WVR	Water Vapor Radiometer

List of Operators

$\Delta\nabla$	Double difference between receivers and satellites
$m(e)$	Mapping function of elevation angles
$MF(e)$	Mapping function of elevation angles
X^T	Transpose of X
X^{-1}	Inverse of X

CHAPTER 1

INTRODUCTION

1.1 Atmosphere and radio wave propagation

As radio signals propagate through the atmosphere, they are delayed by the atmosphere where different layers refract it in various ways, as shown in figure 1.1 (McCorkle 1998).

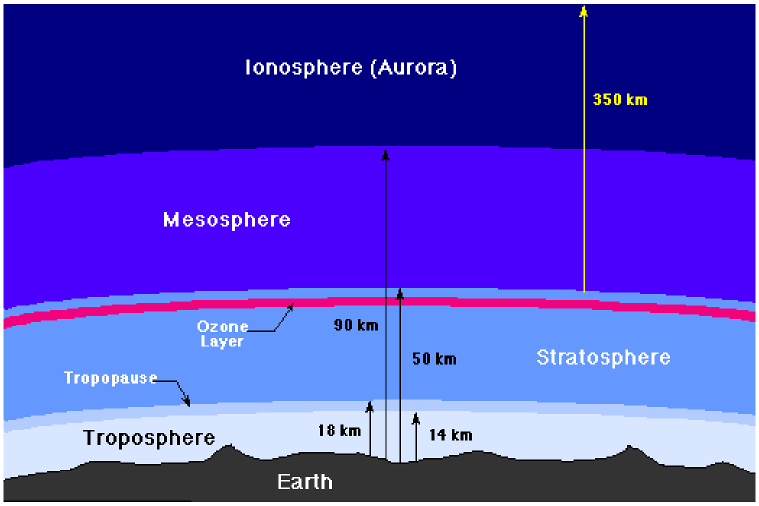

Figure 1.1: Atmosphere different layers

The first layer it encounters is the ionosphere, which is charged with a large number of free electrons that refract the signal. The resulting delay depends on the signal frequency (because the ionosphere is a dispersive medium), which is why it is possible to use data from dual-frequency receivers to estimate and almost entirely eliminate the delay by a linear combination of these dual frequency data.

Having passed through the ionosphere, the signal then undergoes a different kind of the delay in the neutral atmosphere, which is non-dispersive at GPS frequencies and thus cannot be eliminated by dual frequency measurements. The neutral atmosphere consists of the troposphere, stratosphere and part of the mesosphere. The delay in the radio signal propagation through the neutral atmosphere is mostly due to the effect of the troposphere. The neutral atmosphere is also often referred to as the troposphere in GPS applications. The tropospheric delay consists of two components. The hydrostatic (or "dry") component, which is dependent on the dry air gases in the atmosphere, accounts for approximately 90% of the delay. The "wet" component, which depends upon the moisture content of the atmosphere and contains significant levels of water vapor, accounts for the remaining effect of the delay (Emardson 1998, Dodson & al 1996). Although the dry component is the larger effect, the errors in the models for the wet component are larger than the errors in the models for the dry component because the wet component varies more spatially and temporally. Usually, the hydrostatic component is called “dry delay” and the wet component is called “wet delay” (Davis & al 1985).

The hydrostatic delay is caused by the non-water portion of the atmosphere. It is the larger of the two parts of the delay. The hydrostatic delay in the zenith direction is typically about 2.3 m (Businger & al 1996, Dodson & al 1996). This hydrostatic component has a smooth, slowly time-varying characteristic due to its dependence on variations in surface air pressure (weather cells), so this part can be modeled and removed with an accuracy of a few millimetres or better using a surface model (including pressure, temperature and humidity). It does not therefore create much of a problem as far as its effect on GPS signals (Saastamonien 1972, Tralli & Lichten 1990). However, the wet delay, which is mostly dependent on water vapor pressure and strongly influenced by small to large scale turbulence, is as small (in the zenith component) as a few centimetres or less in arid regions and as large as 35 centimetres in humid regions. This delay component is usually far more variable and more difficult to remove based on standard tropospheric models using surface measurements (Bevis & al 1992, Darin & al 1997, Duan & al 1996). Therefore, the residual delay remaining after applying a standard troposphere model is mostly due to the wet component. If this residual delay can be estimated or predicted in some way, GPS accuracy performance can be enhanced significantly for high precision relative GPS positioning, especially in the context of carrier phase integer ambiguity resolution.

1.2 Measurement approaches of residual tropospheric delays

To determine the amount of residual tropospheric delay that is not removed by a standard tropospheric model, three major methods have been developed during the past several years.

1.2.1 Radiosondes

Radiosondes are weather measurement instruments that measure upper air profiles of pressure, temperature and humidity when launched into the upper atmosphere on a weather balloon (see figure 1.2). Wind speed and direction are also measured by monitoring the balloon's progress from ground level to altitudes in excess of 30 km. Radioactivity and ozone measurements can also be made. The observed data are transmitted to ground equipment that processes the data into weather messages.

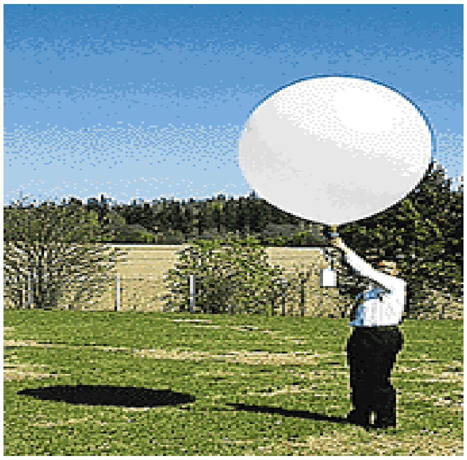

Figure 1.2: Radiosondes for water vapor measurement

Using the obtained profiles it is possible to calculate the total amount of water vapor by integrating the data according to

$$\int r_v(z)dz \tag{1.1}$$

where r_v is the water vapor mass density at the altitude z, which is available from the relative humidity U and the temperature measurement T, as

$$r_v = U \times e_s \times \frac{1}{R_v \times T} \tag{1.2}$$

where e_s is the saturation water vapor pressure and R_v is the specific gas constant for water vapor.

If the atmospheric water vapor has been measured by radiosondes, the tropospheric wet delay can be derived from it. Therefore, radiosondes can measure the tropospheric wet delay with good vertical resolution but poor horizontal resolution, and varying temporal resolution. Because most of the residual tropospheric delays result from the tropospheric wet component, radiosondes provide a good way to measure the residual tropospheric delay. However, they are expensive and inconvenient because only limited measurements are available (2 launches per day).

1.2.2 Water vapor radiometer

The Water Vapor Radiometer (WVR) is an instrument that can provide the wet delay estimates along the signal propagation path and accordingly information on the integrated water vapor. The WVR measures the background microwave radiation produced by the atmosphere, usually at two frequencies centred at the water vapor absorption line (22.235 GHz) and, using various conversion algorithms, transforms these measurements into integrated line-of-sight precipitable water vapor. Its intensity output will depend on the amount and distribution of water vapor in the slant path direction of the antenna. It has the high temporal resolution of the wet delay, but is costly and does not function well in all weather conditions, especially under rainy and heavy cloud conditions. Figure 1.3 shows the appearance of a WVR (Onsala Space Observatory 1998).

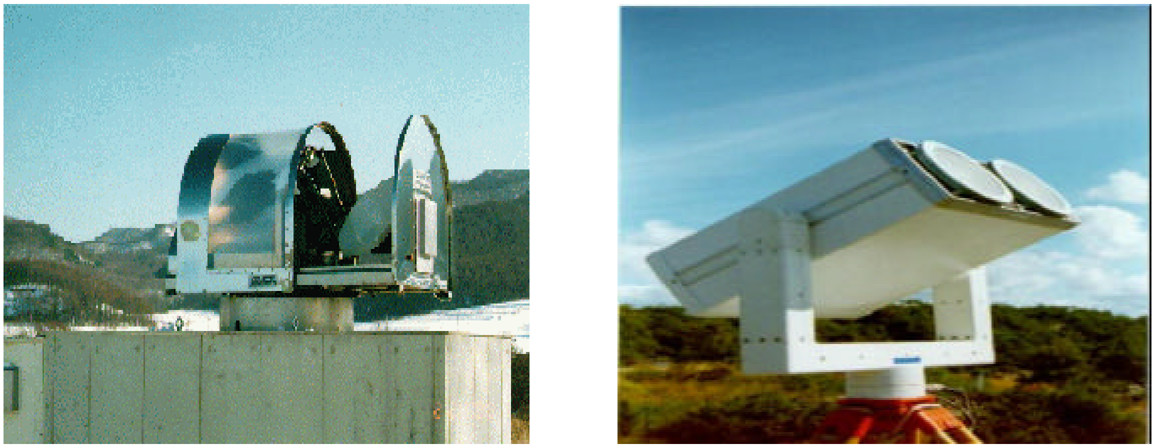

Figure 1.3: Water vapor radiometer

1.2.3 Global Positioning System

The Navigation System with Timing And Ranging (NAVSTAR) Global Positioning System (GPS) is a satellite-based navigation system run by the US Department of Defense (DoD), which is conceived as a ranging system from known positions of satellites in space to unknown positions on land, sea, in air and space.

Each GPS satellite currently transmits data on two carrier frequencies, L1 (1575.42 MHz) and L2 (1227.60 MHz). Atomic clocks onboard the satellite produce a fundamental L-band frequency, namely 10.23 MHz. The L1 and L2 carrier frequencies are generated by multiplying the fundamental frequency by 154 and 120, respectively. Two pseudorandom noise (PRN) codes, along with satellite ephemerides (broadcast ephemerides), ionospheric modeling coefficients, status information, system time, and satellite clock corrections, are superimposed onto the two carrier frequencies. The measured travel times of the signals from the satellites to the receivers are used to compute the pseudoranges.

GPS is becoming an important tool to measure the tropospheric wet delay caused by atmospheric water vapor. Because the ionospheric delay is dispersive and can be determined by observing both frequencies transmitted by the satellites, these kinds of delays affecting observations recorded by a dual-frequency GPS receiver can be eliminated directly without reference to observations recorded by other GPS receivers in the same network. If the position of the receiver is accurately known and the ionospheric delay has been accounted for, an estimate of the tropospheric wet delay overlying the receiver can be derived from the GPS signals. Usually additional measurements of the surface temperature and pressure with good temporal and spatial resolutions are required for the standard troposphere model corrections.

Reviews of the principles of the tropospheric delays of radio signals can be found from a wide library of authors, namely Brunner (1984), Dixon (1991), Elegered (1992), Langley (1992), Trehauft (1992), Brunner and Welsch (1993), and Hofmann-Wellenhof & al (1993). Dixon (1991) gives an introduction to the troposphere delay of radio waves, especially for reducing residual tropospheric delay effects. Trehauft (1992) reviews troposphere delays in very long baseline interferometry (VLBI), which applies similarly to GPS. Based on significant tropospheric research, several theoretical troposphere zenith models and associated mapping functions have been developed during the last several decades. Modeling atmosphere delays was reviewed by Herring (1992), who describes the separation of the neutral atmosphere into wet and hydrostatic components. Janes & al (1991) compares several models and mapping functions with ray traced standard atmosphere conditions. They conclude that the Saastamoinen (1973) zenith delay model, in conjunction with either the Davis (1986) or Goad and Goodman (1974) mapping functions are best suited for GPS relative positioning. Mendes and Langley (1994) comprehensively compare 15 geodetic-quality mapping functions, determining that the Lanyi (1984), Herring (1992), Ifadis (1986), and Neill (1993) mapping functions are the most reliable for high precision positioning applications.

However, these theoretical troposphere models are not able to always satisfy the requirements of high precision GPS applications because of the significant residual tropospheric delay that cannot be well modeled nor removed. In order to estimate the residual tropospheric delays, conventional weighted least squares and Kalman filter algorithms have been developed by various researchers. Reviews of various estimation techniques are covered in: Lichten and Border (1987), Dixon and Kornreich Wolf (1990), Herring & al (1990), Lichten (1990), Tralli and Lichten (1990), and Elgered & al (1991). Lichten and Border (1987) give a review, describing in functional form of the modeling of the tropospheric delay as a random walk or Gauss-Markov stochastic process. Lichten (1990) gives a comprehensive review of a Kalman filter approach to stochastic estimation of the troposphere delay and achieves better than 5mm r.m.s delay estimates. They conclude that the random walk or Gauss-Markov process provides equivalent estimates of residual tropospheric delays. They predict that GPS has the potential to resolve, in near real-time (on the order of a few minutes), zenith delay fluctuations at the centimetre level.

1.3 Research statement and objective

1.3.1 Research objective

The intent of this thesis is to develop and test a new method to predict the residual tropospheric delay in real-time on GPS carrier phase observables using the redundant measurements available in a network of GPS reference stations. For any GPS network, the redundant information available through the availability of multiple reference stations should intuitively be useful in improving the prediction accuracy. The prediction method is based on a least-squares criteria and enables one to predict the residual tropospheric delay remaining after a standard model has been applied to the data.

This method to estimate the residual tropospheric delay is different compared with traditional approaches, such as conventional weighted least squares and Kalman filtering. Two specific sub-objectives are

- Optimal prediction of residual tropospheric delays for an existing satellite at any user location using the satellite measurements available from a network of fixed reference stations. This will result in a faster estimation of the integer ambiguities at the user since a large part of the carrier phase errors are due to the troposphere.

- Prediction of residual tropospheric delays for new satellites being observed by the network stations and user alike, using other satellite measurements available in the network. This implies that tropospheric delays between satellites and observation points are spatially correlated, which is indeed the case. This is important in order to resolve quickly ambiguities involving new satellites. These satellites are initially relatively low and their tropospheric delays relatively high.

1.3.2 Thesis outline

The remaining parts of this thesis consist of the following chapters.

Chapter 2 describes GPS carrier phase observables as well as double difference error sources. Each carrier phase double difference error source is analyzed. The ionospheric delay and satellite position errors are described in detail.

Chapter 3 describes the effects of the troposphere on the GPS signals. Characteristics of the troposphere are first reviewed. Secondly, the refraction of GPS signals in the troposphere is presented. Along with the analysis of the physics associated with the troposphere, several typical troposphere models are introduced with associated mapping functions. Finally, the ionospheric-free (IF) double difference observable is provided as a measurement of the residual tropospheric delay.

In Chapter 4, a review of the traditional estimation approaches for residual tropospheric delays is first presented based on conventional weighted least squares and Kalman filtering. Secondly, the basic methodology of Trop_NetAdjust is introduced for the estimation of the residual tropospheric delay using a GPS network adjustment. Based on the network optimal estimation, the Trop_NetAdjust method is mathematically derived based on least squares prediction for two different predicting cases: a new station and a new satellite. The covariance function of the residual tropospheric delay is derived from GPS network field data based on the analysis of its temporal and spatial correlation.

In Chapter 5, the derived covariance function and the Trop_NetAdjust method are applied to data from a GPS network located in Norway. New station prediction and new satellite prediction for residual tropospheric delays are considered independently. The results are analyzed in the measurement domain. The Trop_NetAdjust performance improvement with respect to satellite elevation angles is also investigated in the latter part of this chapter.

In Chapter 6, the Trop_NetAdjust method is applied to a GPS network located in Sweden. In this case, the residual tropospheric delay can also be measured by a water vapor radiometer. A performance comparison of the estimated results between Trop_NetAdjust and the WVR is presented in the latter part of this chapter.

Chapter 7 provides the conclusions and recommendations for future research.

CHAPTER 2

GPS CARRIER PHASE OBSERVABLES AND DOUBLE DIFFERENCE ERROR SOURCES

In this chapter, various GPS error sources and their influence on carrier phase double difference observables are analysed. Double differencing is described as an approach to eliminate or reduce most errors, and each significant error source that remains after double differencing is analysed in greater detail.

2.1 Carrier phase observables and double differencing

Most GPS receivers generate two primary observables: the pseudorange measurement based on tracking of the GPS signal code, and a measurement of the carrier phase from the integrated beat frequency between the received GPS carrier signal and the carrier signal generated locally within a GPS receiver.

2.1.1 Carrier phase observables

The carrier phase can be measured by beating the received Doppler-shifted satellite carrier with a signal of the constant frequency generated in a GPS receiver. The carrier transmitted by a satellite can be extracted either by complete knowledge of the pseudo-random noise code (C/A code or P code), or by codeless signal processing techniques, such as squaring, or cross-correlation (Hofmann-Wellenhof & al 1993). Since a receiver can only measure the fractional part of the beat carrier phase, the integer number of whole wavelengths in each phase measurement is unknown. This integer number is called the initial carrier phase ambiguity. In essence, this integer number N can be thought of as a constant, adding an unknown bias in each of the carrier phase measurements. The values for N are independent for measurements between different receivers or different satellites. But the values of N are constant for successive measurements taken at different epochs (assuming no cycle slips between those epochs). If the initial integer cycle ambiguity could be resolved reliably, the phase measurement would provide a very precise position in differential mode.

The measured carrier phase range observable f (Lachapelle, 1997) can be written in the following form, where all quantities are in units of distance:

$$f = r + dr + cdt - cdT - d_{Iono} + d_{Trop} + e_f + lN \tag{2.1}$$

where

r is the geometric range from satellite to receiver,

dr is the satellite orbit error,

c is the light speed,

dt is the satellite clock error,

dT is receiver clock error,

d_{Iono} is the ionospheric delay,

d_{Trop} is the tropospheric delay,

e_f is the carrier phase measurement noise (receiver noise and multipath),

l is the wavelength of GPS carrier, and

N is the carrier phase integer ambiguity (in cycles).

2.1.2 Double differencing

In order to eliminate or reduce many of the errors for precise differential GPS, a "double difference" observable is generated. That is, the carrier phase observables are first differenced between different satellites. Then these differenced observables for the same set of satellites are further differenced between the receivers. This is illustrated in figure 2.1.

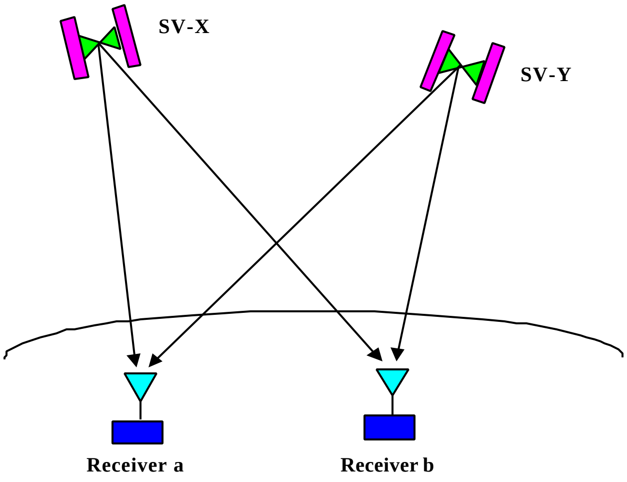

Figure 2.1: GPS double difference

First, a single difference observable is generated by differencing simultaneous measurements between two satellites and a receiver:

$$\nabla f_{a}^{xy} = f_{a}^{x} - f_{a}^{y} \tag{2.2}$$

where subscripts $'a'$ refers to receiver a and superscripts $'x'$ and $'y'$ refer to satellite x and satellite y. For instance, f_{a}^{x} is the carrier phase observable at receiver a for satellite x.

Next, single difference observables between two receivers for the same pair of satellites are differenced in order to form the following double difference observable

$$\Delta\nabla f_{ab}^{xy} = \nabla f_{a}^{xy} - \nabla f_{b}^{xy} \tag{2.3}$$

According to equations 2.1, 2.2 and 2.3, the double difference observable is written as

$$\begin{aligned}\Delta\nabla f_{ab}^{xy} &= (f_{a}^{x} - f_{a}^{y}) - (f_{b}^{x} - f_{b}^{y}) \\ &= \{[(r_{a}^{x} - r_{a}^{y}) - (r_{b}^{x} - r_{b}^{y})] + [(dr_{a}^{x} - dr_{a}^{y}) - (dr_{b}^{x} - dr_{b}^{y})] \\ &+ [c(dt_{a}^{x} - dt_{a}^{y}) - c(dt_{b}^{x} - dt_{b}^{y})] - [c(dT_{a}^{x} - dT_{a}^{y}) - c(dT_{b}^{x} - dT_{b}^{y})] \\ &- [(d_{Iono\,a}^{\;x} - d_{Iono a}^{\;y}) - (d_{Iono b}^{\;x} - d_{Iono\,b}^{\;y})] + [(d_{Trop_a}^{\;x} - d_{Trop_a}^{\;y}) - (d_{Trop_b}^{\;x} - d_{Trop_b}^{\;y})] \\ &+ [(e_{f_a}^{\;x} - e_{f_a}^{\;y}) - ((e_{f_b}^{\;x} - e_{f_b}^{\;y})] + l[(N_{a}^{x} - N_{a}^{y}) - (N_{b}^{x} - N_{b}^{y})]\end{aligned} \tag{2.4}$$

Equation 2.4 can be simplified as follows with the assumption that the measurements were collected at both receivers simultaneously ($dT_a^x = dT_a^y$ and $dT_b^x = dT_b^y$) and the signals were transmitted at the same time from satellites x and y ($dt_a^x = dt_a^y$ and $dt_b^x = dt_b^y$):

$$\Delta\nabla f_{ab}^{xy} = \Delta\nabla r_{ab}^{xy} + \Delta\nabla dr_{ab}^{xy} - \Delta\nabla d_{Iono\,ab}^{\;\;xy} + \Delta\nabla d_{Trop\,ab}^{\;\;xy} + \Delta\nabla e_{f\,ab}^{\;xy} + l\Delta\nabla N_{ab}^{xy} \tag{2.5}$$

In this equation, each of the error sources is presented in the form of a double difference, where

$\Delta\nabla dr_{ab}^{xy}$ is the double differenced satellite orbit error,

$\Delta\nabla d_{Iono\,ab}^{\;\;xy}$ is the double differenced ionospheric delay,

$\Delta\nabla d_{Trop\,ab}^{\;\;xy}$ is the double differenced tropospheric delay, and

$\Delta\nabla e_{f\,ab}^{\;xy}$ is the double differenced measurement noise which includes multipath and receiver noise.

Here, only the satellite position error dr is considered in equation 2.5. But most DGPS algorithms involves generating a nominal "computed" range between the receiver and the satellite from the best known coordinates of the receiver and the satellite. Further considering the errors in the "known" receiver positions relative to the true positions, the double differenced geometric true range $\Delta\nabla r_{ab}^{xy}$ can be written in the following form (Raquet 1998):

$$\Delta\nabla r_{ab}^{xy} = \Delta\nabla R_{ab}^{xy} - \Delta\nabla dR_{ab}^{xy} \tag{2.6}$$

where R is the computed range between the satellite and the receiver, and dR is the receiver position error.

Combining equation 2.6 with 2.5 results in

$$\Delta\nabla f_{ab}^{xy} = \Delta\nabla R_{ab}^{xy} + \Delta\nabla dr_{ab}^{xy} - \Delta\nabla dR_{ab}^{xy} - \Delta\nabla d_{Iono\,ab}^{\;\;xy} + \Delta\nabla d_{Trop\,ab}^{\;\;xy} + \Delta\nabla e_{f\,ab}^{\;xy} + l\Delta\nabla N_{ab}^{xy} \tag{2.7}$$

In the following, the measurement-minus-range observable $\Delta\nabla \bar{f}$ is used in order to give a good representation of the error sources themselves. equation 2.7 can be written in another form as:

$$\Delta\nabla \bar{f}^{xy}_{ab} = \Delta\nabla f^{xy}_{ab} - \Delta\nabla R^{xy}_{ab} = \Delta\nabla dr^{xy}_{ab} - \Delta\nabla dR^{xy}_{ab} - \Delta\nabla d^{xy}_{Iono_{ab}} + \Delta\nabla d^{xy}_{Trop_{ab}} + \Delta\nabla e^{xy}_{f_{ab}} + l\Delta\nabla N^{xy}_{ab} \quad (2.8)$$

Equation 2.8 can also be written in units of cycles as:

$$\Delta\nabla \bar{f}^{xy}_{ab} = \frac{1}{l}(\Delta\nabla dr^{xy}_{ab} - \Delta\nabla dR^{xy}_{ab} - \Delta\nabla d^{xy}_{Iono_{ab}} + \Delta\nabla d^{xy}_{Trop_{ab}} + \Delta\nabla e^{xy}_{f_{ab}}) + \Delta\nabla N^{xy}_{ab} \quad (2.9)$$

where, l is the wavelength of GPS carrier phase (L1 or L2 frequency).

2.2 Carrier phase double difference error sources

To achieve millimetre precision using GPS, it is necessary to analyze GPS carrier phase measurements and eliminate or significantly reduce the biases and errors influencing the measurements. According to equation 2.9, it is clear that the major error sources of the double difference GPS carrier phase measurements are atmospheric refraction in the ionosphere and troposphere (neutral atmosphere), satellite orbit errors, measurement errors (multipath bias and receiver noise), as well as reference station coordinates errors. Here, it is assumed that the carrier phase ambiguity is resolved correctly to an integer.

The following discussion highlights the significant error sources in double difference precise GPS positioning. Further information on GPS biases and errors can be found in: Kroger & al (1986), Wells & al (1986), Dixon (1991), and Blewitt (1993). In order to describe the troposphere effect in greater detail, it is discussed in the next chapter. In this section, other error sources that affect GPS observations are reviewed.

2.2.1 Ionospheric delay

The ionosphere is the part of the upper atmosphere where free electrons occur in sufficient density to have an appreciable influence on the propagation of radio frequency electromagnetic waves. This ionization depends primarily on the Sun and its activity. Ionospheric structures and peak densities in the ionosphere vary greatly with time (sunspot cycle, seasonally, and diurnally), with geographical location (polar, auroral zones, mid-latitudes, and equatorial regions), and with certain solar-related ionospheric disturbances (Klobuchar 1996).

The region of the ionosphere extends from 50 to 1000 km (Langley 1992). Ionization appears at a number of atmospheric levels, producing layers or regions, which may be identified by their interaction with radio waves. These layers are known as the D, E, and F layers, and their locations are shown in figure 2.2 for both night and day conditions at mid-latitudes. The first ionospheric layer found is the so-called E layer or region at about 90-120 km altitude. It is used by radio operators as a surface from which signals can be reflected to distant stations. It is interesting to note that this works also the other way round and, for example, the auroral kilometric radiation created by the precipitating particles high above the ionosphere does not reach the ground because of the ionospheric E layer. Above the E layer, an F layer consisting of two parts can be found: F1 is at about 170 km altitude, and F2 at about 250 km altitude. The F layer also reflects radio waves. The lowermost region of the ionosphere below 80 km altitude, the D layer, however, principally absorbs radio waves.

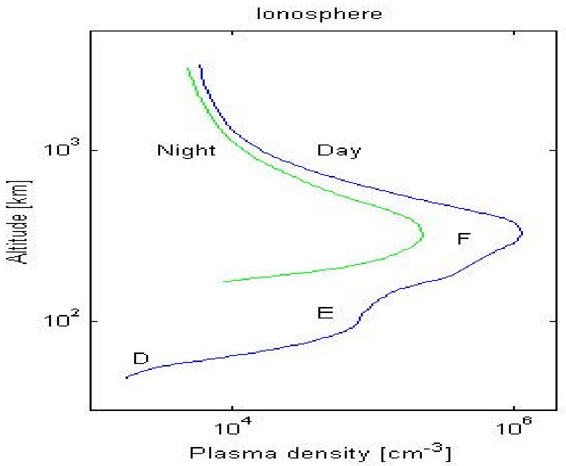

Figure 2.2: Ionosphere layers

Ionospheric temporal variations can be separated into two classes. The first (and most important) class is due to the slowly varying global temporal variations. The second class is due to local variations. The slow global variations are due primarily to solar radiation (i.e., the ionizing source), electron recombination and to some extent atmospheric waves. As the Earth rotates from day to night and back to daylight, the Earth-fixed ionosphere undergoes a quasi-periodic variation in its electron density. The ionospheric correction between a satellite and a receiver is actually a path integral (i.e., the total electron content or TEC) through the ionospheric electron density. The electron density varies with height but an approximation can be obtained by considering the majorities of ionospheric TEC to be at a fixed height and examining the time variation of the electron density.

During daylight hours, the ionizing source (i.e., solar radiation) is strong enough such that the ionospheric electron density approaches a quasi-steady state. The intensity is roughly proportional to the radiation source strength (and the atmospheric density). During the night, no radiation source is freeing electrons (except for auroral activity at the poles) and therefore the existing electrons slowly recombine with the ionospheric ions (the ionosphere is a neutral plasma field). Thus, we expect that the zenith ionospheric electron density is roughly a function of the local earth time of signal transmission.

The major effects the ionosphere can have on GPS are the following: 1) group delay of the signal modulation, or absolute range error; 2) carrier phase advance, or relative range error; 3) Doppler shift, or range-rate error; 4) Faraday rotation of all actually polarized signals; 5) refraction or bending of the radio wave; 6) distortion of pulse waveforms; 7) signal amplitude fading or amplitude scintillation; and 8) phase scintillation. Usually the ionospheric range error can vary from only a few metres, to several tens of metres at the zenith.

Fortunately, the ionosphere is a dispersive medium: the refraction index is a function of the operating frequency, and dual frequency GPS users can take advantage of this property of the ionosphere to measure and correct for the first-order ionospheric range and range-rate effects directly. The refraction index n of the ionosphere can be expressed as (Klobuchar 1996).

$$n^2 = 1 - \frac{X}{1 - iZ - \frac{Y_T^2}{2(1 - X - iZ)} \pm \left[\frac{Y_T^4}{4(1 - X - iZ)^2} + Y_L^2 \right]^{1/2}} \tag{2.10}$$

where $X = N_e e^2 / e_0 m w^2$, $Y_L = f_H \cos(q) / f$, $Y_T = f_H \sin(q) / f$, $Z = v / w$, $w = 2pf$, where

f is the frequency of income signal, in Hz,

N_e is the electron density, in $electrons / m^3$,

e is the electron change, $= -1.602 \times 10^{-19}$ coulomb,

e_0 is the permittivity of free space, $= 8.854 \times 10^{-12}$ farad/m,

m is the rest mass of a electron, $= 9.107 \quad 10^{-31}$ kg,

q is the angle of the ray with respect to the Earth's magnetic field,

v is the electron-neutral collision frequency, and

f_H is the electron gyro frequency, typically 1.5MHz.

For frequencies in the GHz range n can be approximated with an accuracy of better than 1% by:

$$n = 1 - X / 2 \tag{2.11}$$

and

$$I = \frac{40.3}{f^2} \int_S N_e ds . \tag{2.12}$$

The ionospheric group delay is therefore

$$I = \frac{40.3}{f^2} TEC \tag{2.13}$$

where the quantity $\int_S N_e ds$ is the TEC, in el / m^2, integrated along the path from the observer to the satellite. The TEC represents the number of free electrons in a 1-square metre column along the path. The TEC varies both with latitude and time and in the Earth's ionosphere values between 10^{16} and $10^{19}\ el/m^2$ have been measured (Klobuchar 1996).

The phase of the GPS signal is advanced in the ionosphere by the same amount (when converted to metres) that the code is delayed.

2.2.2 Multipath

Multipath is the phenomena whereby a signal travels from a transmitter to a receiver via multiple paths due to refraction and diffraction, as shown in figure 2.3. It is one of the major sources of error in precise GPS applications. Multipath can distort the signal modulation, resulting in measurement errors of the pseudo-random code. Multipath can also degrade the phase of the carrier, resulting in the errors in phase measurements. Unlike other error sources, it is highly localized and does not cancel out through differencing.

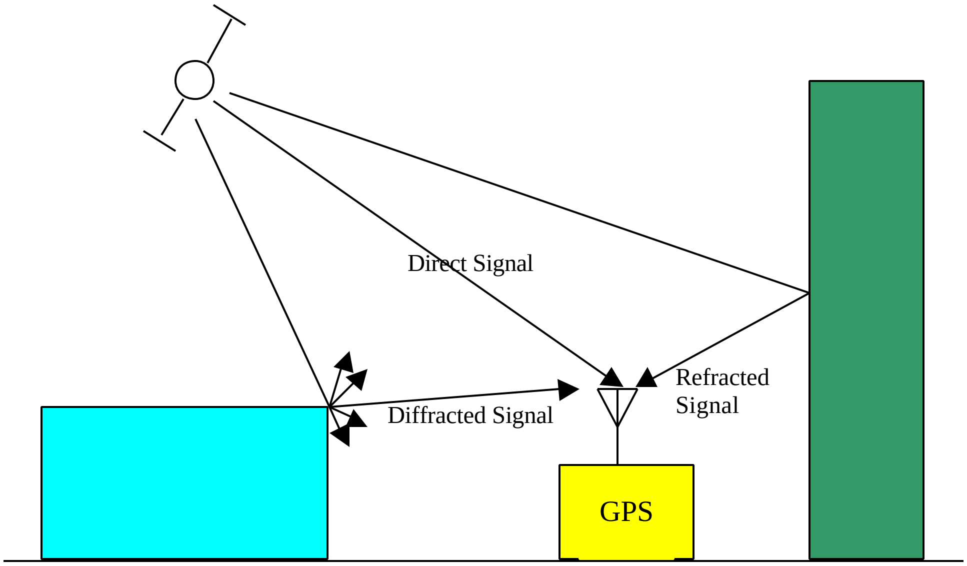

Figure 2.3: Multipath Signal

A mathematical representation of the carrier phase observable for a two-path signal (one reflected signal) to gain insight into multipath errors, can be expressed as

$$S = A\cos(f_d) + aA\cos(f_d + q) \tag{2.14}$$

where

S is the received signal,

A is the ideal (direct) signal amplitude,

f_d is the phase of the ideal (direct) signal,

a is the reflectivity coefficient that relates the relative strength of the reflected signal to the actual signal (typically less than 1), and

q is the phase shift caused by the reflected signal.

Because the direct and reflected signals have the same frequency, the superposition of the two can be written in the form

$$S = a_M A\cos(f_d + q_M) \tag{2.15}$$

where a_M is the attenuation of the signal due to multipath, and q_M is the induced phase shift of the signal due to multipath.

Comparing equations 2.14 and 2.15, yields

$$a_M = \sqrt{1 + a^2 + 2a\cos(q)} \tag{2.16}$$

and

$$q_M = \tan^{-1}\left[\frac{a\sin(q)}{1 + a\cos(q)}\right] \tag{2.17}$$

The case of maximum path delay must fulfill the condition $\partial q_M / \partial q = 0$, which occurs at $q_{Max} = \pm\cos^{-1}(-a)$. Therefore, the maximum carrier phase multipath error induced by a single reflected signal is a function of only the reflected signal strength ratio in this simplistic model. The maximum theoretical error therefore occurs for a value of $a = 1$, which corresponds to $\pm 90^0$. As $\pm 90^0$ is equivalent to one quarter of a cycle, the maximum theoretical carrier phase error due to multipath is $l/4$, or approximately 4.8

cm when converted from L1 cycles to metres (Leick 1995). However, in most real-world applications, the reflected signal will be attenuated to a lesser extent, and typical phase multipath values are more on the order of 1 cm or less (Lachapelle 1994).

Code multipath is similar to carrier phase multipath, only its magnitude tends to be several orders of magnitude higher. For code measurements, the multipath signals are always delayed compared to line-of-sight signals because of the longer travel paths caused by the reflection. The direct and reflected signals will superimpose to produce the received signal and it will have a great effect on the GPS receiver's correlator as shown in figure 2.4 (Lachapelle 1997) and introduce some measurement errors of the calculated GPS signal time delay. The magnitude of this error is site, geometry and equipment dependent, but it is typically less than a few metres. Similar to the carrier phase, in which the maximum multipath is a fraction of the wavelength, multipath for the code is related to the code-chipping rate, and is a function of the length of the codes. The higher the chipping rate, the lower the maximum multipath. Depending upon this rule, the expected multipath on the P-code pseudorange (chipping rate is 10.23MHz) is smaller than for C/A-code pseudorange (chipping rate is 1.023MHz).

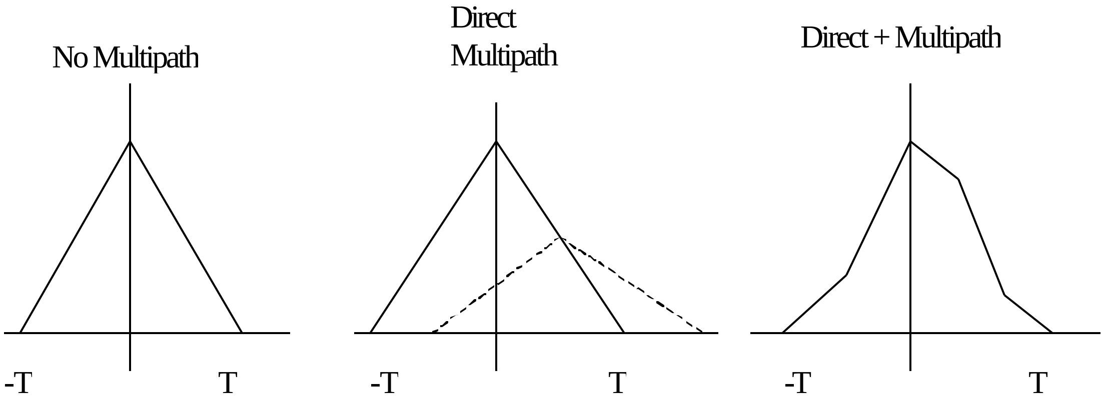

Figure 2.4: Multipath effect on code correlator

A number of significant research work has been done to characterize the effects of the multipath on a Delay Lock Loop (DLL) in a GPS receiver. These multipath effects can be reduced using three typical methods: antenna-based mitigation, improved receiver technology, and signal and data processing. Antenna based mitigation modifies the antenna gain pattern to counter the multipath, such as a chock ring with a ground plane. For receiver technology to mitigate the multipath, the typical example is Narrow Correlator Spacing (Fenton & al 1991, van Dierendonck & al 1992). Multipath mitigation using the signal-to-noise ratio is explored by Axelrad & al (1994), while Raquet and Lachapelle (1996) investigate the use of multiple reference stations to deal with this problem. Regarding carrier phase multipath mitigation, a system comprised of multiple closely-spaced antennas was developed and tested by Ray & al (1998).

2.2.3 Receiver noise

Receiver noise can be considered as white as it is uncorrelated over time. Also, there is no correlation between separate parallel measurements taken at the same time in a GPS receiver, because of the use of independent signal tracking loops for each separate measurement. The noise level is a function of code correlation method, receiver dynamics, and satellite elevation (due to antenna gain) (Lachapelle 1997). Code and carrier phase measurement noise can be estimated by a "zero baseline" test. The GPS signal is split into two and fed to two separate but same-type receivers. Typical receiver noise levels are outlined in Table 2.1.

Table 2.1: Approximate GPS receiver noise level

Observable	Approximate noise level
C/A-code	30 – 300 cm
P-code	3- 30 cm
Carrier Phase (L1)	0.5 –3 mm

2.2.4 Satellite orbit error

Satellite orbit error results from the uncertainties in the orbital information. These uncertainties are due to the accuracy limitations associated with Selective Availability (SA) and the predicted nature of the broadcast ephemeris. The broadcast navigation message includes Keplerian orbital elements and time derivatives for these elements. It is generated using the measurements from five GPS monitor stations and is updated once every two hours. Tests have shown that the orbit error is about 5 to 20 metres when SA is turned off (Lachapelle 1997).

Since most users derive the position of GPS satellites from the broadcast ephemeris, the significant uncertainties of the broadcast ephemeris result in errors in positioning. Orbital errors can be greatly reduced in relative positioning by double differencing because of the spatial correlation of the orbit error. However, the residual orbit error increases as the baseline length increases. Therefore, a more effective way to handle the orbit error for long baseline positioning is to use precise orbits, which are calculated using measurements from many reference stations for many days before and after the time period. These precise orbits typically have an accuracy better than 6 cm (Rothacher 1997). Generally, the following equation gives a simple relationship between satellite orbit error and baseline estimated error for a worst case, as shown in figure 2.5:

$$\overset{\rightarrow}{db}/\,b = \overset{\rightarrow}{dr}/\,r \tag{2.18}$$

where

$\overset{\rightarrow}{db}$ is the baseline error due to a satellite orbit error $\overset{\rightarrow}{dr}$,

b is the baseline length, and

r is the range to satellite (approximately 20,000 km).

The maximum baseline error is therefore 1ppm or better for each 20 m of satellite orbit error.

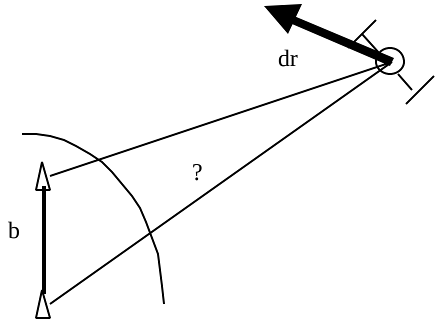

Figure 2.5: Effect of orbit errors on DGPS

2.2.4.1 Samples of satellite orbit errors from field data

In order to evaluate satellite orbit errors, they can be calculated by differencing the position generated from the broadcast ephemeris and the position generated from the precise orbit.

The primary data used in this thesis was from 11 reference receivers spread throughout the southern portion of Norway, as described in detail in Appendix A. The data was collected on September 30, 1997 and a 10^0 cut-off angle is chosen for processing. In the following analysis, two sets of baselines are selected. The direction of one set is North-South and they are Ales-Berg (249km), Ales-Geim (243km) and Ales-Kris (498km), and the associated double differencing errors are shown in figure 2.6. The statistics of these errors are listed in Table 2.2 and shown in figure 2.7. Another set of baselines is along the West-East direction and they are Geim-Geir (29km), Berg-Geir (164km), Geir-Tryr (247km) and Berg-Tryr (407km), and the associated double differencing errors are shown in figure 2.8. The statistical analyses of these baselines are presented in Table 2.3 and in figure 2.9.

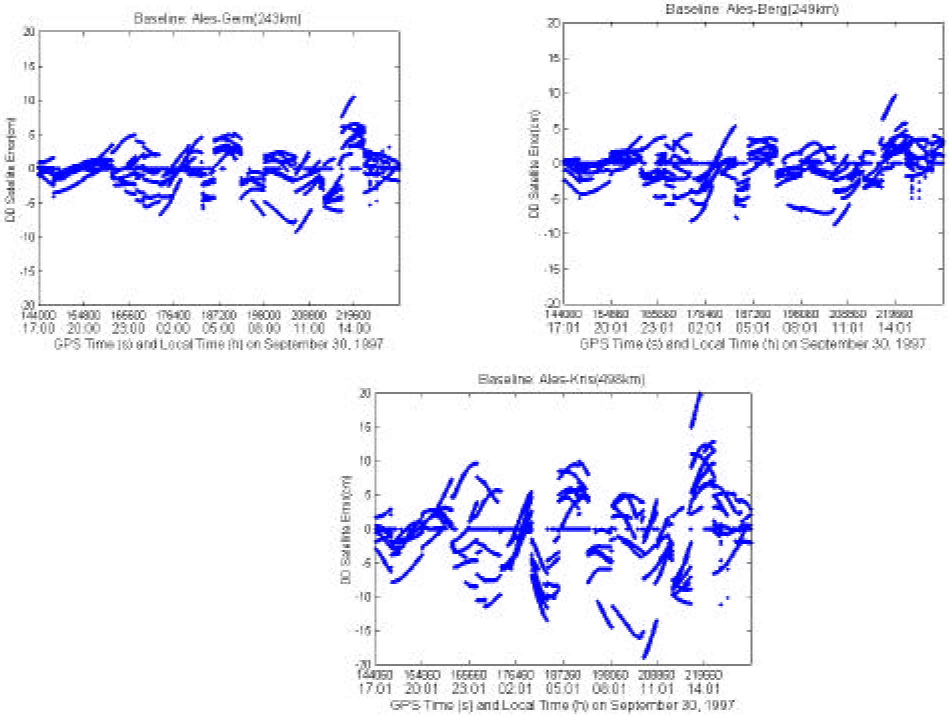

Figure 2.6: DD orbit errors over North-South direction baselines

Table 2.2: Statistics of DD orbit errors over baselines along North-South direction

Baseline Name	Baseline Length (km)	Mean (cm)	RMS (cm)
Ales-Geim	243	-0.12	2.69
Ales-Berg	249	-0.42	2.51
Ales-Kris	498	-0.55	5.50

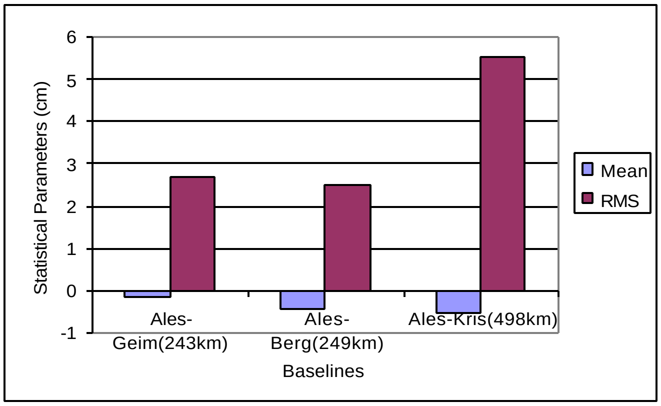

Figure 2.7: Statistics of DD orbit errors over North-South direction baselines

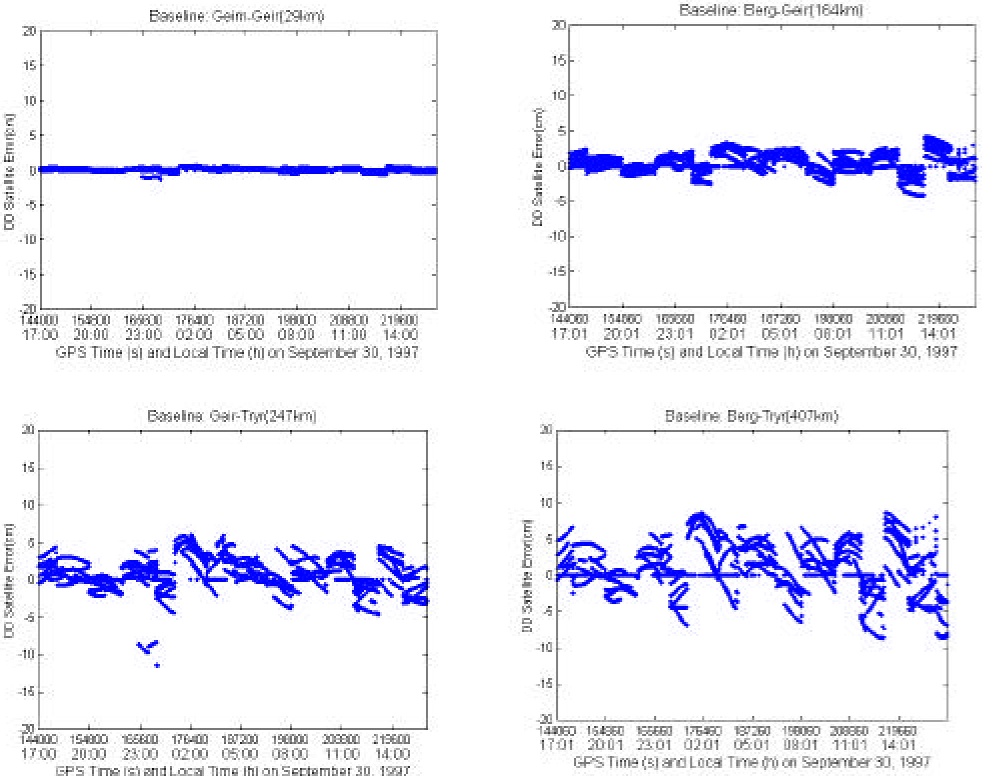

Figure 2.8: Double difference orbit errors over West-East direction baselines

Table 2.3: Statistics of DD orbit errors over baselines along West-East direction

Baseline Name	Baseline Length (km)	Mean (cm)	RMS (cm)
Geim-Geir	29	0.09	0.27
Berg-Geir	164	0.47	1.45
Geir-Tryr	247	0.82	2.35
Berg-Tryr	407	1.01	3.55

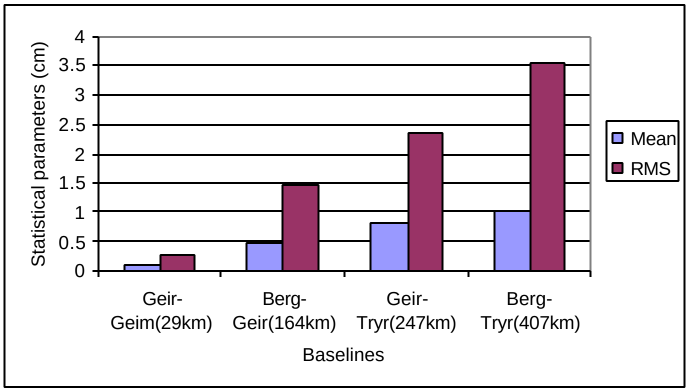

Figure 2.9: Statistics of DD orbit errors over West-East direction baselines

Note that, for the double difference satellite position errors, the rms of this error increases as the baseline length increases. This is because the spatial correlation of satellite orbit errors decreases with the increase of the baseline length. With the decrease of spatial correlation, the residual double difference errors due to satellite orbit errors will increase. Figure 2.10 shows the rms of double difference satllite orbit errors versus the baseline distances by the combination of two baseline sets above. The trend is quasi-linear.

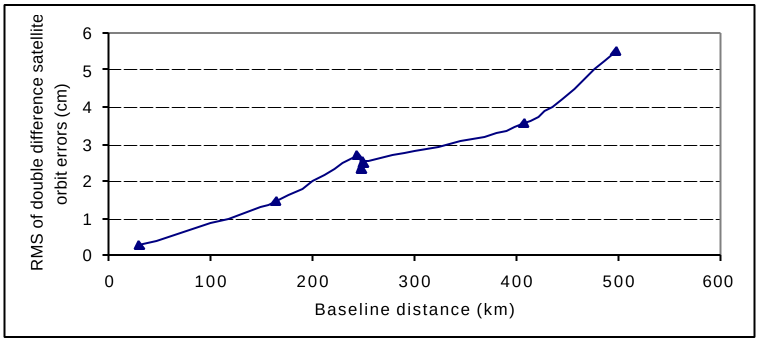

Figure 2.10: RMS of double difference orbit errors versus baseline distance

CHAPTER 3

TROPOSPHERE EFFECT ON GPS SIGNALS

GPS signals have to propagate through the Earth's atmosphere. Two atmospheric regions degrade the quality of GPS observations: the ionosphere and the neutral atmosphere layer. The ionosphere is a frequency-dispersive medium, that is, the free electrons of the ionosphere cause a frequency dependent phase advance or a group delay to the GPS signals. Hence, the first-order ionospheric effects can be removed by dual-frequency observations (Hofmann-Wellenhof & al 1993). However, the neutral atmosphere, which includes the lower part of the stratosphere and the troposphere, is a non dispersive layer. The modeling of this effect on GPS signals requires the information of the atmospheric properties.

In this chapter, the characteristics of the troposphere are reviewed, describing its compositions and significance in GPS relative positioning. Secondly, the refraction of GPS signal in the troposphere is analyzed. Along with the analysis of the physics of the troposphere, several typical tropospheric models are introduced. Thirdly, the ionospheric-free (IF) double difference observable is provided as the measurement of residual tropospheric effects and the concept of residual tropospheric delay is put forward in detail. Finally, the troposphere standard model improvement is tested and analysed using field data.

3.1 Troposphere composition and structure

The neutral atmosphere layer consists of three temperature-delineated regions: the troposphere, the stratosphere and part of the mesosphere. The neutral atmosphere is often simply referred as the troposphere because in radio wave propagation the troposphere effects dominate with respect to other effects. Figure 3.1 gives the temperature profile of the standard atmosphere (Champion & al 1985).

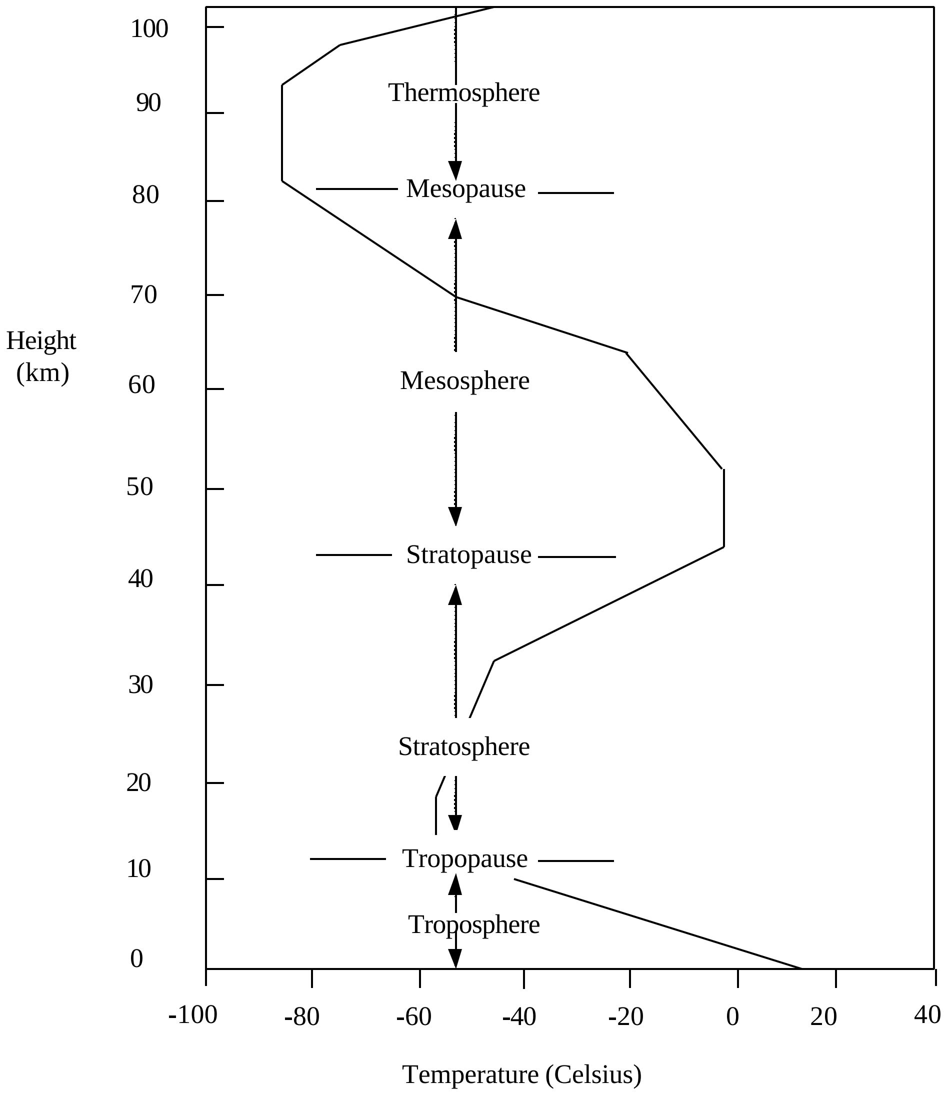

Figure 3.1: Thermal profile of atmosphere showing approximate altitude of temperature regions

From figure 3.1, it is obvious that the temperature in the troposphere region decreases with increasing height at a rate of 6.5°C/km, on average. The actual value of this temperature gradient is a function of height, season and geographical location.

The troposphere contains about 80% of the total molecular mass of the atmosphere (Wallace and Hobbs 1977), and nearly all the water vapor and aerosols. Considering the composition of the troposphere, it can be divided into two parts: dry air and water vapor.

Dry air is a mixture of gases, in which nitrogen, oxygen, and argon are the major constituents and account for about 99.95% of the total volume. Dry air is mixed very consistently up to an altitude of approximately 80km. The main source of water vapor is the evaporation from bodies of water and transpiration by plants. The water vapor content is a function of the local geographic conditions and meteorological phenomenon. Its concentration is less than 1% of the volume of the air in the polar regions and large desert region, but quite significant over tropical rain forests, reaching over 4% of the volume of the air (Lutgens and Tarbuck 1979). Therefore, water vapor in the troposphere is a spatial and temporal variable.

Dry air gases, and water vapor in hydrostatic equilibrium, are easily modeled theoretically with the ideal gas law and the hydrostatic equations. Hence, this is the reason to separate the contents of the troposphere into hydrostatic and non-hydrostatic, or wet components. Since the hydrostatic delay is due to the transient or induced dipole moment of all the gaseous constituents of the atmosphere including water vapor, the term hydrostatic delay is favored over the sometimes used term “dry delay”. The hydrostatic delay can be well determined from pressure measurements, and at sea level it typically reaches about 2.3 m in the zenith direction. The zenith wet delay can be less than 10 mm in arid regions and as large as 400 mm in humid regions. Significantly, the daily variation of the wet delay usually exceeds that of the hydrostatic delay by more than an order of magnitude, especially in temperate regions.

3.2 Refraction of GPS signals in the troposphere

When the radio signals traverse the earth's atmosphere, they are affected significantly by variations in the refractive index of the troposphere. The refractive index is greater than unity and it causes an extra path delay. Simultaneously, the changes in the refractive index with varying height cause a bending of the ray. The combination of these two effects is the so-called troposphere refraction of propagation delay.

The tropospheric propagation delay is directly related to the refractive index (or refractivity). At each point in the troposphere, the refractive index of a particle of air can be expressed as a function of atmospheric pressure, temperature and humidity. The troposphere propagation delay can be usually divided into hydrostatic and wet components and can be determined from models and approximations of the atmosphere profiles.

3.2.1 Refractivity

The refractive index of a medium, n, is defined as the ratio of the speed of propagation of an electromagnetic wave in a vacuum, c, to the speed of propagation in this medium, v:

$$n = \frac{c}{v} \tag{3.1}$$

The refractive index of moist air is different from unity because its constituents suffer polarization induced by the electromagnetic field of the radio signals. As the electromagnetic waves in the atmosphere propagate just slightly slower than in a vacuum, the refractive index is more conventionally expressed by refractivity, N :

$$N = 10^6 (n - 1) \tag{3.2}$$

If we take into account the compressibility factors to account for the non-ideal behavior of gases (Mendes 1999), the refractivity N can be written as

$$N = K_1 (\frac{P_d}{T}) Z_d^{-1} + [K_2 (\frac{e}{T}) + K_3 (\frac{e}{T^2})] Z_w^{-1} \tag{3.3}$$

where P_d is the partial pressure of dry air (mbar), T is the absolute temperature (K), e is the partial pressure of water vapor (mbar), Z_d^{-1} is the inverse compressibility factor for dry air constituents, Z_w^{-1} is the inverse compressibility factor for water vapor, and K_1, K_2, K_3 are empirically determined constants ($K/mb, K/mb, K^2/mb$). Table 3.1 summarizes the most significant recent evaluations of the refractivity constants (Mendes 1999).

Table 3.1: Refractivity empirical constants

Reference	$K_1 (K/mb)$	$K_2 (K/mb)$	$K_3 (10^5 K^2/mb)$
Boudouris (1963)	77.59 ± 0.08	72 ± 11	3.75 ± 0.03
Smith and Weintraub (1953)	77.61 ± 0.01	72 ± 9	3.75 ± 0.03
Thayer (1974)	77.60 ± 0.01	64.79 ± 0.08	3.776 ± 0.004

From equation 3.3, it is obvious that the refractivity N is divided into a dry part and a wet part. According to Davis & al (1985) and Thayer (1974), the refractivity model can be expressed in the more conventional form as follows:

$$N = K_1 R_d r + [K_2 \frac{e}{T} + K_3 \frac{e}{T^2}] Z_w^{-1} \qquad (3.4)$$

where R_d is the gas content for dry air, and r is the total mass density of the troposphere. The first term of equation 3.4 is no longer purely "dry", as there is a contribution of the water vapor hidden in the total density. As opposed to the "dry" component of equation 3.3, the first term of equation 3.4 is the so-called hydrostatic component of the refractivity, a term suggested by Davis & al (1985) which is now widely used. Therefore, the refractivity from equation 3.4 can be divided into hydrostatic and wet components. The errors induced in estimating refractivity assuming the "dry/wet" formalism instead of "hydrostatic/wet" formalism depend upon the errors in the assumption that the dry pressure is equivalent to the total pressure excluding the water vapor pressure. It is more accurate to express the refractivity in terms of hydrostatic and wet components since the hydrostatic components can be described with the equation of state of gases and the hydrostatic equation, but dry components cannot be. Hence the hydrostatic component can be modeled with full accuracy and the zenith delay based on the hydrostatic component is not influenced by the water vapor component, unlike the "dry" component formalism.

3.2.2 Troposphere path delay

The propagation range of a radio signal can be expressed as:

$$L = \int nds \tag{3.5}$$

where L is the so-called optical path length, or the electromagnetic path length, and n is the refractive index described in the previous section. The integral is evaluated along the path of the signal in the troposphere. The geometric path, the corresponding straight-line path, can be expressed by equaling n to unity:

$$S_0 = \int ds_0 \tag{3.6}$$

where the integral is performed in vacuum. Therefore, the troposphere propagation delay is defined as the difference between the electromagnetic path delay and the geometric path delay, neglecting the ray bending,

$$\begin{aligned} d_{Trop} = L - S_0 &= \int (n-1)ds \\ &= 10^{-6} \int Nds0 \end{aligned} \tag{3.7}$$

Considering equation 3.4, the refractivity N can be divided into hydrostatic and wet components. Hence equation 3.7 can be written as

$$d_{Trop} = 10^{-6} \int N_{Hydro} ds + 10^{-6} \int N_{Wet} ds \tag{3.8}$$

or symbolically,

$$d_{Trop} = d_{Hydro} + d_{Wet} \tag{3.9}$$

where d_{Hydro} represents the hydrostatic delay and d_{Wet} is the wet delay.

Propagation delays at arbitrary elevation angles are determined from the zenith delays and the so-called "mapping functions". As the zenith delay can be expressed as the sum of the hydrostatic and wet components, mapping functions can be developed in order to map separately the hydrostatic and wet components. Therefore, in general we have

$$d_{Trop} = d^{Z}_{Hydro} \times m_{Hydro}(e) + d^{Z}_{Wet} \times m_{Wet}(e) \tag{3.10}$$

where d^{Z}_{Hydro} is the hydrostatic zenith delay, d^{Z}_{Wet} is the wet zenith delay, m_{Hydro} is the hydrostatic mapping function, m_{Wet} is the wet mapping function, and e is the elevation angle. In the simplest case which assumes a flat earth and a constant refractivity, the mapping function follows the "cosecant law":

$$m(e) = \frac{1}{\sin(e)} \tag{3.11}$$

But obviously this is not accurate since it depends on assumptions: a flat earth and a constant refractivity.

3.3 Troposphere propagation delay modeling

In the past several decades, a number of troposphere propagation models have been reported in the scientific literature. As for the expression in the previous section, the tropospheric propagation delay can be approximated by finding closed-form analytical models for the zenith delay and then by mapping this delay to the arbitrary elevation angles using a mapping function.

3.3.1 Review of modeling approaches

Much research has gone into the creation and testing of tropospheric refraction models to compute the refractivity N along the path of signal travel: Saastamonien (1972, 1973), Hopfield (1969), Goad and Goodman (1974), and Black (1978). The various tropospheric models differ primarily with respect to the assumptions made regarding the vertical refractivity profiles and the mapping of the vertical delay with elevation angles. The following presents several models where meteorological surface data are taken into account.

Saastamonien model

Saastamonien described a standard model for RF tropospheric delay valid for elevations $e \geq 10^0$ and it is given as follows:

$$d_{Trop} = \frac{0.002277}{\cos Z}\left[p + (\frac{1225}{T} + 0.05)e - \tan^2 Z \right] \tag{3.12}$$

where d_{Trop} is the delay correction in metres, Z denotes the zenith distance of the satellite or apparent zenith angle $Z = 90^0 - e$, and e is the elevation angle, p is the atmospheric pressure in mbar, e is the partial pressure of water vapor in mbar, and T is the surface temperature in Kelvin. Saastamonien has also refined this model by adding two correction terms, one dependent on the height of the observation site and the other on the height and the zenith distance. Equation 3.12 can be refined as:

$$d_{Trop} = \frac{0.002277}{\cos Z}(1+D)\left[p + (\frac{1225}{T} + 0.05)e - B\tan^2 Z \right] + dR \qquad (3.13)$$

where $D = 0.0026\cos(2f) + 0.00028h$, where f is the local latitude and h is the station height in km. The correction terms dR and B can be interpolated from Table 3.2.

Table 3.2: Correction terms for Saastamonien model

Zenith distance		Station height above sea level [km]							
		0	0.5	1	1.5	2	3	4	5
	$60^o00'$	0.003	0.003	0.002	0.002	0.002	0.002	0.001	0.001
	$66^o00'$	0.006	0.006	0.005	0.005	0.004	0.003	0.003	0.002
	$70^o00'$	0.012	0.011	0.010	0.009	0.008	0.006	0.005	0.004
	$73^o00'$	0.020	0.018	0.017	0.015	0.013	0.011	0.009	0.007
	$75^o00'$	0.031	0.028	0.025	0.023	0.021	0.017	0.014	0.011
	$76^o00'$	0.039	0.035	0.032	0.029	0.026	0.021	0.017	0.014
$dR, metre$:	$77^o00'$	0.050	0.045	0.041	0.037	0.033	0.027	0.022	0.018
	$78^o00'$	0.065	0.059	0.054	0.049	0.044	0.036	0.030	0.024
	$78^o30'$	0.075	0.068	0.062	0.056	0.051	0.042	0.034	0.028
	$79^o00'$	0.087	0.079	0.072	0.065	0.059	0.049	0.040	0.033
	$79^o30'$	0.102	0.093	0.085	0.077	0.070	0.058	0.047	0.039
	$79^o45'$	0.111	0.101	0.092	0.083	0.076	0.063	0.052	0.043
	$80^o00'$	0.121	0.110	0.100	0.091	0.083	0.068	0.056	0.047
B, mbar		1.156	1.079	1.006	0.938	0.874	0.757	0.654	0.563

Hopfield model

Hopfield (1969) developed a dual quartic zenith model of the refractivity with different quartics for the dry and wet atmospheric profiles using real data covering the whole earth. The refractivity can be written as a function of height h above the surface by

$$N_d^{Trop}(h) = N_{d,0}^{Trop}(1 - \frac{h}{h_d})^4 \qquad (3.14)$$

under the assumption of a single polytropic layer with thickness

$$h_d = 40136 + 148.72(T - 273.16) \quad [\mathrm{m}] \qquad (3.15)$$

where $N_{d,0}^{Trop}$ is the refractivity of dry component at surface.

and

$$N_w^{Trop}(h) = N_{w,0}^{Trop}(1 - \frac{h}{h_w})^4 \qquad (3.16)$$

where $N_{w,0}^{Trop}$ is the refractivity of wet component at surface and the mean value of $h_w = 11000m$ is used. Unique values for h_d, h_w cannot be given because they depend on location and temperature. The effective troposphere heights are given as $40km \le h_d \le 45km$ and $10km \le h_w \le 13km$.

A slight variation of the Hopfield model contains an arbitrary elevation angle e at the observation site using $\sin(e^2 + 6.25)^{-1/2}$ as a mapping function for the dry component and $\sin(e^2 + 2.25)^{-1/2}$ for the wet component. Therefore, the tropospheric delay can be written as follows:

$$d^{Trop}(e) = d_d^{Trop}(e) + d_w^{Trop}(e) \qquad (3.17)$$

where

$$d_d^{Trop}(e) = \frac{10^{-6}}{5} \frac{77.64 \frac{p}{T}}{\sqrt{\sin(e^2 + 6.25)}} [40136 + 148.72(T - 273.16)]$$

$$d_w^{Trop}(e) = \frac{10^{-6}}{5} \frac{-12.96T + 3.718 \times 10^5}{\sqrt{\sin(e^2 + 2.25)}} \frac{e}{T^2} \times 11000 \qquad (3.18)$$

where p is the atmospheric pressure in mbar, e is the partial pressure of water vapor in mbar and T is the temperature in Kelvin.

Modified Hopfield model

Instead of the height h, the modified Hopfield model is refined as a function of the length of the position vector. Denoting the earth's radius by R_E, the corresponding lengths are $r_d = R_E + h_d$ and $r = R_E + h$, as shown in Figure 3.2.

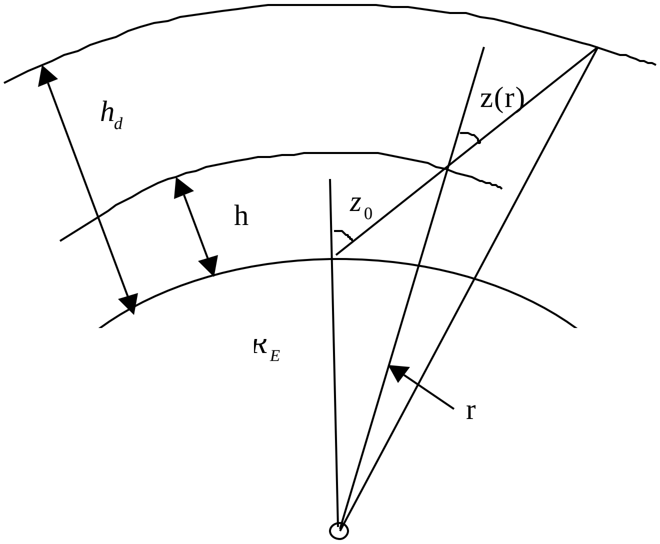

Figure 3.2: Geometry for tropospheric delay

Therefore, the refractivity for the dry and wet components is of the following form

$$N_d^{Trop}(r) = N_{d,0}^{Trop}[\frac{r_d - r}{r_d - R_E}]^4 \tag{3.19}$$

and

$$N_w^{Trop}(r) = N_{w,0}^{Trop}[\frac{r_w - r}{r_w - R_E}]^4 \tag{3.20}$$

Based on a series expansion of the integral, the modified Hopfield model can be expressed in the following form, where a subscript i is introduced which reflects either the dry component (replace i by d) or the wet component (replace i by w). The tropospheric path delay in metres is thus given by

$$d_i^{Trop}(E) = 10^{-6} N_{i,0}^{Trop}[\sum_{k=1}^{9} \frac{a_{k,i}}{k} r_i^k] \qquad (3.21)$$

where

$$r_i = \sqrt{(R_E + h_i)^2 - (R_E \cos e)^2} - R_E \sin e \qquad (3.22)$$

$$a_{1,i} = 1 \qquad a_{2,i} = 4a_i \qquad a_{3,i} = 6a_i^{\;2} + 4b_i$$

$$a_{4,i} = 4a_i(a_i^2 + 3b_i) \qquad a_{5,i} = a_i^4 + 12a_i^2 b_i + 6b_i^2 \qquad a_{6,i} = 4a_i b_i (a_i^2 + 3b_i)$$

$$a_{7,i} = b_i^2(6a_i^2 + 4b_i) \qquad a_{8,i} = 4a_i b_i^3 \qquad a_{9,i} = b_i^4$$

and

$$a_i = -\frac{\sin e}{h_i}$$

$$b_i = -\frac{\cos^2 e}{2h_i R_E}$$

3.3.2 Mapping functions

Over the past 20 years or so, geodesists and radio meteorologists have developed a variety of model profiles and mapping functions for the variation of the delay experienced by signals propagating through the troposphere at arbitrary elevation angles.

The simplest mapping function is the cosecant of the elevation angle that assumes that spherical constant-height surfaces can be approximated as plane surface. This is a reasonably accurate approximation only for high elevation angles and with a small degree of bending. Saastamonien (1973) and Baby & al (1988) mapping functions are basically dependent on this "cosecant law " with extension.

The more complex mapping functions are based on the truncation of the continued fractions. This type of mapping function includes Marini (1972), Chao (1972), Davis & al (1985), and Neil (1996). The mapping functions derived by Marini (1972), Davis & al (1985) and Neil (1996) are described below.

Marini mapping function

Marini (1972) showed that the elevation angles of the tropospheric path delay can be expressed as a continued fraction in terms of the sine of the elevation angle:

$$m(e)=\cfrac{1}{\sin e+\cfrac{a}{\sin e+\cfrac{b}{\sin e+\cfrac{c}{\sin e+\ldots\ldots}}}} \tag{3.23}$$

where the coefficients a , b, c … are constants or linear functions.

Davis & al (1985) have developed a more complex function for the dry (hydrostatic) component based on Marini model (1972) wherein the coefficients a, b, and c are dependent on surface pressure, temperature, lapse rates, and tropospheric height h_T. This model is termed as the Davis mapping function and has the form:

$$m(e)=\cfrac{1}{\sin e+\cfrac{a}{\tan e+\cfrac{b}{\tan e+c}}} \tag{3.24}$$

where a, b, and c depend upon measurements or estimates:

$$\begin{aligned} a &= 0.001185+0.6071\times10^{-4}(p_0-1000)-0.1471\times10^{-3}e_0 \\ &\quad +0.3072\times10^{-2}(T_0-20)+0.1965\times10^{-1}(b+6.5)-0.5645\times10^{-2}(h_T-11.231)] \end{aligned} \tag{3.25}$$

$$\begin{aligned} b &= 0.001144\times[1+0.1164\times10^{-4}(p_0-1000)-0.2795\times10^{-3}e_0 \\ &\quad +0.3109\times10^{-2}(T_0-20)+0.3038\times10^{-1}(b+6.5)-0.1217\times10^{-1}(h_T-11.231)] \end{aligned}$$

$$c=-0.0090$$

where b is the tropospheric temperature lapse rate in ^{o}C/km, h_T is the height of the troposphere in km, T_0 is the surface temperature in ^{o}C, p_0 is the atmospheric surface pressure in mbar, and e_0 is the pressure in mbar of water vapor.

Neil mapping function

Differing from most typical tropospheric delay models, Neil has developed a hydrostatic and wet mapping function with new forms whose combined use reduces errors in geodetic estimation for observations as low as 3^{o} in elevation. Even if it has no parameterization in terms of actual meteorological conditions, they agree as well or better with mapping functions calculated from radiosonde profiles. Instead, when there is no information about the state of the atmosphere other than at the surface, the variation of the mapping function is found to be better modeled in terms of the seasonal dependence of the atmosphere, taken to be sinusoidal, and in terms of the latitude and height above the sea level of the site. In fact, for this model, the coefficients of the continued fraction representation of the hydrostatic mapping function depend on the latitude and height above sea level of the observing site and on the day of the year. The dependence of the wet mapping function is only on the site latitude. The form adopted for this mapping function is the continued fraction of Marini (1972) with three constants but normalized to unity at the zenith as proposed by Herring (1992) and can be expressed in the following form:

$$m(e) = \frac{\dfrac{1}{1+\dfrac{a}{1+\dfrac{b}{1+c}}}}{\dfrac{1}{\sin e+\dfrac{a}{\sin e+\dfrac{b}{\sin e+c}}}} \tag{3.26}$$

In addition to a latitude and seasonal dependence due to varying solar radiation, the hydrostatic mapping function should also be dependent on the height above the geoid of the point of observation because the ratio of the atmosphere "thickness" to the radius of curvature decreases with height. This does not apply to the wet mapping function since the water vapor is not in hydrostatic equilibrium , and the height distribution of the water vapor is not expected to be predictable from the station height. Therefore, the hydrostatic and wet mapping function can be written as:

$$m_{Hydro}(e)=\frac{\dfrac{1}{1+\dfrac{a_{Hydro}}{1+\dfrac{b_{Hydro}}{1+c_{Hydro}}}}}{\dfrac{1}{\sin e+\dfrac{a_{Hydro}}{\sin e+\dfrac{b_{Hydro}}{\sin e+c_{Hydro}}}}}+\left[\frac{1}{\sin e}-\frac{\dfrac{1}{1+\dfrac{a_{ht}}{1+\dfrac{b_{ht}}{1+c_{ht}}}}}{\dfrac{1}{\sin e+\dfrac{a_{ht}}{\sin e+\dfrac{b_{ht}}{\sin e+c_{ht}}}}}\right]\times\frac{H}{1000} \tag{3.27}$$

and

$$m_{wet}(e)=\frac{\dfrac{1}{1+\dfrac{a_{wet}}{1+\dfrac{b_{wet}}{1+c_{wet}}}}}{\dfrac{1}{\sin e+\dfrac{a_{wet}}{\sin e+\dfrac{b_{wet}}{\sin e+c_{wet}}}}} \tag{3.28}$$

where e is the elevation angle, and $a_{ht}=2.53\times10^{-5}, b_{ht}=5.49\times10^{-3}, c_{ht}=1.14\times10^{-3}$. For the coefficients $a_{Hydro}, b_{Hydro}, c_{Hydro}$, they can be interpolated based on the parameter values extracted from Table 3.3 by the following interpolation rule:

$$\begin{aligned}p(f,t) &= p_{avg}(f_i)+[p_{avg}(f_{i+1})-p_{avg}(f_i)]\times\frac{f-f_i}{f_{i+1}-f_i}\\ &\quad+\{p_{amp}(f_i)+[p_{amp}(f_{i+1})-p_{amp}(f_i)]\times\frac{f-f_i}{f_{i+1}-f_i}\}\times\cos(2p\,\frac{t-T_0}{365.25})\end{aligned} \tag{3.29}$$

for the latitude range $15^0 \le |f| \le 75^0$,where f is the user's latitude and the subscripts refer to the nearest tabular latitude, t is the day-of-year, p represents the calculated coefficients a, b or c, and T_0 is the adopted phase, Day-of-year (DOY) 28. The average value of $a_{Hydro}, b_{Hydro}, c_{Hydro}$ and amplitude value of $a_{Hydro}, b_{Hydro}, c_{Hydro}$ are listed in Table 3.3.

Table 3.3: Coefficients of the hydrostatic mapping function

Latitude(degree)	a_{Hydro} (average)	b_{Hydro} (average)	c_{Hydro} (average)
15	1.2769934e-3	2.9153695e-3	62.610505e-3
30	1.2683230e-3	2.9152299e-3	62.837393e-3
45	1.2465397e-3	2.9288445e-3	63.721774e-3
60	1.2196049e-3	2.9022565e-3	63.824265e-3
75	1.2045996e-3	2.9024912e-3	64.258455e-3
Latitude(degree)	a_{Hydro} (amplitude)	b_{Hydro} (amplitude)	c_{Hydro} (amplitude)
15	0.0	0.0	0.0
30	1.2709626e-5	2.1414979e-5	9.0128400e-5
45	2.6523662e-5	3.0160779e-5	4.3497037e-5
60	3.4000452e-5	7.2562722e-5	84.795348e-5
75	4.1202191e-5	11.723375e-5	170.37206e-5

For the latitude $|f| \leq 15^0$,

$$p(f,t) = p_{avg}(15^0) + p_{amp}(15^0) \times \cos(2p\,\frac{t-T_0}{365.25}) \tag{3.30}$$

For the latitude $|f| \geq 75^0$

$$p(f,t) = p_{avg}(75^0) + p_{amp}(75^0) \times \cos(2p\,\frac{t-T_0}{365.25}) \tag{3.31}$$

In case of the wet mapping function, the interpolation rule is also based on the following equation but the average values of $a_{wet}, b_{wet}, c_{wet}$ are listed in the Table 3.4.

$$p(f,t) = p_{avg}(f_i) + [p_{avg}(f_{i+1}) - p_{avg}(f_i)] \times \frac{f - f_i}{f_{i+1} - f_i} \tag{3.32}$$

for the latitude range $15^0 \leq |f| \leq 75^0$ and

For the latitude $|f| \leq 15^0$,

$$p(f,t) = p_{avg}(15^0) \tag{3.33}$$

For the latitude $|f| \geq 75^0$

$$p(f,t) = p_{avg}(75^0) \tag{3.34}$$

Table 3.4: Coefficients of the wet mapping function

Latitude(degree)	a_{wet} (average)	b_{wet} (average)	c_{wet} (average)
15	5.8021879e-4	1.4275268e-3	4.3472961e-2
30	5.6794847e-4	1.5138625e-3	4.6729510e-2
45	5.8118019e-4	1.4572752e-3	4.3908931e-2
60	5.9727542e-4	1.5007428e-3	4.4626982e-2
75	6.1641693e-4	1.7599082e-3	5.4736039e-2

3.4 Residual tropospheric delays and ionospheric-free measurements

As we have mentioned in the previous sections, the hydrostatic delay in the zenith direction is typically about 2.3m (Businger & al 1996, Dodson & al 1996) but this component can be modeled and removed with an accuracy of a few millimetres or better using one of the surface models (including pressure, temperature and humidity) presented in section 3.3. It is actually not much of a problem as far as its effect on GPS signals is concerned. However, the wet delay, which is mostly due to water vapor and is as small (zenith component) as a few centimetres or less in arid regions and as large as 35 centimetres in humid regions, is usually far more variable and more difficult to remove based on standard tropospheric models using surface measurements. Therefore, the delay remaining after applying a standard troposphere model and associated mapping function is called the "residual tropospheric delay" and it is mostly due to the wet component. If this residual tropospheric delay can be estimated or predicted in some way, GPS accuracy performance can be enhanced significantly. The residual tropospheric delay can be expressed as follows:

$$d_{Trop} = d_{Trop}(\text{model}) + d_{Trop}(\text{residual}) \tag{3.35}$$

where d_{Trop} is the total tropospheric path delay, d_{Trop}(model) is the predicted tropospheric path delay using one of the standard models as well as an associated mapping function, and d_{Trop}(residual) is the remaining tropospheric path delay after applying the standard models.

The residual tropospheric delay in some instances can be estimated using GPS data itself. The ionospheric-free combination of GPS carrier phase observations is a good measurement for this residual tropospheric delay computation.

3.4.1 Carrier phase ionospheric-free measurement

In order to study the tropospheric path delay of GPS signals, the ionospheric effect should first be eliminated from the observables. As both ionospheric delays and advances are frequency dependent, it is possible to eliminate the ionospheric effects with dual-frequency receivers. Then, the large part of the tropospheric path delay can be removed by standard models and associated mapping functions. The remaining part is the residual tropospheric delay.

Consider a GPS measurement based on a linear combination of the L_1 and L_2 phase measurements

$$f_{j,k} = j f_{L1} + k f_{L2} \tag{3.36}$$

where f_{L1} is the L_1 carrier phase measurement, f_{L2} is the L_2 carrier phase measurement, j and k are the linear combination coefficients for f_{L1} and f_{L2}; and $f_{j,k}$ is the combination of f_{L1} and f_{L2}.

After applying equation 2.9 and considering the measurement noise e is the combination of multipath error m and receiver noise v, the double difference equation of the measurement-minus-range observable is (Raquet 1998):

$$\begin{aligned}\Delta\nabla \bar{f}^{xy}_{ab(j,k)} = {} & \frac{1}{l_{j,k}}(\Delta\nabla d^{xy}_{Trop\,ab} + \Delta\nabla dr^{xy}_{sv\,ab} - \Delta\nabla dR^{xy}_{rec\,ab}) \\ & + \frac{j}{l_1}(\Delta\nabla m^{xy}_{ab\,L1} + \Delta\nabla v^{xy}_{ab\,L1}) + \frac{k}{l_2}(\Delta\nabla m^{xy}_{ab\,L2} + \Delta\nabla v^{xy}_{ab\,L2}) \\ & - \frac{\Delta\nabla d^{xy}_{Iono\,ab}}{c}\left(\frac{jf_2 + kf_1}{f_1 f_2}\right) + j\Delta\nabla N_1 + k\Delta\nabla N_2\end{aligned} \qquad (3.37)$$

where x and y denote the satellites and a and b the receivers. $\Delta\nabla \bar{f}^{xy}_{ab(j,k)}$ is the double difference (measurement-minus-range observable) in cycles, $l_{j,k} = \frac{l_1 l_2}{j l_2 + k l_1}$ is the wavelength of combined measurement term, d_{Trop} is the residual tropospheric delay (delay remaining after applying the standard troposphere model based on surface meteorological measurements of pressure, temperature and humidity), d_{Iono} is the ionospheric delay, dr_{sv} is the satellite position error, dR_{rec} is the reference receiver position error, m is the multipath error, v is the measurement noise, f_1 is the L_1 frequency (Hz), f_2 is the L_2 frequency (Hz), l_1 is the L_1 wavelength, l_2 is the L_2 wavelength, N_1 is the L_1 ambiguity, N_2 is the L_2 ambiguity, and c is the speed of light.

To extend equation 3.37 from equation 2.9, the ionospheric delay, multipath and receiver noise are considered as the frequency dependent terms, while the remaining satellite orbit error, receiver coordinate error and tropospheric error are considered as the non-frequency dependent terms.

The ionospheric free carrier phase measurement combination is obtained when $j = 1, k = -\frac{f_2}{f_1}$. Depending upon this combination, the ionospheric term is not included yet. However, the integer nature of the initial ambiguities N_1 and N_2 on this new combination is lost because of the non-integer factor k so that the ionospheric-free measurements cannot be used for integer search.

For the case when the integer ambiguities for L1 and L2 have been correctly determined, and if precise satellite orbits are used and receiver coordinates are assumed to be known accurately, that is, the satellite orbit error $\Delta\nabla dr_{sv}$ and receiver position error $\Delta\nabla dR_{rec}$ are small enough to be ignored in equation 3.37, the ionospheric-free double difference measurement can be simplified as

$$\Delta\nabla \bar{f}_{IF} = \frac{1}{l_{IF}}(\Delta\nabla d_{Trop}) + \frac{1}{l_1}(\Delta\nabla m_{L1} + \Delta\nabla v_{L1}) - \frac{f_2}{f_1 l_2}(\Delta\nabla m_{L2} + \Delta\nabla v_{L2}) + \Delta\nabla N_1 - \frac{f_2}{f_1}\Delta\nabla N_2 \tag{3.38}$$

where

$$l_{IF} = l_{j=1,k=-\frac{f_2}{f_1}} = \frac{l_1 l_2}{l_2 - \frac{f_2}{f_1} l_1} = 0.4844 \quad (m) \tag{3.39}$$

For long inter-receiver distances, the tropospheric term in equation 3.38 will dominate the residual errors which also include carrier phase multipath and receiver noise. Therefore, equation 3.38 represents a good measurement of the residual tropospheric delay assuming that the L1 and L2 ambiguities have been solved already. The objective of this thesis is to find a method to estimate residual tropospheric delays using all ionospheric-free carrier phase measurements simultaneously available from a network.

3.5 Field data tests for troposphere standard model improvement

In this section, the performance improvement prior to and after applying the troposphere standard model is analysed based on the field data from the Norway network, where there are total 11 reference receivers spread throughout the network and is described in Appendix A. The data was collected on September 30, 1997 and a 10^{o} cut-off angle was selected for the processing and analysis.

The test results depend on the analysis of the ionospheric-free double difference measurement, which is the phase combination of L1 and L2 and a good measurement of the residual tropospheric delay as presented in section 3.4.1. The statistical performance of ionospheric-free double difference measurements are first analysed with and without applying the standard troposphere model. For this analysis, the modified Hopfield model is chosen as one of the standard troposphere model and the defined sea level values of the pressure P_0, temperature T_0 and relative humidity f_0 are used: $P_0 = 1013.25mb$, $T_0 = 291.12K$, $f_0 = 50\%$.

Two sets of double difference baselines are chosen. The direction of one set is North-South and they are Ales-Geim (243km) and Ales-Kris (498km). The ionospheric-free double difference measurements, with and without applying the modified Hopfield model on the raw GPS measurements are shown in figures 3.3 and 3.4.

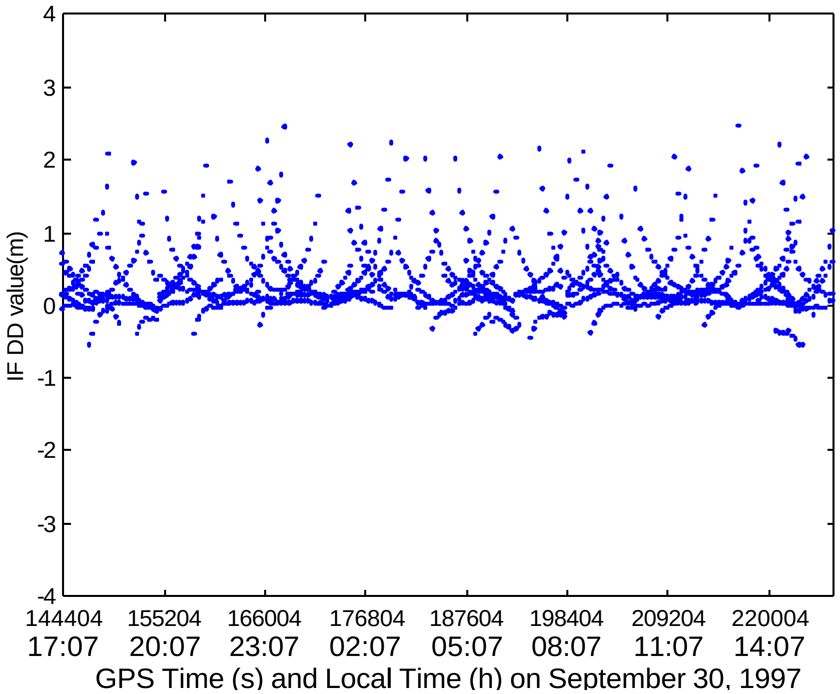

Figure 3.3 (a): IF DD measurements without applying modified Hopfield model for baseline Ales-Geim (243km)

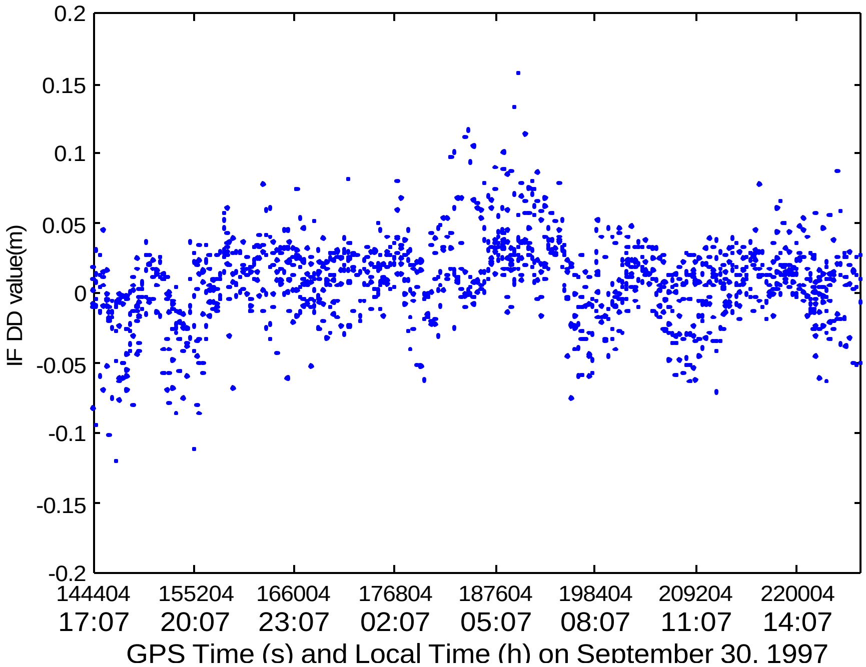

Figure 3.3 (b): IF DD measurements with applying modified Hopfield model for baseline Ales-Geim (243km)

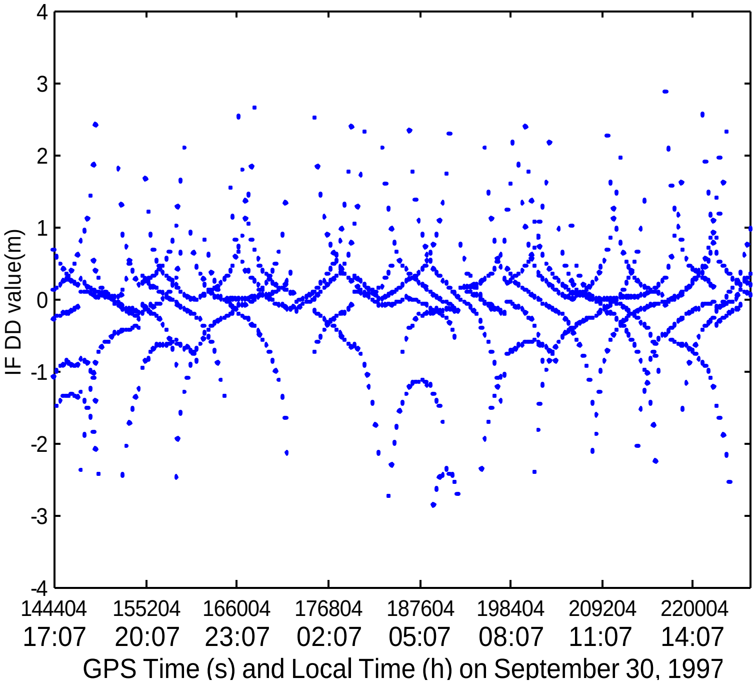

Figure 3.4 (a): IF DD measurements without applying modified Hopfield model for baseline Ales-Kris (498km)

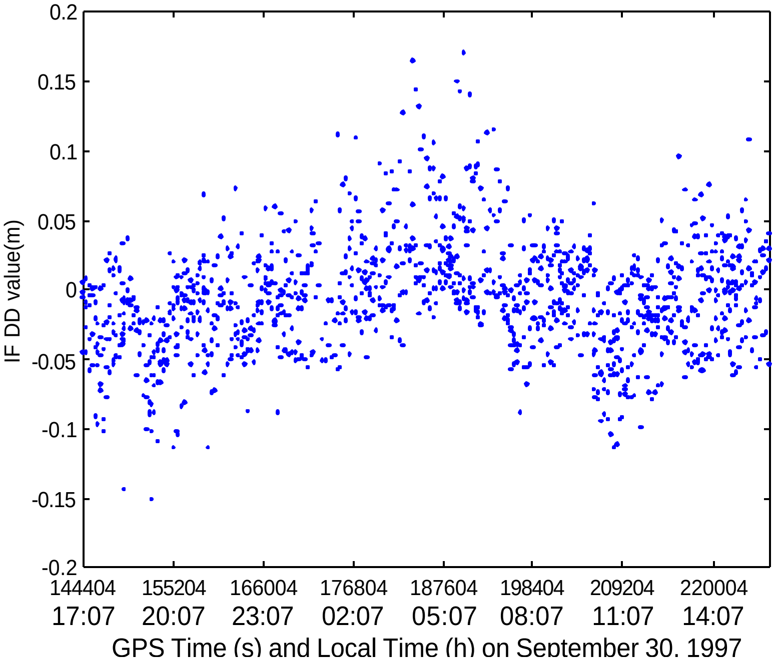

Figure 3.4 (b): IF DD measurements with applying modified Hopfield model for baseline Ales-Kris (498km)

The statistics of the test results for this set of baselines are listed in Table 3.5.

Table 3.5: Statistics of IF DD measurements with and without applying modified Hopfield model over the baselines along the North-South direction

Baseline Name	DD RMS without tropo model (m)	DD RMS with tropo model (m)	Percentage improvement (%)
Ales-Geim (243km)	0.53	0.03	94.3%
Ales-Kris (498km)	0.78	0.04	94.9%

The direction of another set is the West-East direction and they are Tryr-Geir (247km) and Tryr-Berg (407km). The ionospheric free double difference measurements, with and without applying the modified Hopfield model on raw GPS measurements are shown in figure 3.5 and 3.6.

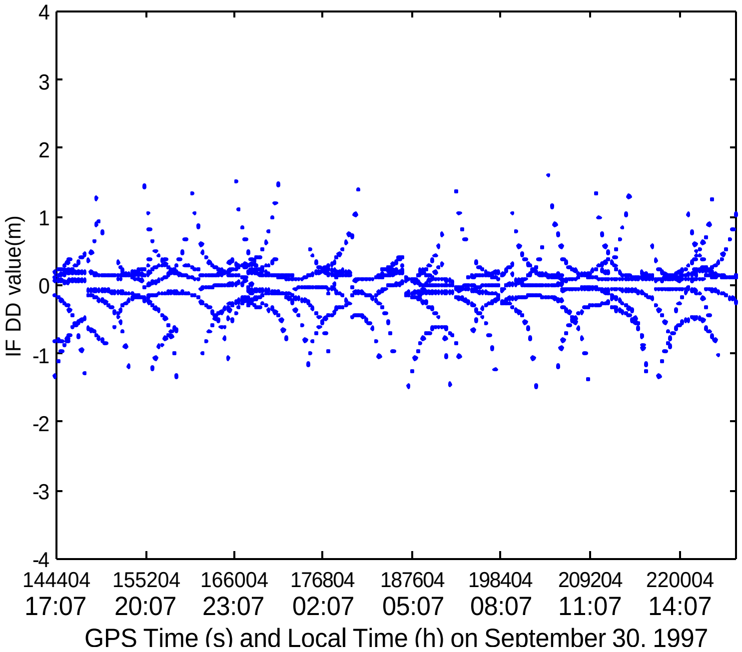

Figure 3.5 (a): IF DD measurements without applying modified Hopfield model for baseline Tryr-Geir (247km)

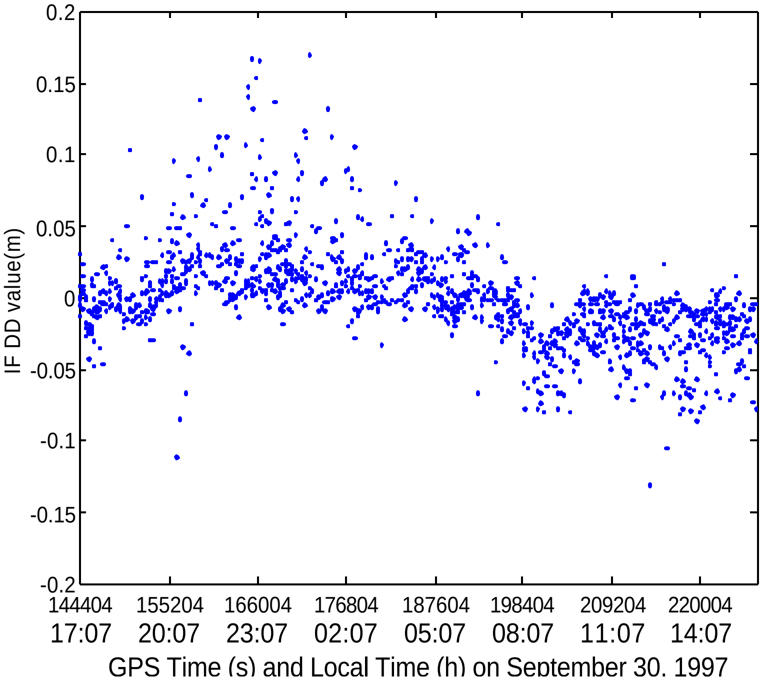

Figure 3.5 (b): IF DD measurements with applying modified Hopfield model for baseline Tryr-Geir (247km)

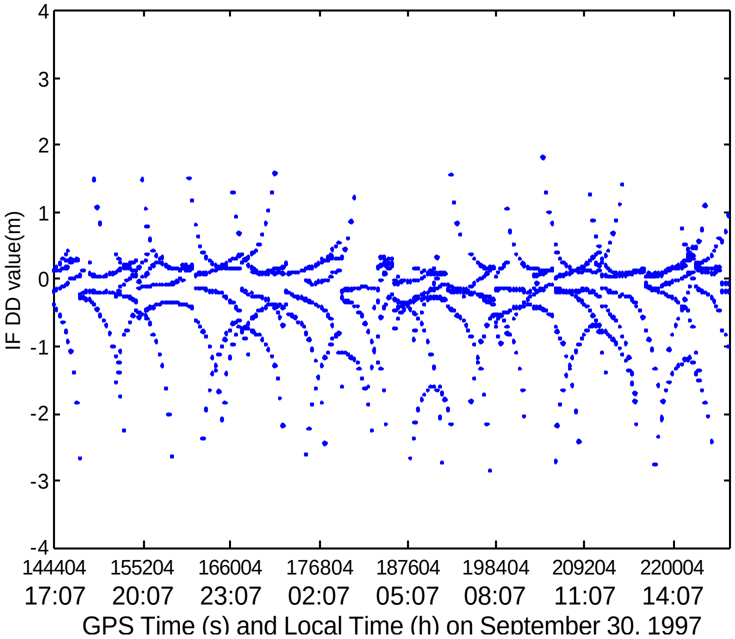

Figure 3.6 (a): IF DD measurements without applying modified Hopfield model for baseline Tryr-Berg (407km)

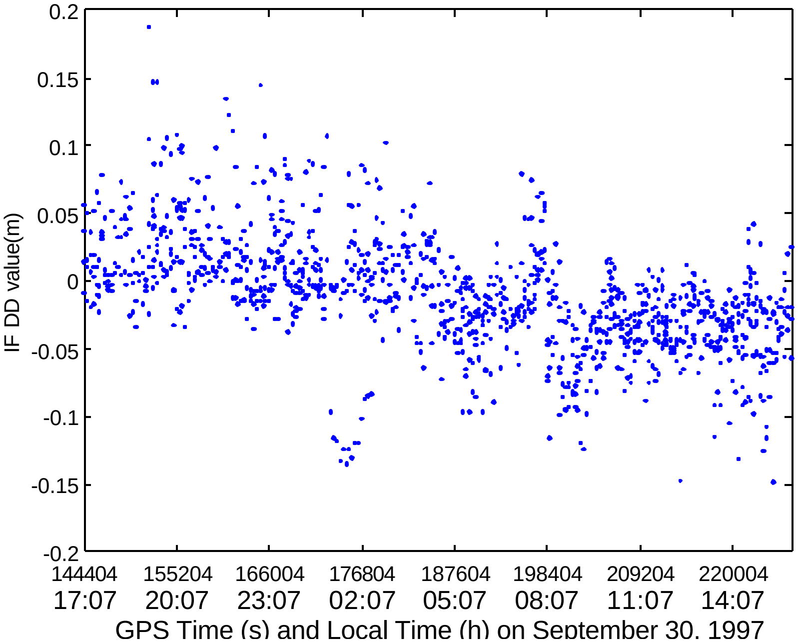

Figure 3.6 (b): IF DD measurements with applying modified Hopfield model for baseline Tryr-Berg (407km)

The statistics of the test results for this set of baselines are listed in Table 3.6.

Table 3.6: Statistics of IF DD measurements with and without applying modified Hopfield model over the baselines along the West-East direction

Baseline Name	DD RMS without tropo model (m)	DD RMS with tropo model (m)	Percentage improvement (%)
Tryr-Geir (247km)	0.41	0.03	92.7%
Tryr-Berg (407km)	0.73	0.05	93.1%

Based on the test results shown in figures 3.3 to 3.6, a significant improvement can be obtained if a standard model of the troposphere correction (such as modified Hopfield model) is applied to the GPS measurements. Tables 3.5 and 3.6 show an improvement of 92% to 95% on ionospheric-free double difference measurements prior to and after applying the modified Hopfield model. For the Tryr-Berg baseline (407km), the rms of ionospheric-free double difference measurements without applying the modified Hopfield model can be as much as 0.73 metres. The rms value decreases significantly after applying the modified Hopfield model to 0.05 metres. From figures 3.3 to 3.6, it is obvious that the maximum value of the ionospheric-free double difference measurements is greatly decreased from 3.0 metres level to 0.2 metres level, an improvement of 93%.

From Tables 3.5 and 3.6, it is obvious that the double difference residual tropospheric delays (based on the ionospheric-free double difference measurements), after applying the modified Hopfield model, are still at the centimetre level with a possible maximum of 20 centimetres. The goal of this thesis is to develop and test a network adjustment method in order to have accurate estimations and predictions of the remaining tropospheric delay.

CHAPTER 4

ESTIMATION OF RESIDUAL TROPOSPHERIC DELAYS USING A GPS NETWORK ADJUSTMENT APPROACH

Residual tropospheric delays can be estimated using GPS observables. In the last ten years several approaches were developed to independently determine the residual tropospheric delay, which is mostly caused by the variable wet component of the troposphere. In this chapter, a review of conventional estimation approaches is presented. Following that, a new method called "Trop_NetAdjust", which is derived from the NetAdjust method proposed by Raquet (1998), is described to estimate the residual tropospheric delay for two cases: 1) residual tropospheric delay prediction for new users and 2) residual tropospheric delay prediction for new satellites.

4.1 Review of conventional estimation approaches

The conventional estimation approaches for residual tropospheric delays can be classified into two categories: least-squares, and Kalman filtering. Usually only one unknown residual tropospheric zenith delay per site and observation session can be estimated in a conventional weighted least-squares algorithm. Such a method tends to average any temporal variation of the residual tropospheric zenith delay. A logical extension of this method is to estimate several residual tropospheric delay parameters per session. Alternatively an individual delay constrained by a stochastic model can be estimated for every observation epoch.

4.1.1 Least-squares method

Least-squares methods have been successfully applied to the estimation of the residual tropospheric delay. Equation 2.5 can be written as

$$\Delta\nabla f_{ab}^{xy} = \Delta\nabla r_{ab}^{xy} + \Delta\nabla dr_{ab}^{xy} - \Delta\nabla d_{Iono_{ab}}^{xy} + (1+a_{ab})\Delta\nabla d_{Trop_{ab}}^{xy} + \Delta\nabla e_{f_{ab}}^{xy} + l\Delta\nabla N_{ab}^{xy} \qquad (4.1)$$

where a_{ab} is the double difference scale factor (Dodson & al 1996). Typically, one factor is solved for per session, whereby a constant offset to the surface standard tropospheric model is determined depending on the double difference scale factor. In equation 4.1, $\Delta\nabla d_{Trop_{ab}}^{xy}$ is the double difference tropospheric delay determined from surface standard model. The difference between the actual tropospheric delay and the modeled delay is presented by the double difference scale factor a_{ab}. Such an algorithm does not allow for the time-varying nature of the atmosphere. An alternative to that is to introduce a polynomial tropospheric zenith delay scale factor given by

$$\begin{aligned}\Delta\nabla f_{ab}^{xy} = \Delta\nabla r_{ab}^{xy} + \Delta\nabla dr_{ab}^{xy} - \Delta\nabla d_{Iono_{ab}}^{xy} + \\ [1 + a_0 + a_1(t_i - t_0) + a_2(t_i - t_0)^2 + ... + a_n(t_i - t_0)^n]\Delta\nabla d_{Trop_{ab}}^{xy} \\ + \Delta\nabla e_{f_{ab}}^{xy} + l\Delta\nabla N_{ab}^{xy}\end{aligned} \quad (4.2)$$

This model is correlated through time via the connection of the start epoch t_0 and the current epoch t_i. The behavior of this model is dictated by the order (n) of the polynomial. For instance, a first-order polynomial will solve for an offset (constant) and a rate. Depending upon the least-squares criteria, the scale factors a_i can be solved based on the measurements from several different pairs of satellites combination at two reference stations a and b. The design matrix for a system of equations, such as equation 4.2, contains residual tropospheric delay scale factors valid for "n" observations. Then it would contain a banded hyper-matrix of unknown delay parameters. The general form of a parametric least-squares adjustment is

$$\hat{x} = -(A^T P A)^{-1} A^T P l \quad (4.3)$$

where

$\hat{x}$ is the least-squares optimized vector of estimated parameter corrections,
A is the first design matrix,
P is the observation weight matrix ($P = C_l^{-1}$, and C_l is the observation covariance matrix),
and l is the observation vector.

4.1.2 Kalman Filtering

An alternative to the previous technique is to model the temporal (and spatial) fluctuation in the atmosphere statistically or by some probabilistic law (Tralli and Lichten 1990). The spatial and temporal characteristics of the residual tropospheric delay, which is mostly due to the water vapor fluctuation in the atmosphere, can be characterized by probabilistic laws or statistical models. The effects of the troposphere on radio wave propagation then can be predicted over varying spatial dimensions and temporal scales according to a given probability density function or stochastically in terms of the spatial and temporal correlations of the fluctuations. In general, we can consider that the residual tropospheric delay is correlated in time by a sum of some stochastic processes, such as first-order Gauss-Markov, random walk, random ramp and bias.

A stochastic process needs to be defined by some model characterizing the nature of the atmosphere. For example in a first-order Gauss-Markov process, the correlation time (t_{GM}) and stochastic process noise (s_{GM}) need to be determined. Here the stochastic model is assumed to be a first-order Gauss-Markov process. In the following, based on the analysis of the autocorrelation and power spectral density for residual tropospheric delays, the stochastic model and its parameters are identified.

4.1.2.1 Analysis of the autocorrelation and power spectral density of the residual tropospheric delay

In order to model the residual tropospheric delay, its autocorrelation function and power spectral density are analyzed. From the analysis, it is found that the residual tropospheric delay can be modeled as a first-order Gauss-Markov process.

In general, a first-order Gauss-Markov process can be expressed by the differential form:

$$d\Delta\nabla d_{Troo} / dt = -\Delta\nabla d_{Trop}(t) / t_{GM} + w(t) \tag{4.4}$$

where t_{GM} is the correlation time and w(t) is a zero-mean white noise of variance s_w^2 given by the ensemble average of its square,

$$E[w(t)w(\tau)^T] = \sigma_w^2 \delta(t-\tau) \qquad (4.5)$$

where E[ ] denotes the expectation operator and $\delta(t-\tau)$ is the Dirac delta function.

The discrete solution of equation 4.4 can be written as:

$$\Delta\nabla d_{Trop}(t+\Delta t) = m\Delta\nabla d_{Trop}(t) + (1-m)^{1/2} w_{GM}(t) \qquad (4.6)$$

where the parameter m is given by

$$m = \exp(-\Delta t / \tau_{GM}) \qquad (4.7)$$

which is a measurement of the exponential correlation between adjacent measurements of sampling interval Δt. In figure 4.1, a typical system representation of the first-order Gauss-Markov process is shown.

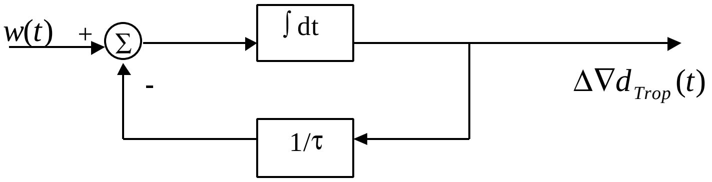

Figure 4.1: First-order Gauss-Markov process

The autocorrelation function of a first-order Gauss-Markov process is given by:

$$R(\tau) = \sigma_{GM}^2 e^{-|\tau|/\tau_{GM}} \qquad (4.8)$$

where

$$E[w(t)w(t+\tau)] = [2\sigma_{GM}^2 / \tau_{GM}]\delta(\tau) \qquad (4.9)$$

and σ_{GM}^2 is the steady-state variance of the first-order Gauss-Markov process and it is satisfied with the differential equation:

$$\frac{d}{dt}\sigma_{GM}^2(t) = -(2/\tau_{GM})\sigma_{GM}^2(t) + \sigma_w^2 \qquad (4.10)$$

and the relationship between the correlation time τ_{GM} and the steady-state variance σ_{GM}^2 is

$$\sigma_{GM}^2 = \tau_{GM}\sigma_w^2 / 2 \qquad (4.11)$$

By taking the Fourier transform of the autocorrelation function, the power spectral density can be obtained:

$$\Psi(w) = \frac{2s_{GM}^{\;2} / t_{GM}}{w^2 + (1/t_{GM})^2} \tag{4.12}$$

In figures 4.2 and 4.3, the typical autocorrelation function plot and power spectral density of a first-order Gauss-Markov are shown, respectively.

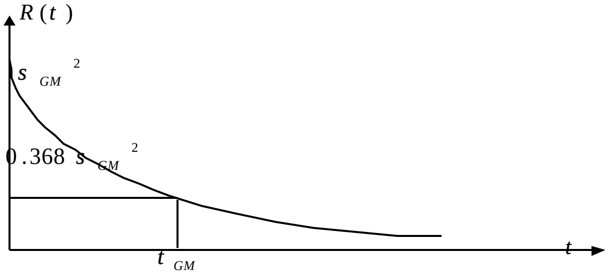

Figure 4.2: The autocorrelation of first-order Gauss-Markov process

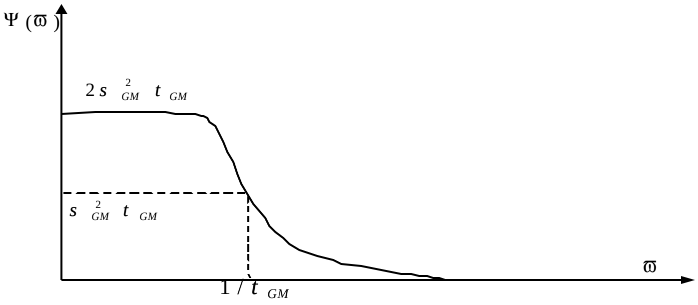

Figure 4.3: The power spectral density of first-order Gauss-Markov process

In order to stochastically analyse the residual tropospheric delays, the test data from the network described in Appendix A are used for the following analysis. The analysis is based on the calculation of autocorrelation function of ionospheric-free double difference measurements for the selected receiver-satellite pairs. All the double difference pairs are based on the Berg-Tryr baseline (407km) and two sets of satellite pairs (PRN 16-14, and PRN 16-18) are chosen for the tests.

The following figures (figure 4.4 and 4.5) show the ionospheric-free double difference measurements (residual tropospheric delays) and their normalized autocorrelation functions for the selected satellite pairs. The data period of the ionospheric-free double difference measurements is 1000 seconds (about 17 minutes) and the data sampling rate is 10 seconds. Comparing these plots with the typical plot of the autocorrelation of first-order Gauss-Markov processes (figure 4.2), it is reasonable to consider that the double difference residual tropospheric delays are first-order Gauss-Markov processes because their autocorrelation functions show a clear exponential attenuation trend similar to figure 4.2.

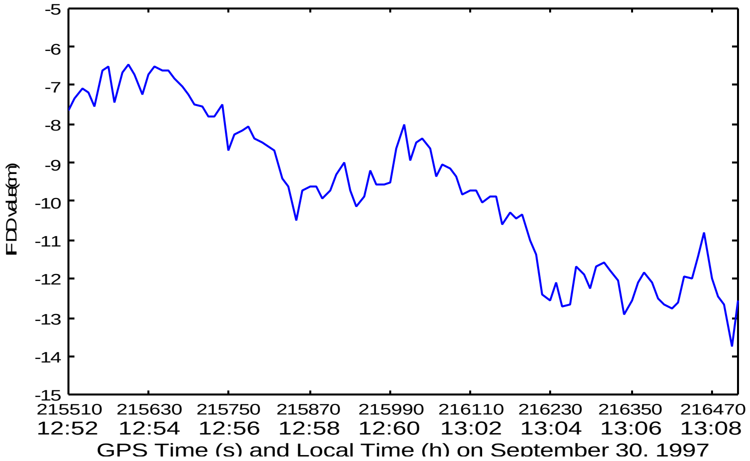

Figure 4.4(a): IF DD measurements for satellite pair 16-14

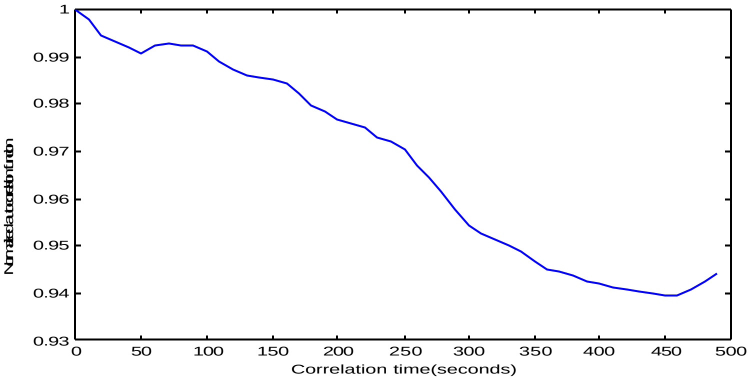

Figure 4.4(b): The normalized autocorrelation of IF DD measurements for satellite pair 16-14

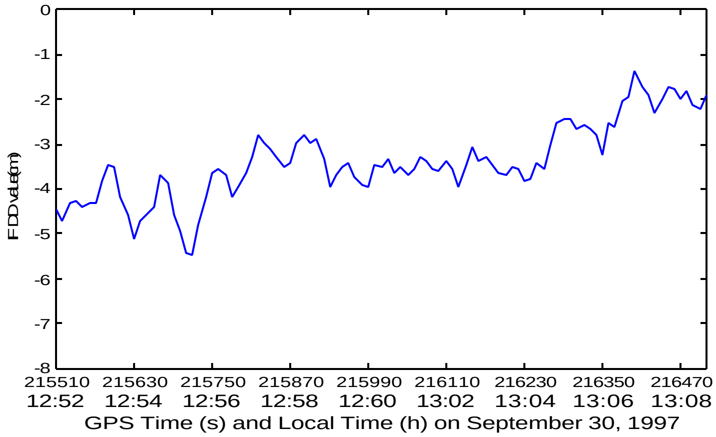

Figure 4.5(a): IF DD measurements for satellite pair 16-18

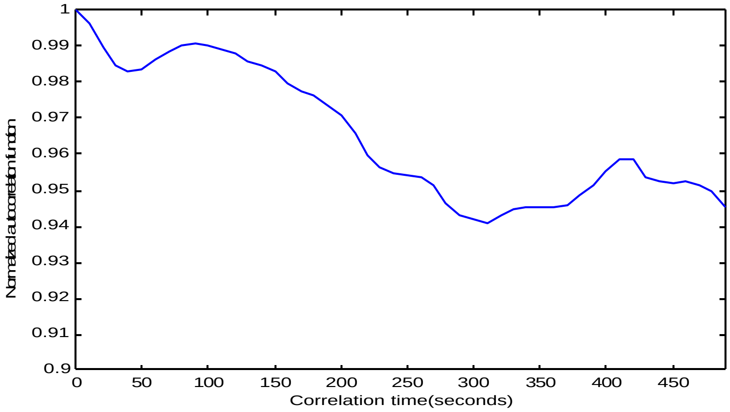

Figure 4.5(b): The normalized autocorrelation of IF DD measurements for satellite pair 16-18

Residual tropospheric zenith delays are modeled as Gauss-Markov processes and parameterized by the steady-state standard deviation s_{GM} and correlation time t_{GM}. The correlation time t_{GM} can be obtained from the value of m and sampling interval Δt, using equation 4.7:

$$t_{GM} = -\Delta t / \ln(m) \tag{4.13}$$

Given m, the expression

$$s_{GM}^{2} = \frac{[\Delta\nabla d_{Trop}(t+\Delta t) - m\Delta\nabla d_{Trop}(t)]^{2}}{(1-m^{2})} \tag{4.14}$$

yields the steady-state variance for the first-order Gauss-Markov process. In the limit of infinite or large correlation time relative to data sampling interval Δt, modeling the residual tropospheric delay as a Gauss-Markov process becomes equivalent to modeling it as a random walk process. Since the first-order Gauss-Markov process has zero mean, a constant term is estimated and added as an additional parameter. In fact, this is equivalent to adding a random ramp process into the statistical model.

4.1.2.2 Kalman Filtering Parameter Estimation

A Kalman filter is an optimal LMV (Linear Minimum of Variance of error) estimator that processes measurements to deduce a minimum error estimate of the state of a system by utilizing the knowledge of the system and measurement dynamics, assumed statistics of system noises and measurement errors, and initial condition information (Gelb 1974). For instance, given a linear system model and any measurements of its behavior, plus statistical models which characterize system and measurement errors, plus initial condition information, the Kalman filtering describes how to process the measurement data.

Let us consider any linear system that can be described using the following space-state model:

$$x_k = \Phi_{k,k-1} x_{k-1} + G_{k,k-1} w_{k-1} \tag{4.15}$$

where

x_k is the state vector ($n \times 1$),

$\Phi_{k,k-1}$ is the transition matrix ($n \times n$),

$G_{k,k-1}$ is the input matrix ($n \times r$), and

w_{k-1} is the input white noise ($r \times 1$) with zero mean and known covariance matrix $E[w_{k-1} w_{k-1}{}^T] = Q$, which describes the uncertainty of the system model.

Part of the state vector components or their linear combinations are directly observable according to the measurement equation:

$$z_k = Hx_k + v_k \tag{4.16}$$

where

z_k is the measurement vector ($m \times 1$),

v_k is the measurement white noise ($m \times 1$) with zero mean and known covariance matrix $E[v_k {v_k}^T] = R$.

Optimal Kalman filtering minimizes the trace of the corresponding covariance matrix of error estimates using the state model equation 4.15 and the measurement model equation 4.16. The Kalman filtering is carried out sequentially: prediction and update. The prediction equations are:

$$\hat{x}_{k/k-1} = \Phi_{k,k-1} \hat{x}_{k-1} \tag{4.17}$$

$$P_{k/k-1} = \Phi_{k,k-1} P_{k-1} \Phi^T_{k,k-1} + G_{k,k-1} Q G^T_{k,k-1} \tag{4.18}$$

where

$\hat{x}_k$ is the optimal estimate of the state vector,

$\hat{x}_{k/k-1}$ is the prior estimate of the state vector;

P_k is covariance matrix of the error estimates and

$P_{k/k-1}$ is the priory covariance matrix of the error estimates.

The update equations are:

$$K_k = P_{k,k-1} H^T [HP_{k,k-1} H^T + R]^{-1} \tag{4.19}$$

$$\hat{x}_k = \hat{x}_{k/k-1} + K_k (z_k - H \hat{x}_{k/k-1}) \tag{4.20}$$

$$P_k = (I - K_k H)P_{k/k-1} \tag{4.21}$$

where K_k is the optimal gain matrix.

The calculation scheme of Kalman filtering is shown in figure 4.6 (Gelb, 1974).

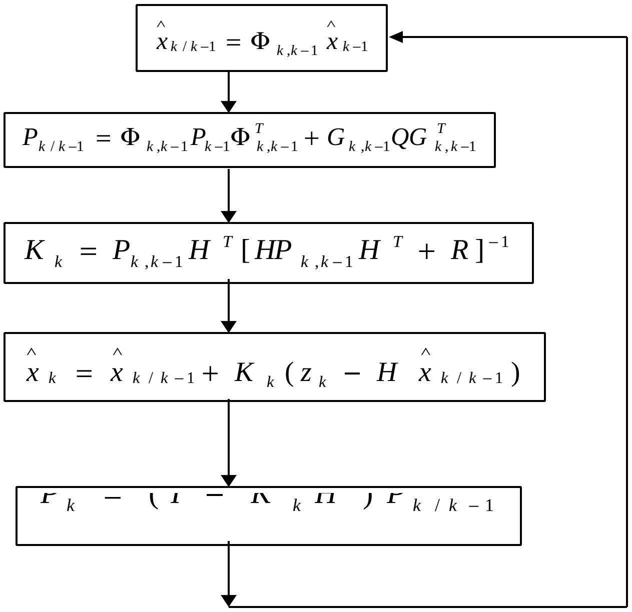

Figure 4.6: Calculation scheme of Kalman filtering

Implementation of this process requires two input "parameters": the transition matrix of the system model and the noise variance matrix of the system model. The transition matrix elements corresponding to the residual tropospheric delay parameters are m (equation 4.6) for the first-order Gauss-Markov process. The system noise covariance elements are given by equation 4.14.

Although Kalman filtering is an optimal solution to the filtering problem, the algorithm is prone to serious numerical difficulties. For instance, although it is theoretically impossible for the covariance matrix to have a negative eigenvalue, such a situation can, and often does result due to numerical computation using finite wordlengths. It may happen especially when 1) the measurements are very accurate and/or 2) a linear combination of state vector components is known with great precision while other combinations are nearly unobservable (i.e., there is a large range of magnitude of state covariance eigenvalues). Such a condition can lead to subsequent divergence or total failure of the recursion. Therefore, numerical instability can be a problem for a conventional Kalman filtering.

To circumvent this inherent numeric problem in a Kalman filter, alternate recursion relationships have been developed to propagate and update a state estimate and its error covariance matrix. Methods such as SRIF (square root information filter) and U-D factorization are proposed by Bierman (1977) to provide greater numerical stability. Lichten (1990) describes the use of the SRIF and U-D factorization to the application of satellite orbit and geodetic parameter estimation using GPS. Here, for the residual tropospheric delay estimation, U-D factorization algorithm is recommended. A flowchart of estimating the tropospheric delay using Kalman filtering is presented in figure 4.7.

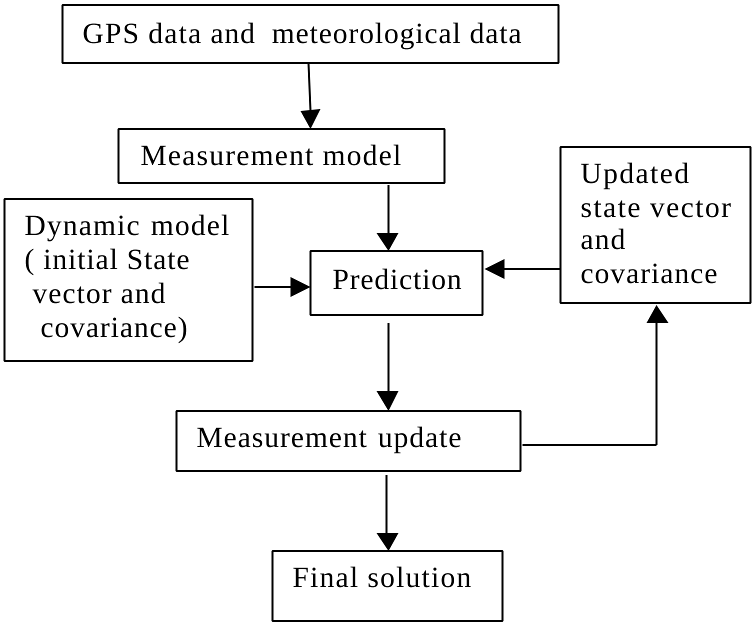

Figure 4.7: Flowchart of the tropospheric delay estimation using Kalman filtering

4.2 Mathematical review of NetAdjust method

For differential GPS, two or more reference receivers collect simultaneous measurements from common satellites at each epoch. In the case of a GPS network, there are three or more reference receivers and, usually at least one mobile receiver (Emardson 1998, Raquet 1998). All phase measurement-minus-range observables from the reference receivers are used to form an observation vector l_n

$$l_n = [\bar{f}_1^1, \dots \bar{f}_1^{n_{sv}}, \bar{f}_2^1, \dots \bar{f}_2^{n_{sv}}, \dots\dots \bar{f}_{n_{rec}}^1, \dots \bar{f}_{n_{rec}}^{n_{sv}}]^T \tag{4.22}$$

where $\bar{f}_a^x$ is the phase measurement-minus-range observable from receiver a to satellite x, n_{rec} is the number of reference receivers in the network, and n_{sv} is the number of observed satellites. Next, all the linearly independent double difference combinations of l_n can be used to form the vector $\Delta\nabla l_n$ as

$$\Delta\nabla l_n = [\Delta\nabla \bar{f}_{12}^{12}, \dots \Delta\nabla \bar{f}_{12}^{1n_{sv}}, \dots\dots \Delta\nabla \bar{f}_{1n_{rec}}^{12}, \dots \Delta\nabla \bar{f}_{1n_{rec}}^{1n_{sv}}]^T \tag{4.23}$$

where $\Delta\nabla \bar{f}_{ab}^{xy}$ is the double difference measurement-minus-range observables between receivers a and b and satellites x and y. The double difference matrix B_n for the network is defined as

$$B_n = \frac{\partial \Delta \nabla l_n}{\partial l_n} \tag{4.24}$$

Since the double difference observation vector elements of $\Delta\nabla l_n$ are direct linear combinations of the observation vector l_n, the B_n matrix is made up of the values +1, -1, and 0. Therefore, the double difference observation vector $\Delta\nabla l_n$ can be expressed by multiplying the observation vector l_n by the B_n matrix:

$$\Delta\nabla l_n = B_n l_n \tag{4.25}$$

4.2.1 Least Squares Prediction

Least squares estimation is a standard method to obtain a unique set of values for a set of unknown parameters from a redundant set of observables through a known mathematical model. The standard cases of least squares estimation have been discussed by numerous authors, e.g. Schmid and Schmid (1965), Wolf (1968), and Wells and Krakiwsky (1971).

Moritz (1972) made a modification of the original least squares estimation to least squares collocation (prediction). Assuming a predictable process, the problem is to estimate a quantity at certain points using measured quantities at other points. Let l be the measurement vector including n measured quantities:

$$l = [l_1, l_2, ...l_n]^T \tag{4.26}$$

and s is the vector of m unknown signals to be predicted:

$$s = [s_1, s_2, ...s_m]^T \tag{4.27}$$

where the superscript T represents transposition.

Next, let us assume each measured quantity l_i and signal s_i has zero expectation, i.e.,

$$\begin{aligned} E[l] &= 0 \\ E[s] &= 0 \end{aligned} \tag{4.28}$$

where E denotes the mathematical expectation. In practice, these characteristics normally exist.

The degree of correlation between the measurement vector l and the signal vector s is given by a cross-covariance matrix C_{sl}. The statistical characteristics of the measurement vector l and the signal vector s are given by their covariance matricies C_{ll} and C_{ss}, respectively. Assuming l and s are zero expectation vectors, the covariance matrix and cross-covariance matrix are given by

$$C_{ll} = E[ll^T] \tag{4.29}$$

$$C_{sl} = E[sl^T] \tag{4.30}$$

and

$$C_{ss} = E[ss^T] \tag{4.31}$$

where the dimensions of C_{ll}, C_{sl}, C_{ss} are $n \times n$, $m \times n$ and $m \times m$ respectively.

In order to find the best estimate for the signal vector s based on measurement vector l, a linear minimum variance unbiased estimate $\hat{s}$ can be expressed as

$$\hat{s} = Hl \tag{4.32}$$

where H is a matrix with dimension $m \times n$. Because of the zero-expectation of l and linear property of the H matrix, $\hat{s}$ is an unbiased estimate of s, i.e., $E[\hat{s}] = E[s]$. The problem is to find the best H that satisfies the least-squares criterions, namely that the error variance of the predicted signals is minimized. The estimation error vector is defined as

$$e = \hat{s} - s \tag{4.33}$$

and the error covariance matrix C_{ee} is written as

$$C_{ee} = E[ee^T] = E[(\hat{s} - s)(\hat{s} - s)^T] \tag{4.34}$$

Applying equation 4.32 into equation 4.34, the error covariance function can be rewritten as

$$C_{ee} = HE[ll^T]H^T - E[sl^T]H^T - HE[ls^T] + E[ss^T] \tag{4.35}$$

Noting that $C_{ls} = E[ls^T] = C_{sl}^T$, equation 4.35 can be written in the following form using equations 4.29, 4.30, and 4.31,

$$C_{ee} = HC_{ll}H^T - C_{sl}H^T - HC_{sl}^T + C_{ss} \tag{4.36}$$

Adding and subtracting the same term $C_{sl}C_{ll}^{-1}C_{ls}$ into the right hand of equation 4.36, one obtains

$$C_{ee} = C_{ss} - C_{sl}C_{ll}^{-1}C_{ls} + HC_{ll}H^T - C_{sl}H^T - HC_{sl}^T + C_{sl}C_{ll}^{-1}C_{ls} \tag{4.37}$$

Performing the operations in equation 4.37 using the relation

$$C_{ll}C_{ll}^{-1} = C_{ll}^{-1}C_{ll} = I \tag{4.38}$$

where I is the unit matrix, the following formula is obtained

$$C_{ee} = C_{ss} - C_{sl}C_{ll}^{-1}C_{ls} + (H - C_{sl}C_{ll}^{-1})C_{ll}(H - C_{sl}C_{ll}^{-1})^T \tag{4.39}$$

According to the above equation 4.39, the error covariance matrix is consisted of two matrices U and V:

$$U = C_{ss} - C_{sl} C_{ll}^{-1} C_{ls}$$
$$V = (H - C_{sl} C_{ll}^{-1}) C_{ll} (H - C_{sl} C_{ll}^{-1})^T \tag{4.40}$$

Since U is independent from H, C_{ee} is minimized when V is equal to zero. Hence,

$$H = C_{sl} C_{ll}^{-1} \tag{4.41}$$

Inserting equation 4.41 into equation 4.32, the desired solution for the unknown signal s is:

$$\hat{s} = C_{sl} C_{ll}^{-1} l \tag{4.42}$$

The estimated error covariance matrix is equal to U,

$$C_{ee} = C_{ss} - C_{sl} C_{ll}^{-1} C_{ls} \tag{4.43}$$

Equations 4.42 and 4.43 give the best solution of least squares prediction based on the principle of least squares. Depending on these two equations, it is possible to predict the signals at a point where measurements are not available.

4.2.2 Residual Tropospheric Delay Estimation using Least Squares Prediction

The goal of this research is to develop a method based on least squares prediction, using a GPS network of reference receivers that predicts the residual tropospheric delay of GPS observations at existing or new points and for existing or new satellites. In figure 4.8, this problem is illustrated. The reference receivers are represented by circles, and a mobile receiver is represented by a triangle.

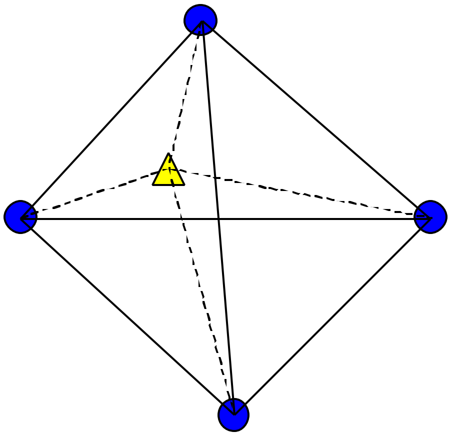

Figure 4.8 GPS Network of four reference receivers and one mobile receiver

Based on the theory of least squares prediction presented in the previous section, a network adjustment method called "NetAdjust" algorithm, was developed by Raquet (1998). This method is modified herein to estimate the residual tropospheric delay and the modified method is referred to as "Trop_NetAdjust".

4.2.2.1 Definition of measurement equation for residual tropospheric delays

Let us rewrite equation 3.38 and the ionospheric-free double difference measurement-minus-range observable $\Delta\nabla \bar{f}_{IF}$:

$$\Delta\nabla \bar{f}_{IF} = \frac{1}{l_{IF}}(\Delta\nabla d_{Trop}) + \frac{1}{l_1}(\Delta\nabla m_{L1} + \Delta\nabla v_{L1}) - \frac{f_2}{f_1 l_2}(\Delta\nabla m_{L2} + \Delta\nabla v_{L2}) + \Delta\nabla N_{IF} \tag{4.44}$$

where d_{Trop} is the residual tropospheric delay after applying a standard tropospheric model and is of interest to us. Assuming that the residual tropospheric error has some spatial correlation, i.e, it is a function of receiver position p_{rec}, it can be referred to as the correlated term. The uncorrelated error term includes all the errors which are not eliminated in the double difference and usually consists of multipath (m) and measurement noise (v).

A point p_0 is defined as a fixed position from where all the differential errors will be referred and is called the "zero-point". Usually it is chosen to be somewhere near the center of the network, in order to minimize the distances to the reference receivers. In fact, the results are not very sensitive to the location of p_0. Define the relative residual tropospheric delay, which is assumed as the correlated term in equation 4.44,

$$dd_{Trop}(p_{rec}, p_0) = d_{Trop}(p_{rec}) - d_{Trop}(p_0) \tag{4.45}$$

Therefore, equation 4.44 can be written in metres as

$$\Delta\nabla \bar{f}_{IF} - l_{IF}\Delta\nabla N_{IF} = \Delta\nabla dl_c + \Delta\nabla dl_u \tag{4.46}$$

where the correlation term is

$$dl_c = dd_{Trop}(p_{rec}, p_0) \tag{4.47}$$

and the uncorrelated term is

$$\Delta\nabla dl_u = \frac{l_{IF}}{l_1}(\Delta\nabla m_{L1} + \Delta\nabla v_{L1}) - \frac{f_2 l_{IF}}{f_1 l_2}(\Delta\nabla m_{L2} + \Delta\nabla v_{L2}) \tag{4.48}$$

Inserting equation 4.25 into equation 4.46,

$$B\bar{f}_{IF} - l_{IF}\Delta\nabla N_{IF} = \Delta\nabla(dl_c + dl_u) = \Delta\nabla dl = Bdl \tag{4.49}$$

where the elements in the left hand side are the known quantities. The problem is how to calculate the dl_{cp} at the computation point, which is the location of the mobile receiver. Here cp means the computation point. Because the vector dl is the misclosure vector from the phase observation, it is expected to have zero-mean. Raquet (1998) has shown some results from real field data to confirm this property. Applying the least squares prediction equation 4.42 into equation 4.49, the prediction solution for the computation point can be written as

$$d\hat{l}_{cp} = C_{dl_{cp},\Delta\nabla dl}\, C^{-1}_{\Delta\nabla dl}\, \Delta\nabla dl \tag{4.50}$$

where the double difference measurement covariance matrix $C_{\Delta\nabla dl}$ is

$$C_{\Delta\nabla dl} = E[(\Delta\nabla dl)(\Delta\nabla dl)^T] = E[(Bdl)(Bdl)^T] = BC_{dl}B^T \tag{4.51}$$

and the cross-covariance matrix is

$$C_{dl_{cp},\Delta\nabla dl} = E[(dl_{cp})(\Delta\nabla dl)^T] = E[(dl_{cp})(Bdl)^T] = C_{dl_{cp},dl}B^T \tag{4.52}$$

Substituting equations 4.51 and 4.52 into 4.50, the final form of the least squares prediction solution for the computation point (cp) is written as

$$d\hat{l}_{cp} = C_{dl_{cp},dl} B^T (BC_{dl} B^T)^{-1} (Bl - l_{IF} \Delta\nabla N_{IF}) \tag{4.53}$$

and for the corrected measurement from one of the reference receivers,

$$d\hat{l} = C_{dl} B^T (BC_{dl} B^T)^{-1} (Bl - l_{IF} \Delta\nabla N_{IF}) \tag{4.54}$$

where $\hat{dl}$ and $\hat{dl}_{cp}$ are the estimates of the GPS errors at the reference receiver locations and at the computation point(s). N_{IF} is the ionospheric-free ambiguity which does not preserve the integer ambiguity property. Generally N_{IF} can be presented by the linear combination of L1 ambiguity N_1 and L2 ambiguity N_2 ($N_{IF} = N_1 - \frac{f_2}{f_1} N_2$). Provided that the double difference ambiguities $\Delta\nabla N_1$ and $\Delta\nabla N_2$ are already resolved, therefore the value of $\Delta\nabla N_{IF}$ can be derived from them ($\Delta\nabla N_{IF} = \Delta\nabla N_1 - \frac{f_2}{f_1} \Delta\nabla N_2$) (Sun & al 1999). The measurement-minus-range vector l comes directly from the GPS measurements made by the network receivers. In addition, C_{dl} is the covariance matrix between the network measurement errors and $C_{dl_{cp},dl}$ is the cross-covariance matrix between the network and mobile measurement errors. As in any other prediction process, the effectiveness of the network adjustment method is dependent on the accuracy of the covariance matrices C_{dl} and $C_{dl_{cp},dl}$ (Raquet & al 1998). The covariance matrices are formed using the residual tropospheric delay covariance function which is discussed in the next section.

4.3 Calculation of residual tropospheric delay covariance function parameters

In the "Trop_NetAdjust" method, it is important to develop the covariance function with enough accuracy so that good prediction results can be obtained. In this section, the detailed steps for calculation of this covariance function are presented.

4.3.1 Determination of mapping function for residual tropospheric delay from field data test

For the standard tropospheric model, the simplest cosine-law mapping function can be used. This mapping function is developed for the total tropospheric path delay. However, for the residual tropospheric delay, it is not clear whether this simple cosine-law mapping function can be used. In this section, the mapping function for the residual tropospheric delay is calculated from GPS network data described in Appendix A.

For the data set, the ionospheric-free double difference measurement errors $\Delta\nabla \bar{f}_{abIF}^{xy}$ are valid measurements of the residual tropospheric delays, if the multipath and measurement noise are small enough to be ignored. So the ionospheric-free double difference measurement errors $\Delta\nabla \bar{f}_{abIF}^{xy}$ are used for estimating the mapping function.

In the Norway network, there are 11 reference receivers and 55 baselines. In order to make sure that the tropospheric delay effects dominate the ionospheric-free double difference residuals of equation 3.38, the short baselines (< 100km) are not used for our calculations and only 50 baselines (not including the five short baselines Tryr-Trym, Geir-Geim, Arer-Arem, Arer-Kris, and Arem-Kris) will be used. For a fixed set of elevations, the estimates of the mapping function will be calculated for each baseline. Then a function is generated to fit the averaged mapping function estimates (Raquet 1998). The main steps for these calculations are:

1. All independent combinations of ionospheric-free double difference measurement errors $\Delta\nabla \bar{f}_{abIF}^{xy}$ are calculated for the 50 baselines. The measurement interval is assigned to be one minute, and the time period is 24 hours.
2. Reject any double difference combination which does not have a satellite above 45^{o} (making sure the higher satellite's elevation is high enough).
3. Group the double differences $\Delta\nabla \bar{f}_{abIF}^{xy}$ into bins according to the lower satellite elevation angle: each bin size is 3^{o}.

4. The variance of ionospheric-free double differences $\Delta\nabla \bar{f}_{abIF}^{xy}$ is calculated for each bin.
5. The average of variances for the 50 baselines is calculated with respect to the lower satellite elevation angles.
6. Based on the relationship between the double difference residual tropospheric delay variance $E[(\Delta\nabla d_{Trop_{ab}}^{xy})^2]$ and the double difference residual tropospheric delay variance in the zenith direction $E[(\Delta\nabla d_{Trop_{abZ}}^{xy})^2]$, the mapping function for lower elevation satellite is

$$MF(e^{LOW}) = \sqrt{\frac{2E[(\Delta\nabla d_{Trop_{ab}}^{xy})^2]}{E[(\Delta\nabla d_{Trop_{abZ}}^{xy})^2]} - MF(e^{HIGH})^2} \tag{4.55}$$

In our calculations, the double difference residual tropospheric delays $\Delta\nabla d_{Trop_{ab}}^{xy}$ are derived from the ionospheric-free double difference measurement errors $\Delta\nabla \bar{f}_{abIF}^{xy}$, assuming the tropospheric term dominates it. On the other hand, because of the high elevation angle for higher satellites, and the fact the mapping function changes very little for high elevation angles, $MF(e^{HIGH})$ can be calculated using the average value of high satellite elevation angles over 24 hours. In our current data, the high averaging elevation angle is about 62^{o}.

Based on the above six steps, the mapping function was calculated using actual ionospheric-free double difference measurement error data. Firstly, in figure 4.9, the average RMS value and $\pm 1 - s$ window for ionospheric-free double difference measurement errors of the different baseline combinations are calculated and shown with respect to the elevation angles of lower satellites. Depending on them, the mapping function can be derived from equation 4.55. The resulting mapping function is shown in figure 4.10.

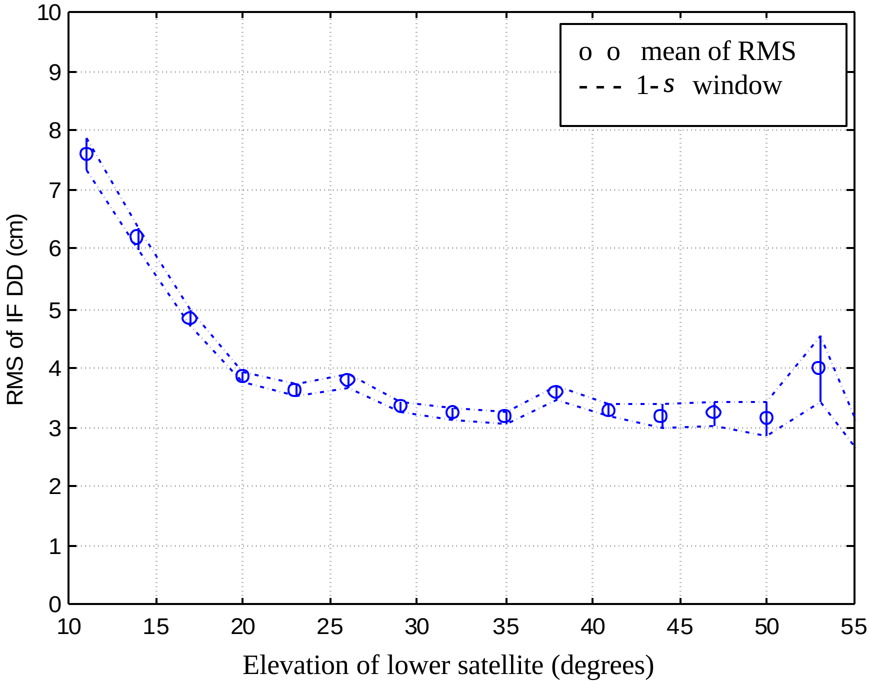

Figure 4.9: Average RMS values of ionospheric-free double difference measurement errors for the different baselines in the Norway network

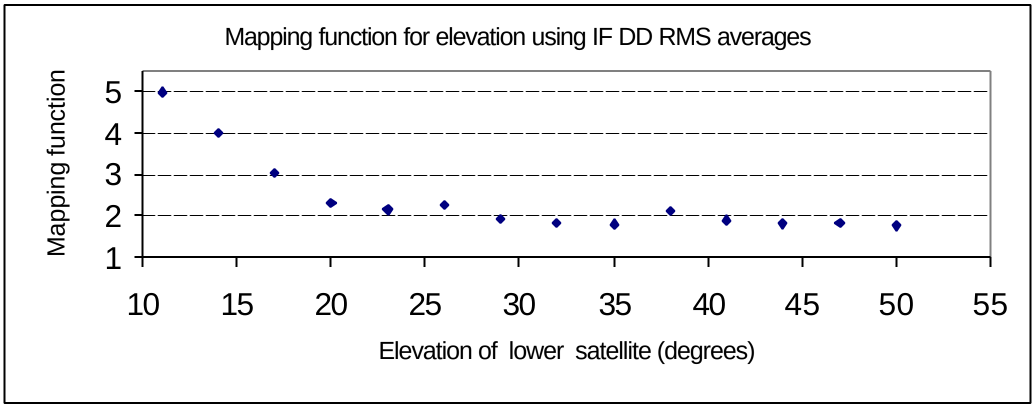

Figure 4.10: Mapping Function using IF DD measurement error RMS averages

Finally, the data shown in figure 4.10 was used in a least squares fit to determine the coefficients of the elevation mapping function. The mapping function can be given in the following form:

$$MF(e) = \frac{a}{\sin(e)} \qquad (4.56)$$

where a is the coefficient which is determined by least squares fitting. As shown in figure 4.11, if we consider this type of mapping function, the coefficient a is calculated as 0.97, which is very near 1. In order to simplify our calculation, we assume that a=1 and then the mapping function is given by

$$MF(e) = \frac{1}{\sin(e)} \qquad (4.57)$$

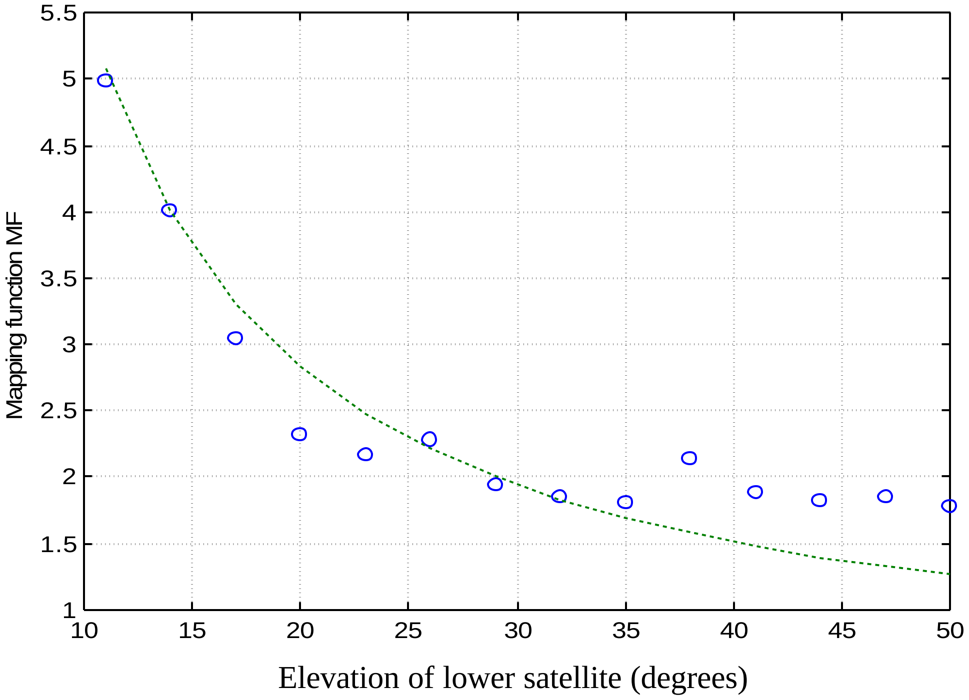

Figure 4.11: Mapping function points and functional fit of mapping function for ionospheric-free carrier phase combinations

Based on the above results, it is obvious that for the residual tropospheric delays the simplest cosine-law mapping function illustrated by equation 4.57 can be used to map the zenith residual tropospheric delay to an arbitrary elevation. In the following analysis, this form of mapping function is used for all calculations.

4.3.2 Relative residual tropospheric zenith delay

4.3.2.1 Definition of relative residual tropospheric zenith delay

If we use T to represent the tropospheric delay, the double difference residual tropospheric delay $\Delta\nabla T_{ab}^{xy}$ is given by

$$\Delta\nabla T_{ab}^{xy} = [T_{aZ} MF(e_a^x) - T_{bZ} MF(e_b^x)] - [T_{aZ} MF(e_a^y) - T_{bZ} MF(e_b^y)] \tag{4.58}$$

where, T_{aZ} and T_{bZ} are the residual tropospheric zenith delays at receivers a and b. $MF(e)$ is a mapping function with respect to the elevation angle e, which is used to map the zenith delay to an arbitrary elevation. Clearly, as reference receivers a and b get closer to each other, there is a little difference between the satellite observed elevation angles from the two different receivers and this can be easily found from the following examples of the selected baseline Berg-Ales (248 km) for satellite PRN 16,14 and 18, shown in figure 4.12.

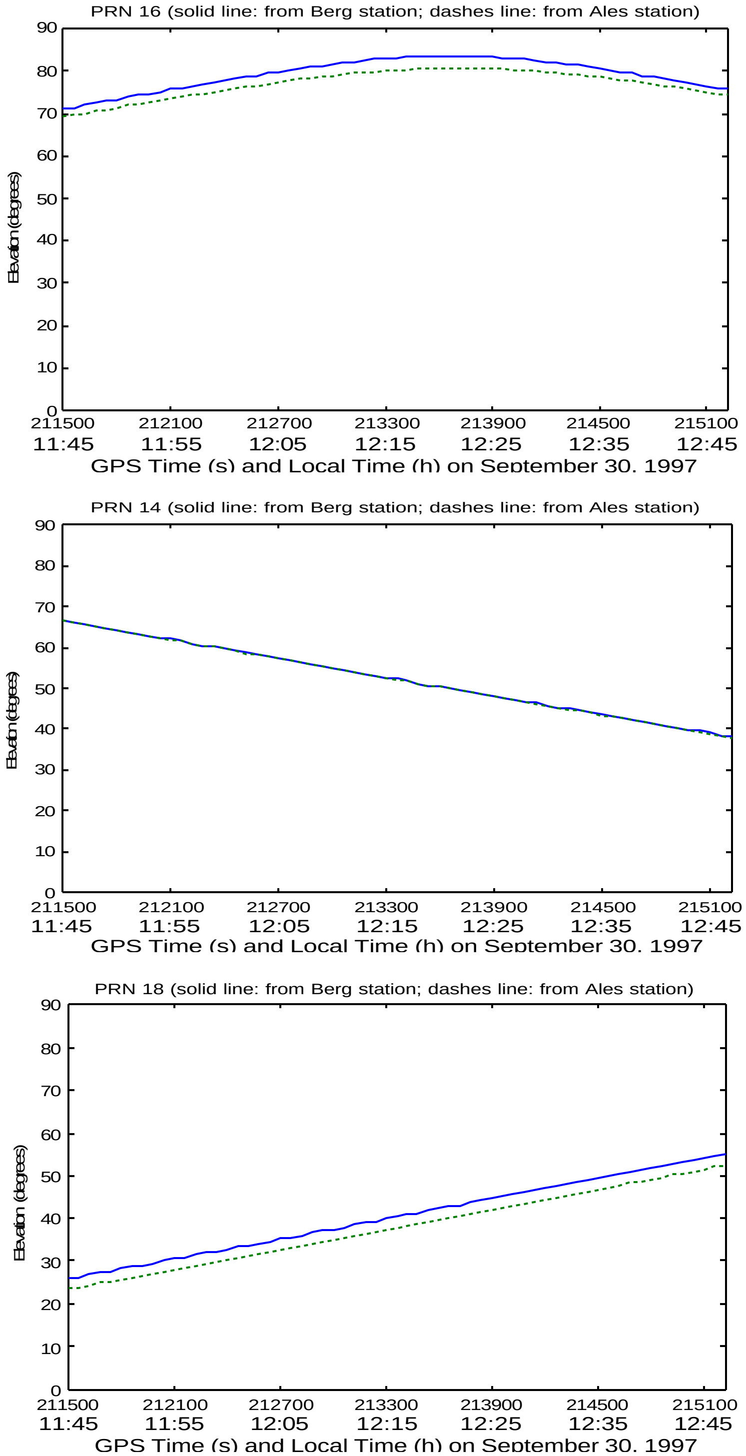

Figure 4.12: The satellite elevation angles from Berg and Ales stations for PRN 16, PRN 14 and PRN 18

Therefore,

$$MF(e_a^x) \rightarrow MF(e_b^x)$$
$$MF(e_a^y) \rightarrow MF(e_b^y)$$

and

$$\Delta\nabla T_{ab}^{xy} \cong MF(e^x)(T_{aZ} - T_{bZ}) - MF(e^y)(T_{aZ} - T_{bZ}) \qquad (4.59)$$

where e^x and e^y are the average elevation angles of the two receivers for satellite x and y, respectively.

Hence, we can rewrite Equation 4.59 as

$$\Delta\nabla T_{ab}^{xy} \cong (T_{aZ} - T_{bZ})[MF(e^x) - MF(e^y)] \qquad (4.60)$$

Defining the relative tropospheric zenith delay (RTZD) as (Duan & al 1996, Businger & al 1996)

$$RTZD = (T_{aZ} - T_{bZ}) \qquad (4.61)$$

The double difference can be represented as a function of RTZD,

$$\Delta\nabla T_{ab}^{xy} = [MF(e^x) - MF(e^y)] \times RTZD \qquad (4.62)$$

4.3.2.2 Use of $MF(e)$ to map double difference tropospheric residual variance to RTZD

The variance of the double difference residual tropospheric delay $\Delta\nabla T_{ab}^{xy}$ is defined by its stochastic expectation $E[(\Delta\nabla T_{ab}^{xy})^2]$ assuming that $\Delta\nabla T_{ab}^{xy}$ is zero-mean. If the mapping function is used, the following equation represents the relationship between $E[(\Delta\nabla T_{ab}^{xy})^2]$ and $E[(RTZD)^2]$,

$$E[(\Delta\nabla T_{ab}^{xy})^2] = [MF(e^x) - MF(e^y)]^2 \times E[(RTZD)^2] \qquad (4.63)$$

where $E[(RTZD)^2]$ is the variance of the relative residual tropospheric zenith delay assuming that the mean of RTZD is zero. Based on equation 4.63, the variance of the double difference residual tropospheric delay is linked to the variance of relative residual tropospheric zenith delay through the mapping function.

4.3.2.3 RTZD variance calculation from field data

The 24-hour double difference data set from the network shown in figure 4.13 was used to estimate the RTZD variance. The data was collected at a 1-Hz rate from 16:00 UTC (17:00 local) on September 29, 1997 to 16:00 UTC the following day, and it was thinned to two-second intervals. This data set will be used for the tests in this thesis. The cut-off elevation angle was chosen as 10^o. Post-mission precise orbits were used to fix the integer ambiguities between the network stations and to obtain the ionospheric-free double difference measurements.

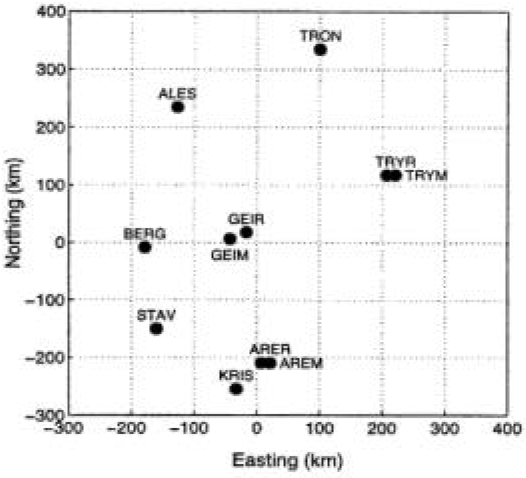

Figure 4.13: Southern Norway GPS reference Network

In the calculation of the relative residual delay stochastic parameters, baselines shorter than 100 km were not used because noise and carrier phase multipath errors are expected to be significant relative to the residual tropospheric errors. The 50 baselines described earlier were used. Two different sizes of sub-networks are analyzed. The first one includes all of the 11 reference receivers and it is called "LargeNet", which includes Ales,Tron, Tryr, Trym, Arer, Arem, Kris, Stav, Berg, Geim, and Geir (see figure 4.14). In figure 4.14, 50 used baselines are shown.

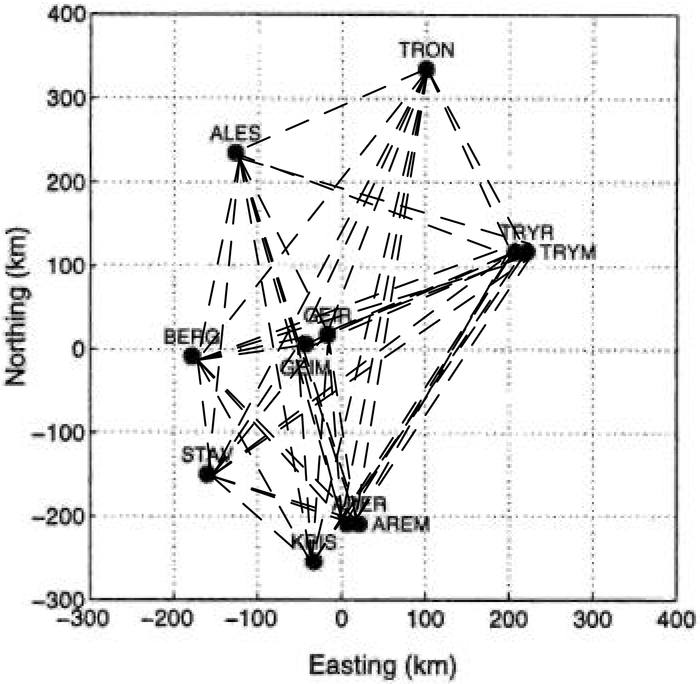

Figure 4.14: 50 baselines used in LargeNet

Also, as mentioned in the calculation of RTZD based on equation 4.62, all the double difference measurements used to calculate the RTZD should have enough elevation angle difference. Otherwise the mapping function difference with respect to two observed satellites is near zero and this results in the divergence of RTZD. The variance calculation consists of two components:

1. Firstly, based on our selected long baselines, calculate the relative residual tropospheric zenith delay RTZD from equation 4.62.
2. The variance of the RTZD is calculated for each of the long baselines in the network, as shown in figure 4.15, where each circle represents the RTZD variance of one baseline.

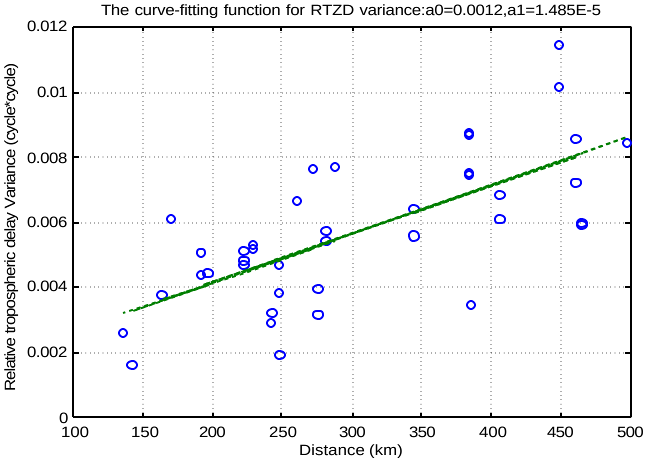

Figure 4.15: Calculated RTZD variances (circles) and curve fitting function for LargeNet

Based on figure 4.15, the RTZD variances (circles) show a power-law dependence on the baseline distance r, i.e.,

$$E[(RTZD)^2] = a_0 + a_1 \times r^n \qquad (4.68)$$

where, a_0, a_1 and n are constants.

Following this and function fitting the calculated variance of RTZD in figure 4.15, it can be found that n=1, $a_0 = 0.0012(cycle^2)$ and $a_1 = 1.485 \times 10^{-5}(cycle^2/km)$ for LargeNet. Therefore, the following curve fitting function of RTZD variances can be given by

$$E[(RTZD)^2] = 0.0012 + 1.485 \times 10^{-5} \times r\,(cycle^2) \qquad (4.69)$$

A small size GPS network is then considered in order to compare the performance of the tropospheric estimation as compared to LargeNet. This small size network is called SmallNet and it includes eight stations as shown in figure 4.16 (Berg, Geim, Geir, Tryr, Trym, Arer, Arem and Stav). As shown in figure 4.16, three short baselines (Geim-Geir, Tryr-Trym and Arer-Arem) were not used and the other 25 baselines were used for SmallNet computations and analysis.

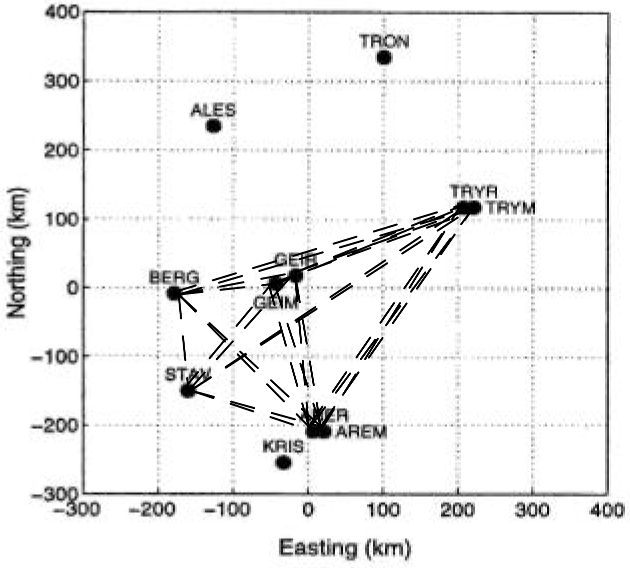

Figure 4.16: 25 baselines used in SmallNet

The variance of the RTZD is calculated for each of the long baselines shown in figure 4.16. The results are shown in figure 4.17, where each circle represents the RTZD variance of one baseline.

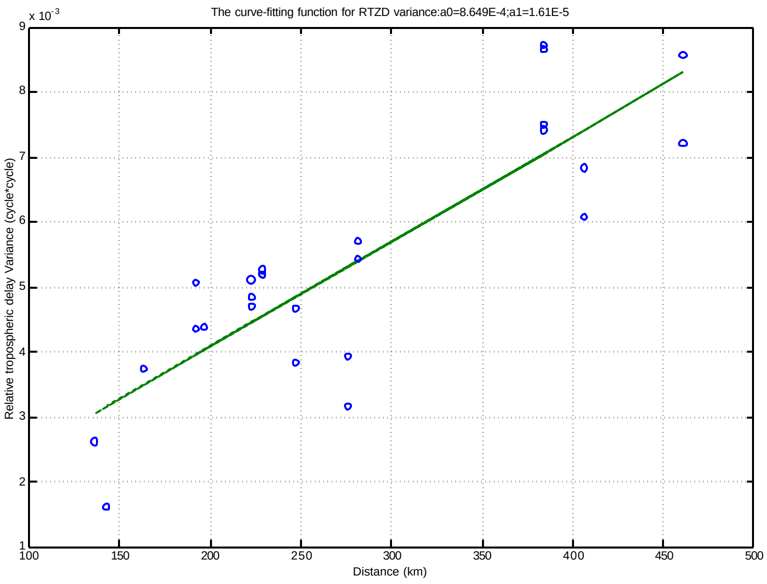

Figure 4.17 : Calculated RTZD variances (circles) and curve fitting function for SmallNet

From figure 4.17, it is also obvious that the RTZD variances (circles) have a power-law dependence on baseline distance. Depending on function fitting of the calculated variances of RTZD in Fig.4.17, we can find that n=1, $a_0 = 0.0008649(cycle^2)$ and $a_1 = 1.61\times10^{-5}(cycle^2/km)$ for SmallNet (only using eight reference stations for calculation). Therefore, the curve fitting function can be expressed as

$$E[(RTZD)^2] = 0.0008649 + 1.61\times10^{-5}\times r\,(cycle^2) \qquad (4.70)$$

4.3.3 Calculation of covariance function parameters

Now we investigate how to calculate the actual residual tropospheric delay variance by taking into account the RTZD variances estimated in the previous section. Clearly, the ionospheric-free double difference measurement error $\Delta\nabla\bar{f}_{IF}$ can be divided into a correlated term $\Delta\nabla d_c f(p_{rec}, p_0)$, which can be estimated by Trop_NetAdjust, and an uncorrelated term $\Delta\nabla d_u f$ as

$$\Delta\nabla\bar{f}_{IF} = \Delta\nabla d_c f(p_{rec,} p_0) + \Delta\nabla d_u f + \Delta\nabla N \qquad (4.71)$$

where $d_c f(p_{rec}, p_0)$ is the correlated term which includes all errors which are purely a function of the receiver position p_{rec} and the point p_0 (Raquet 1998). The point p_0 is defined as a fixed position from which all of the differential errors will be referenced and is called the "zero-point". $d_u f$ is the uncorrelated error term that includes all errors which cannot be estimated by the network adjustment procedure and includes measurement noise and multipath. We can define the function

$$s^2_{cz}(p_m, p_n) = E[(d_c f_Z(p_m) - d_c f_Z(p_n))^2] \qquad (4.72)$$

to be the variance of the differential correlated zenith errors $d_c f_Z$ between two arbitrary points p_m and p_n. The relationship between $E[(RTZD)^2]$, $E[(\delta_c\phi_Z(p_m)-\delta_c\phi_Z(p_n))^2]$ and $E[(\delta_u\phi_Z)^2]$ must be established in order to find the covariance function parameters of the residual tropospheric delay. Expanding the RTZD within the expectation yields

$$\begin{aligned} E[(RTZD(p_a, p_b))^2] &= E[(dl_{aZ} - dl_{bZ})^2] \\ &= E[((d_C f_{aZ}(p_a) - d_C f_{bZ}(p_b)) + (d_u f_{aZ} - d_u f_{bZ}))^2] \\ &= E[(d_C f_{aZ}(p_a) - d_C f_{bZ}(p_b))^2] + E[(d_u f_{aZ} - d_u f_{bZ}))^2] \\ &= E[(d_C f_{aZ}(p_a) - d_C f_{bZ}(p_b))^2] + E[(d_u f_{aZ})^2] + E[(d_u f_{bZ})^2] \end{aligned} \quad (4.73)$$

assuming no correlation between the uncorrelated zenith error $d_u f_z$ with other error sources. According to equation 4.72, equation 4.73 can be written as

$$\begin{aligned} E[(RTZD(p_a, p_b))^2] = s_{cZ}^2(p_a, p_b) + s_{uZ}^2(rec_a) \\ + s_{uZ}^2(rec_b) \end{aligned} \quad (4.74)$$

where $s_{uZ}^2(rec_a)$ and $s_{uZ}^2(rec_b)$ are uncorrelated error variances with respect to receiver a and receiver b, respectively. Taking equation 4.69 into account, equation 4.74 can be rewritten as

$$E[(RTZD(p_a, p_b))^2] = a_1 \times r + s_{uZ}^2(rec_a) + s_{uZ}^2(rec_b) \quad (4.75)$$

where r is the distance between reference stations a and b. For the test network used, the parameters a_1 and the constant $s_{uZ}^2(\cdot)$ are given in Table 4.1. Based on the covariance parameters given in Table 4.1, the covariance matrix of the residual tropospheric delays can be easily calculated for any receiver-satellite pair.

Table 4.1: Covariance function parameters of residual tropospheric delays for LargeNet and SmallNet

Network Type \ Parameters	a_1 (unit: $(cycle)^2/km$)	$s_{uZ}^2(\cdot)$ (unit: $(cycle)^2$)
LargeNet	1.485×10^{-5}	0.0006
SmallNet	1.610×10^{-5}	0.0004

4.4 Summary of covariance function calculation for residual tropospheric delays

In this section, we summarize the covariance function calculation for residual tropospheric delay estimation based on the previous discussion.

The covariance matrix C_{dl} consists of individual elements c_{ab}^{xy}, which correspond to the ionospheric-free measurements dl_a^x (from receiver a to satellite x) and dl_b^y (from receiver b to satellite y) as

$$c_{ab}^{xy} = E[(dl_a^x)(dl_b^y)] \tag{4.76}$$

Receiver a is located at p_a, and receiver b is located at p_b.

Actually, four possible cases of receivers and satellites exist, namely

1. when $a = b$ and $x = y$ (same receivers and same satellites)

$$c_a^x = MF^2(e^x)[f_{zC}(p_a, p_a, p_0) + s_{uZ}^2(rec_a)] \tag{4.77}$$

where $f_{zC}(p_a, p_a, p_0)$ is the correlated variance function (here is referred to residual tropospheric delay), e^x is the elevation angle and $MF(e^x)$ is the mapping function, which is given by

$$MF(e) = \frac{1}{\sin e} \tag{4.78}$$

and $s_{uZ}^2(rec_a)$ is taken from Table 4.1.

2. when $a \neq b$ and $x = y$ (different receivers and same satellites)

$$c_{ab}^x = MF^2(e_{ab}^x) f_{zC}(p_a, p_b, p_0) \tag{4.79}$$

where e_{ab}^x is the average elevation angle between two elevation angles with respect to two receivers and the mapping function is the same form of equation 4.78.

3. when $x \neq y$ and $a = b$ (different satellites and same receivers)

$$c_a^{xy} = MF(e_a^x) MF(e_a^y)[f_{zC}(p_a, p_a, p_0) + s_{uZ}^2(rec_a)] \tag{4.80}$$

where the mapping function is the same form of equation 4.78.

4. when $x \neq y$ and $a \neq b$ (different satellites and different receivers)

$$c_{ab}^{xy} = MF(e_a^x) MF(e_b^y) f_{zC}(p_a, p_b, p_0) \tag{4.81}$$

where e_a^x and e_b^y are the satellite elevation angles and the mapping function is the same form of equation 4.78.

For the above covariance function, the correlated variance function is presented as

$$f_{zC}(p_a, p_b, p_0) = \frac{s^{2}_{cZ}(p_a, p_0) + s^{2}_{cZ}(p_b, p_0) - s^{2}_{cZ}(p_a, p_b)}{2} \tag{4.82}$$

The differential variance function is described by

$$s^{2}_{cZ}(p_1, p_2) = a_1 \times r \tag{4.83}$$

where r is the distance between p_1 and p_2, and a_1 is taken from Table 4.1.

4.5 Trop_NetAdjust algorithm flowchart

The Trop_NetAdjust software was developed to estimate residual tropospheric delays based on the algorithm presented in the previous sections, using the information available from the reference stations. It requires measurements from the network reference stations and it performs double differencing, calculates the misclosure of the ionospheric-free double difference measurements and then it generates network estimates of the residual tropospheric delays using least squares prediction. The measurement vector l_n is generated directly from the reference receiver network measurements, and it is independent of the computation point. The residual tropospheric delay at the computation point is not only dependent upon the measurements from the reference receivers, but also a function of the computation point. Figure 4.18 gives a brief flow diagram of the Trop_NetAdjust software.

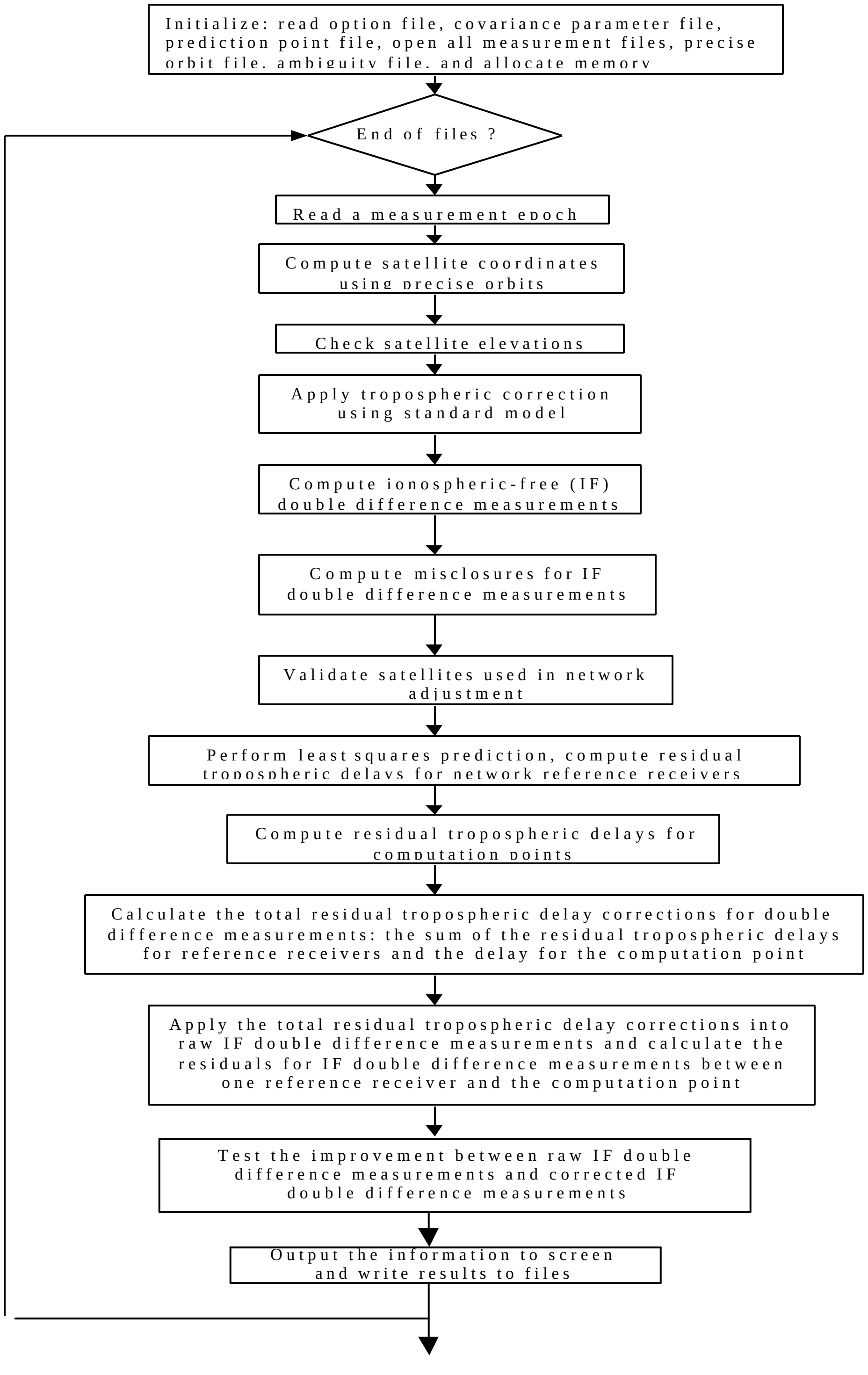

Figure 4.18: Flowchart of Trop_NetAdjust software

CHAPTER 5

ANALYSIS OF RESIDUAL TROPOSPHERIC DELAY ESTIMATION PERFORMANCE

In this chapter, the Trop_NetAdjust algorithm presented in Chapter 4 is used to estimate the residual tropospheric delay using the redundant information available through the multiple reference stations in a GPS network. Two specific cases are addressed, namely:

- Prediction of residual tropospheric delays for existing satellites at a user location optimally using the satellite measurements available from a network of reference stations. This will result in a faster estimation of the integer ambiguities at the user since a part of the carrier phase errors are due to the troposphere.

- Prediction of residual tropospheric delays for new satellites being observed by the network stations and user alike, using existing satellite measurements available in the network. This implies that tropospheric delays between satellites and observation points are spatially correlated, which is indeed the case. This case is important in order to resolve quickly ambiguities involving new satellites. These satellites are initially at relatively low elevation angles and their tropospheric delays relatively high.

5.1 Use of test network

The Norway network, which is described in detail in Appendix A, consists of 11 reference receivers as shown in figure 5.1.

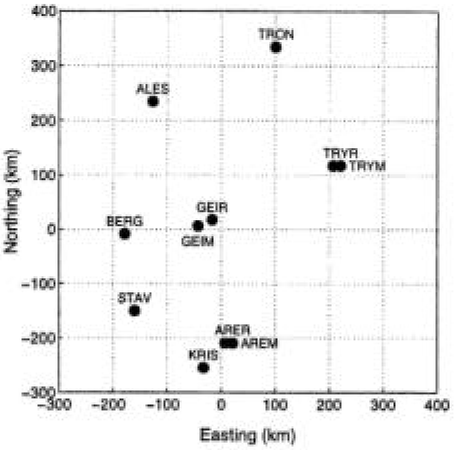

Figure 5.1: Southern Norway GPS reference Network

To analyse the impact of network geometry on Trop_NetAdjust performance, two different "mobile" receiver locations are chosen. One is located at the center of the network at the Geim reference station and this case is referred to as the Geim-Net, as shown in figure 5.2. An existing reference station is used as the location of the mobile user because the actual measurements at the reference station can be used to externally assess the accuracy of the predicted values. In the Geim-Net, the Geir station is not used for Trop_NetAdjust prediction because it is near Geim (<100km). The measurements at the reference station are naturally excluded from the data set used in the prediction, otherwise predicted and measured values would be practically identical and no performance assessment could be made. Likewise for the second test, the mobile receiver location is chosen to be Tryr, as shown in figure 5.3. In the Tryr-Net, the Trym station is not used because of the short distance between Tryr and Trym. A mobile receiver is treated as though it was moving, even though it is actually stationary. It yields the results which are very similar to the results obtained if the receiver were actually moving, as long as tuning parameters (such as process noise in a Kalman filtering) are set to the values for a moving receiver. This approach can be taken because most of the differential GPS errors (atmospheric and satellite position errors) are independent of receiver dynamics. In general, the multipath decreases with dynamics (relative to a stationary receiver). Therefore, a stationary receiver treated as a mobile receiver often represents a worst-case scenario. In figures 5.2 and 5.3, circles represent reference receivers and triangles represent the test receivers. Each receiver is identified by a four letter designation. Table 5.1 summarizes the characteristics of each of the test nets.

Table 5.1: Summary of test network characteristics

Network	Mobile Receiver	Network Reference Receivers
Geim-Net	Geim	Ales, Tron, Tryr,Trym,Arer, Arem, Kris,Stav, Berg
Tryr-Net	Tryr	Ales, Tron, Arer, Arem, Kris, Stav,Berg, Geim,Geir

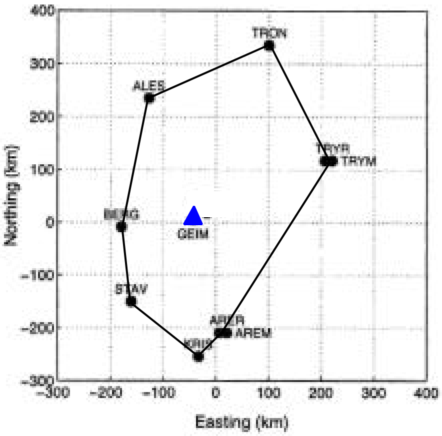

Figure 5.2: Geim Test Net

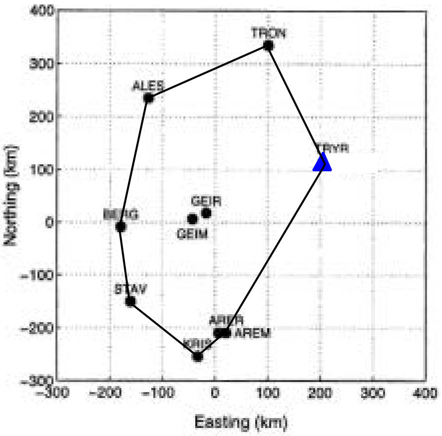

Figure 5.3: Tryr Test Net

5.2 Prediction of residual tropospheric delays at a mobile receiver and for an existing satellite

The goal is to estimate the residual tropospheric delay at a mobile receiver based on the ionospheric-free double difference measurements from the reference network receivers. The individual ionospheric-free double difference measurement-minus-range observables were calculated over the sampling period using the data from the test network. These ionospheric-free observables are the direct measurements of the residual tropospheric delays assuming multipath and measurement noises are small enough to be neglected.

These ionospheric-free double difference observables were computed between the selected "mobile" receiver and one of the reference receivers in the test network using raw (uncorrected) data. After this, Trop_NetAdjust was used to calculate estimates of the residual tropospheric delays for this "mobile" receiver based on all of the redundant measurements from the reference receivers of the network. Then the residual tropospheric delay estimates were applied to the raw measurements in order to test how well the residual tropospheric delays were estimated by analysing the reduction in the double difference error. Reducing these errors improves the ability to resolve the carrier phase ambiguities, and provides better positioning performance once the ambiguities are known. It also provides a means to measure the tropospheric wet delay and monitor its change because the major part of the residual tropospheric delay results from water vapor.

5.2.1 Geim-Net test network

In this analysis, the "mobile" receiver is located at the Geim reference station, which is near the center of the Norway network, as shown in figure 5.4.

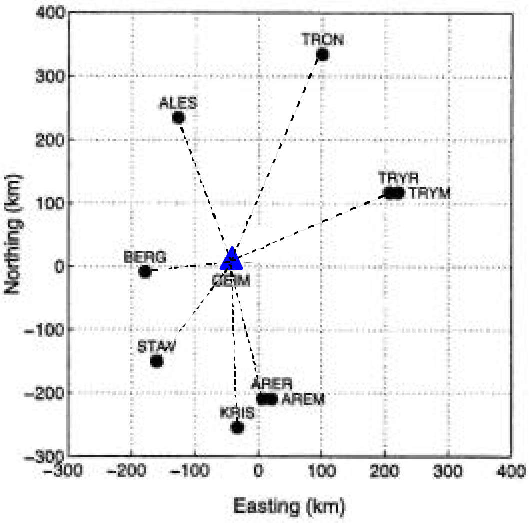

Figure 5.4: Seven test baselines in Geim-Net

In order to illustrate the effectiveness of Trop_NetAdjust, results are illustrated in figure 5.5 to figure 5.8. Trop_NetAdjust was used to calculate the corrections for ionospheric-free (IF) carrier phase measurements using the methods and covariance function described in Chapter 4. Actually Trop_NetAdjust generates estimates of the residual tropospheric delays for both reference receiver measurements and the unknown measurements at the "mobile" receiver (computation point). The total corrections are calculated as the sum of the estimates of the residual tropospheric delay at the reference receiver and the "mobile" receiver. After calculating these estimated tropospheric corrections, they are then applied to the raw ionospheric-free double difference measurements to reduce the residual tropospheric delay errors.

Shown in figures 5.5(a) and 5.5(b) are the ionospheric-free double difference measurements for the mobile reference pair Geim-Tron, prior to and after including the tropospheric corrections calculated by Trop_NetAdjust. The results for two different pairs of satellites 27-2 and 27-17 are shown and their elevation and azimuth changes are shown in figure 5.5(c). The data period is about one hour and the residuals decrease by 72% when the Trop_NetAdjust corrections are used, demonstrating the effectiveness of the approach in this case.

In figures 5.6, 5.7, and 5.8, three sets of results corresponding to three different directions from Geim are shown. They are based on three testing baselines (Geim-Kris: southern direction; Geim-Tryr: Eastern direction; and Geim-Berg: Western direction). The change of elevation and azimuth angles for the selected satellite pairs are also shown. From these figures, it is obvious that a significant improvement has been achieved. The improvement ranges from 35% to 72%.

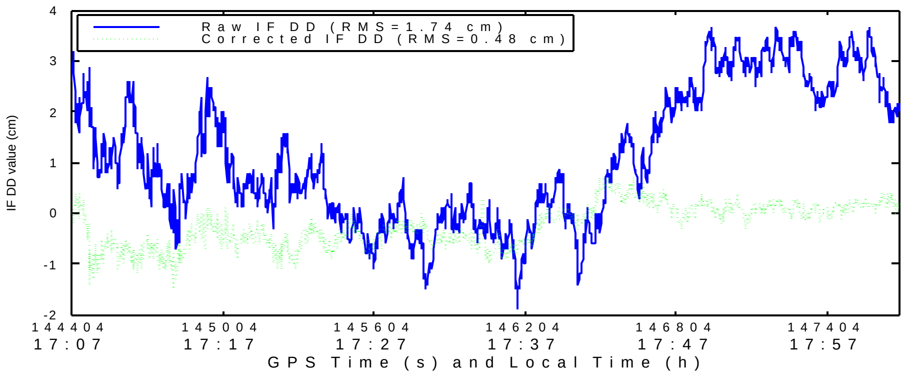

Figure 5.5(a): Geim-Tron (372km) for PRN 27-2 (RMS improvement = 72%)

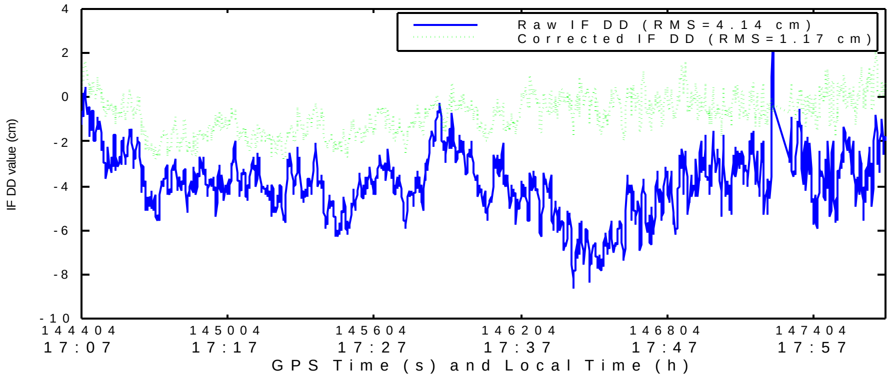

Figure 5.5(b): Geim-Tron (372km) for PRN 27-17 (RMS improvement = 72%)

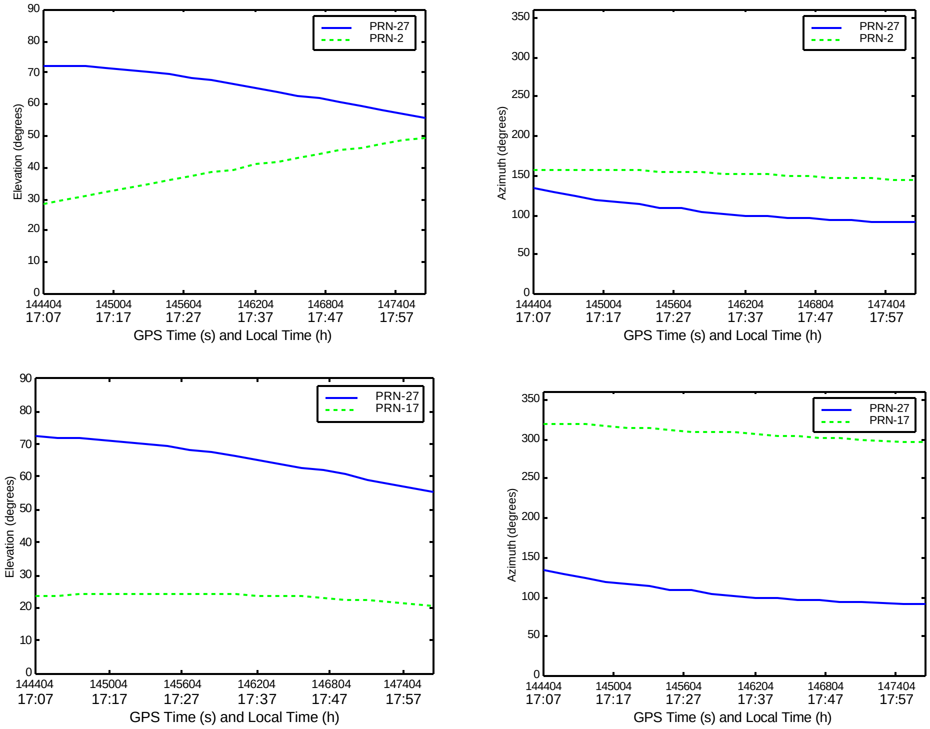

Figure 5.5(c): Elevation and azimuth angles for satellite pairs 27-2 and 27-17

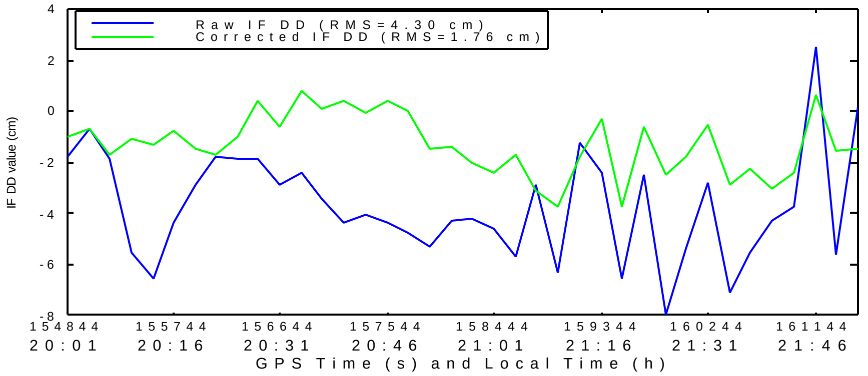

Figure 5.6(a): Geim-Kris (272km) for PRN 9-21 (RMS improvement = 59%)

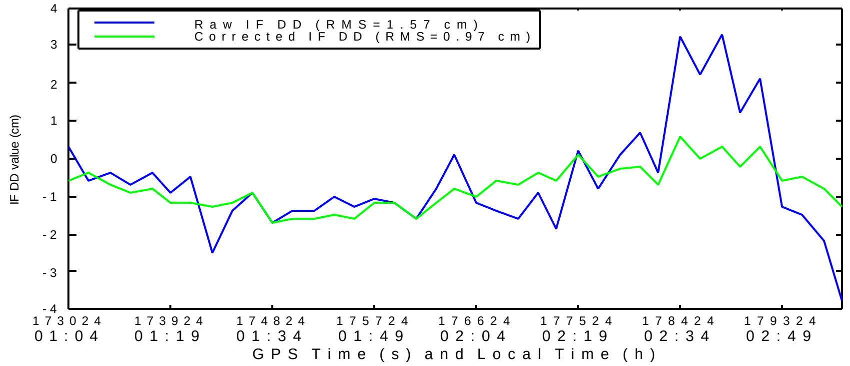

Figure 5.6(b): Geim-Kris (272km) for PRN 6-25 (RMS improvement = 38%)

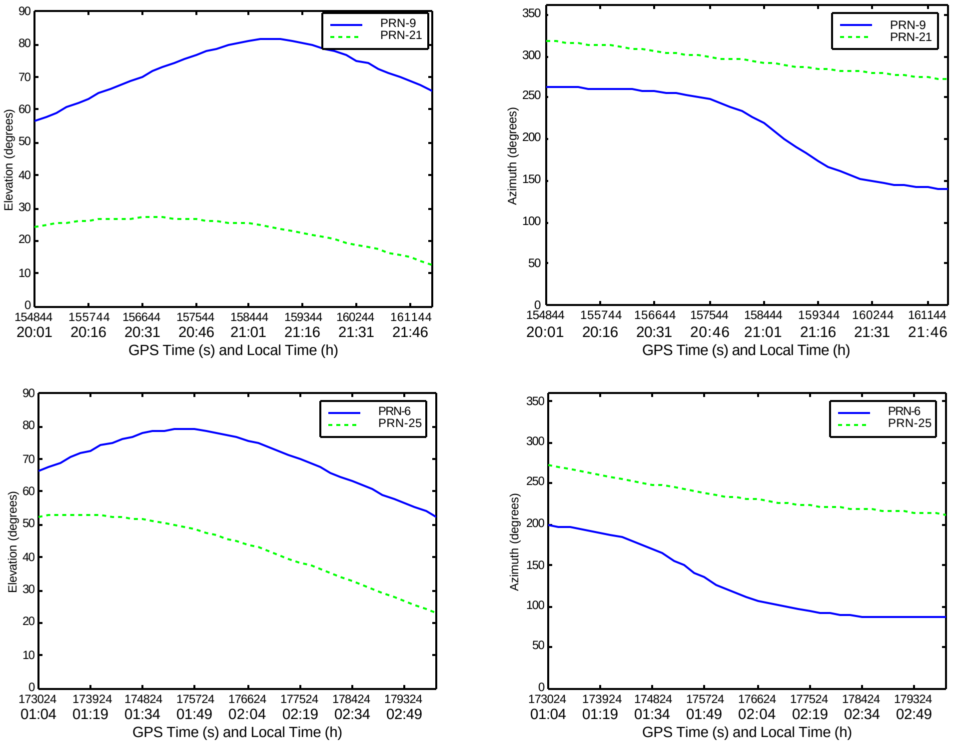

Figure 5.6(c): Elevation and azimuth angles for satellite pairs 9-21 and 6-25

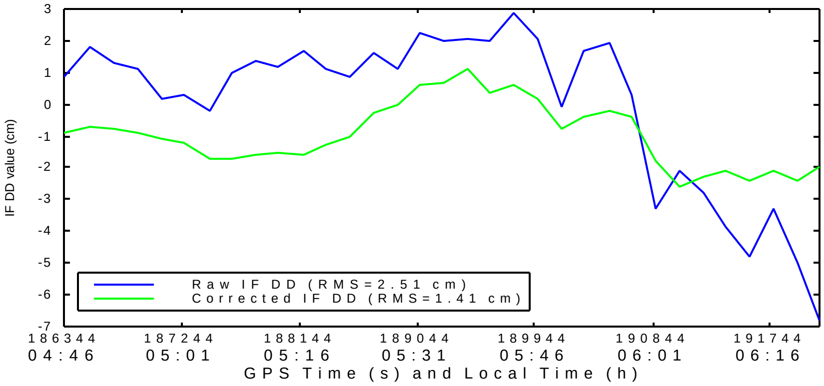

Figure 5.7(a): Geim-Tryr (276km) for PRN 3-17 (RMS improvement = 43.8%)

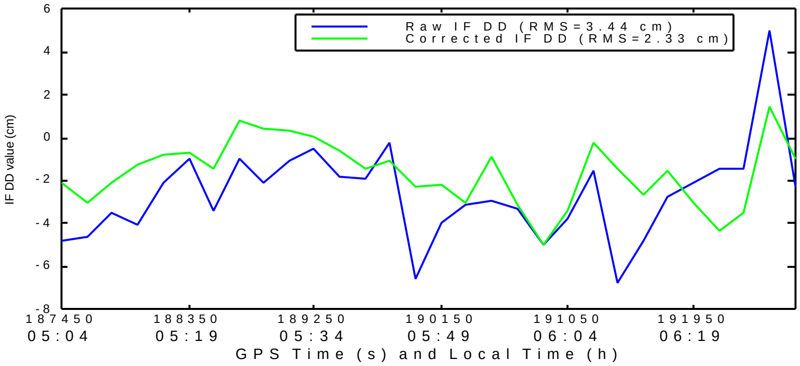

Figure 5.7(b): Geim-Tryr (276km) for PRN 3-26 (RMS improvement = 35%)

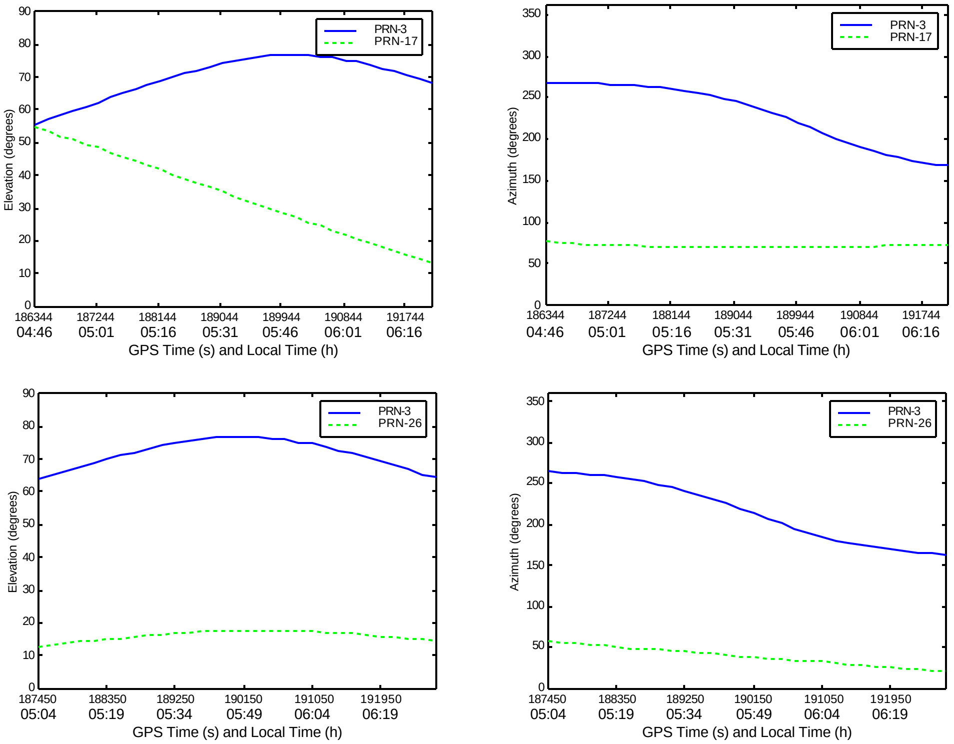

Figure 5.7(c): Elevation and azimuth angles for satellite pairs 3-17 and 3-26

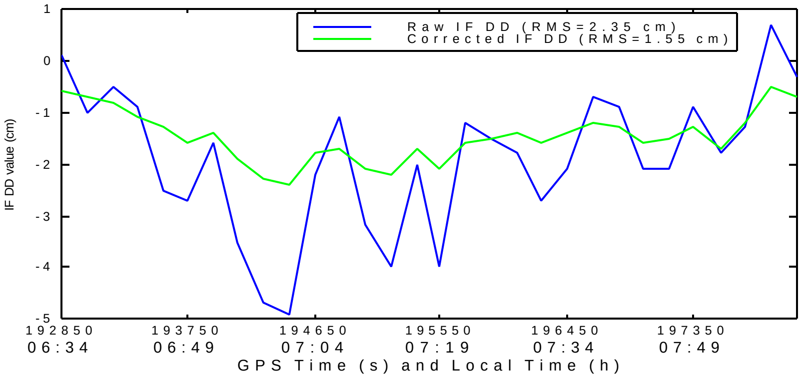

Figure 5.8(a): Geim-Berg (163km) for PRN 31-21 (RMS improvement = 35%)

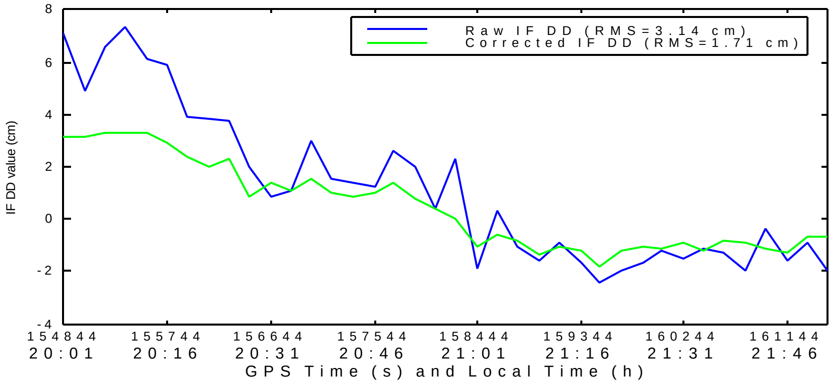

Figure 5.8(b): Geim-Berg (163km) for PRN 9-7 (RMS improvement = 46%)

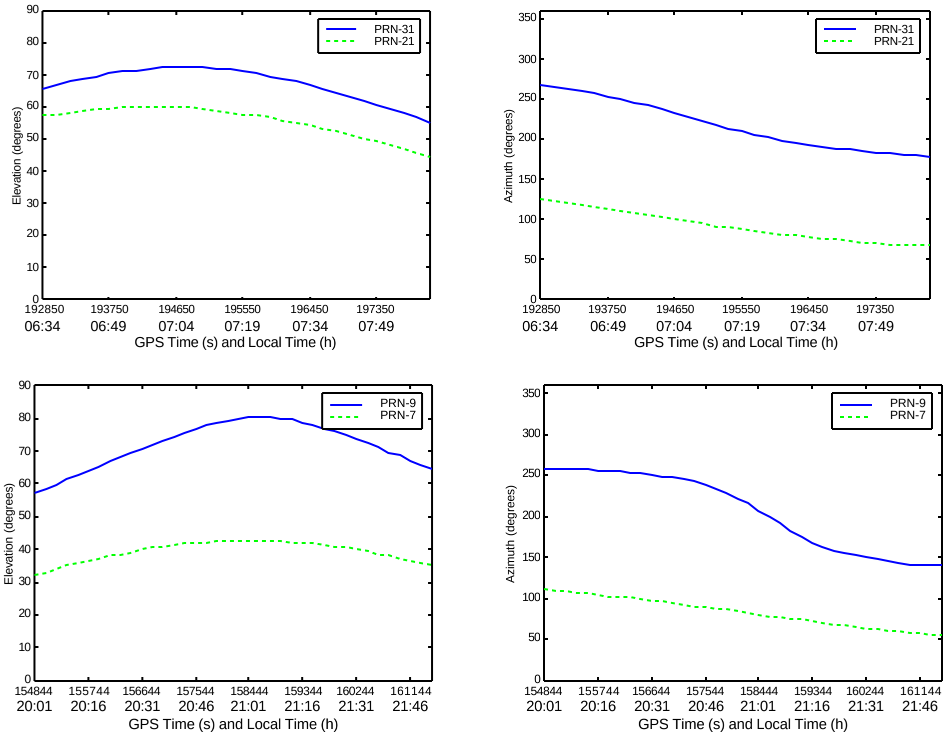

Figure 5.8(c): Elevation and azimuth angles for satellite pairs 31-21 and 9-7

5.2.1.1 Statistical analysis of Trop_NetAdjust performance

In order to analyze the performance improvement of Trop_NetAdjust, 15 hours of data at a 3-minute sampling rate were processed for statistical analysis. To implement this statistical analysis, the steps followed are listed below:

1) Choose "Geim" as the "mobile" receiver (computation point).
2) Choose seven test baselines from Geim whose directions are different from each other, as shown in figure 5.4.
3) For each baseline, Trop_NetAdjust residual tropospheric delay corrections were calculated as the sum of the estimates at the "mobile" receiver and the estimate at the corresponding reference receiver.
4) For each baseline, apply this Trop_NetAdjust residual tropospheric delay correction to the raw ionospheric-free double difference measurements.
5) For each baseline, calculate the RMS of each double difference (DD) satellite-receiver pair for raw measurements and corrected measurements, respectively.
6) Compare the RMS percentage improvement between raw measurements and corrected measurements.

For instance, since typically seven satellites were available above 10^{o}, six DD satellite-pairs were selected, as one of the satellites is chosen as the base satellite for each baseline. If the sampling interval is three minutes, the total number of measurements for each baseline over 15 hours is given by

$$\text{Total DD Measurements} = \frac{(7-1)\times 15\times 60(\text{min})}{3(\text{min})} = 1800$$

In figure 5.9 to figure 5.12, comparisons between raw and corrected measurements are shown as time series for four test baselines, which have the following directions: Geim-Tron: Northern direction; Geim-kris: Southern direction; Geim-Tryr: Eastern direction; and Geim-Berg: Western direction. From these figures, the improvement of Trop_NetAdjust is consistently over 50%.

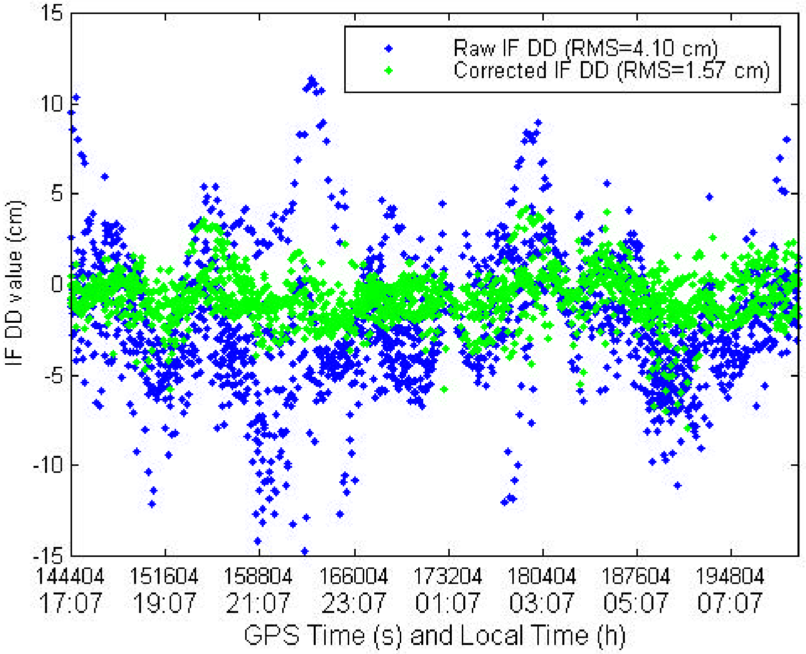

Figure 5.9: Time series of IF double difference measurements for Geim-Tron baseline (372km)—62% improvement percentage

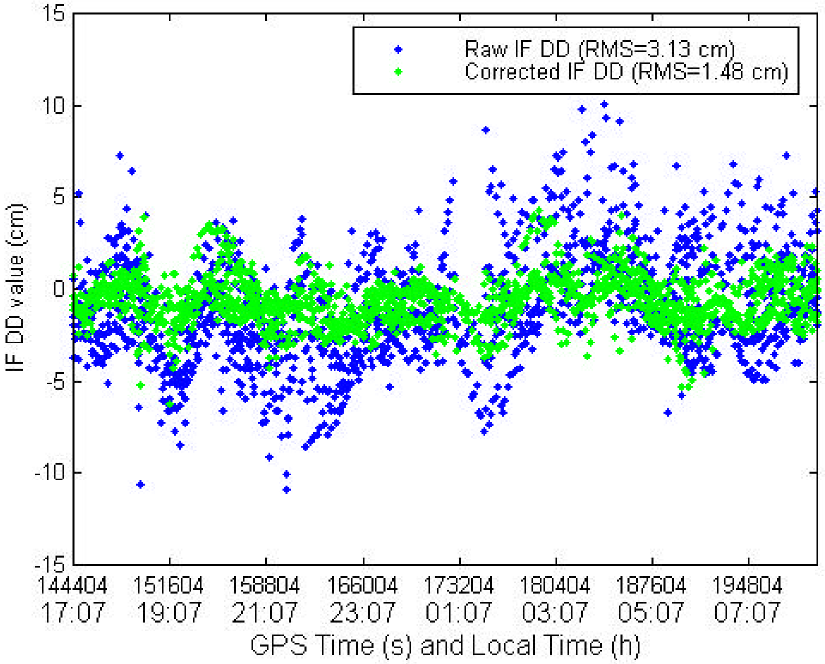

Figure 5.10: Time series of IF double difference measurements for Geim-Kris baseline (272km)—53% improvement percentage

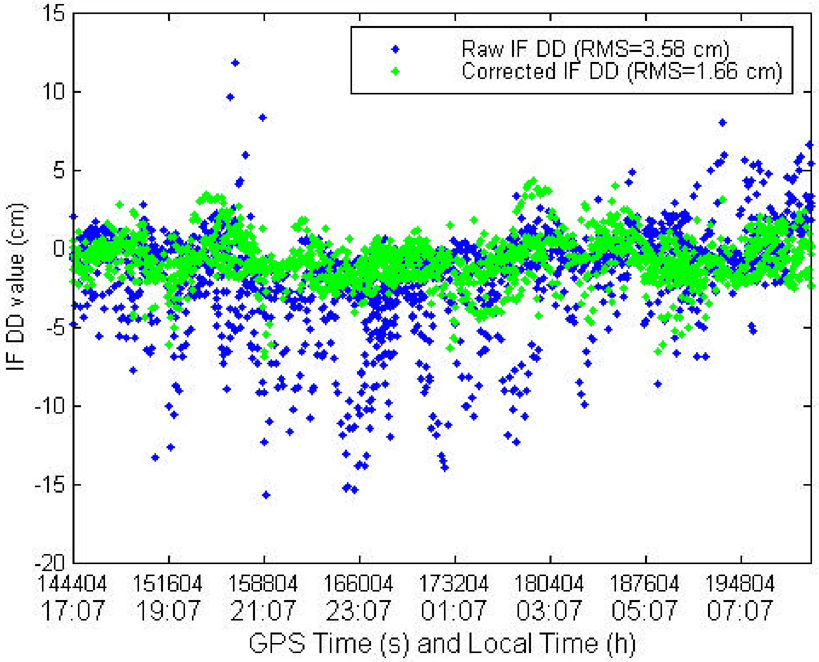

Figure 5.11: Time series of IF double difference measurements for Geim-Tryr baseline (276km)—54% improvement percentage

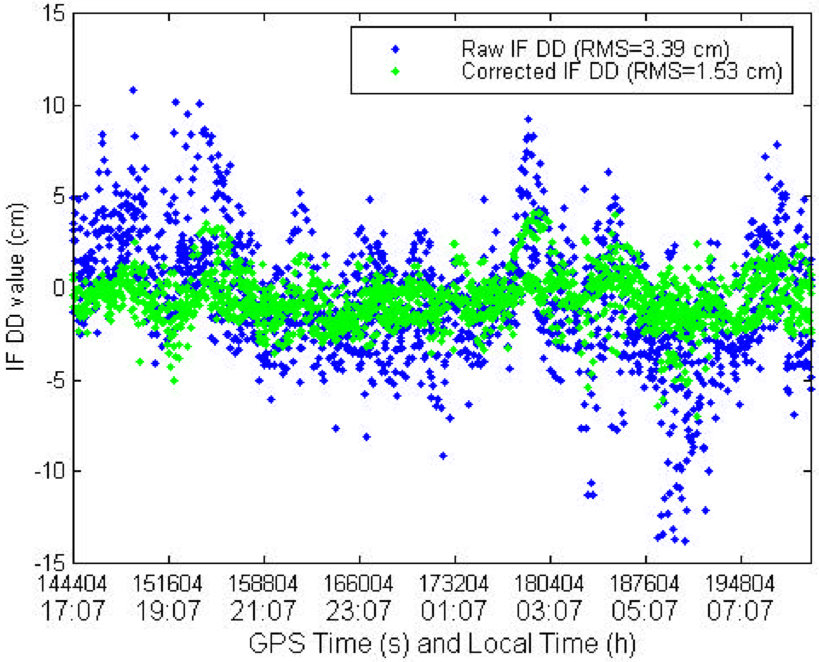

Figure 5.12: Time series of IF double difference measurements for Geim-Berg baseline (163km)—55% improvement percentage

Seven baseline test results are summarized in figure 5.13 and Table 5.2. The improvement when the residual tropospheric delay corrections are applied is consistently at the 55% level for this case.

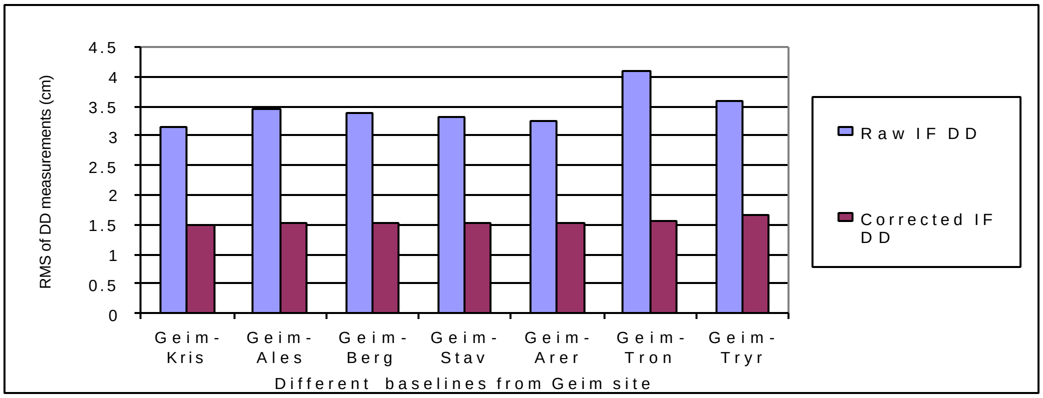

Figure 5.13: Stochastic RMS residual analysis -Geim-Net (seven baselines), new station case

Table 5.2: RMS residual improvement - Geim-Net, New station case

Baselines	DD RMS residuals (no residual tropo corr) (cm)	DD RM residuals (residual tropo corr) (cm)	Percentage improvement (%)
Geim – Kris (272 km)	3.13	1.48	53%
Geim – Ales (242 km)	3.46	1.51	56%
Geim – Berg (163 km)	3.39	1.53	55%
Geim – Stav (222 km)	3.33	1.53	54%
Geim – Arer (223 km)	3.24	1.52	54%
Geim – Tron (372 km)	4.10	1.57	62%
Geim – Tryr (276 km)	3.58	1.66	54%

5.2.2 Tryr-Net test network

For the second test net, the "mobile" receiver is located at the Tryr reference station, which is at the edge of the network, as shown in figure 5.14, and different network geometry occurs.

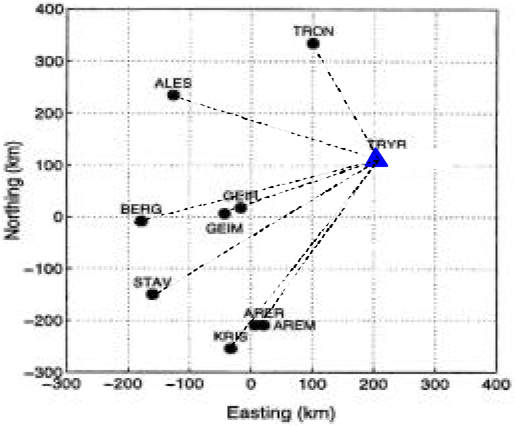

Figure 5.14: Seven test baselines in Tryr-Net

In order to illustrate the effectiveness of Trop_NetAdjust, results are illustrated in figure 5.15 to figure 5.18 corresponding to the following four different baselines: Tryr-Tron: Northern direction; Tryr-Kris: Southern direction; Tryr-Geim: Western direction (medium baseline); and Tryr-Berg: Western direction (long baseline). For the western direction, two baselines with different lengths are chosen, which shows the increase of residual tropospheric delays with the increase of the baseline length. Similar to the Geim-Net test network, the total corrections applied to raw measurements were calculated as the sum of the estimates of residual tropospheric delays at the reference receiver and the "mobile" receiver-Tryr.

Figures 5.15(a) and 5.15(b) show the ionospheric-free double difference measurements for the mobile reference pair Tryr-Tron. The double difference residuals prior and after including the residual tropospheric delay corrections were calculated by Trop_NetAdjust. The elevation and azimuth changes corresponding to the related two different satellite pairs 27-2 and 27-10 are shown in figure 5.15(c). The residuals still decrease over 36% when the Trop_NetAdjust corrections are used, demonstrating the effectiveness of this approach. Figures 5.16, 5.17 and 5.18 show the significant improvements for three sets of results, namely Tryr-Geim, Tryr-Berg and Tryr-Kris baselines. The elevation and azimuth changes of selected satellite pairs for each baseline are also presented.

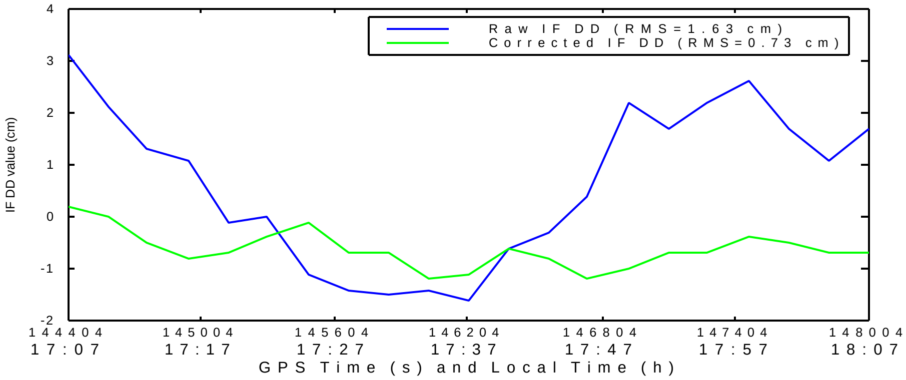

Figure 5.15(a): Tryr-Tron (220km) for PRN 27-2 (RMS improvement = 55%)

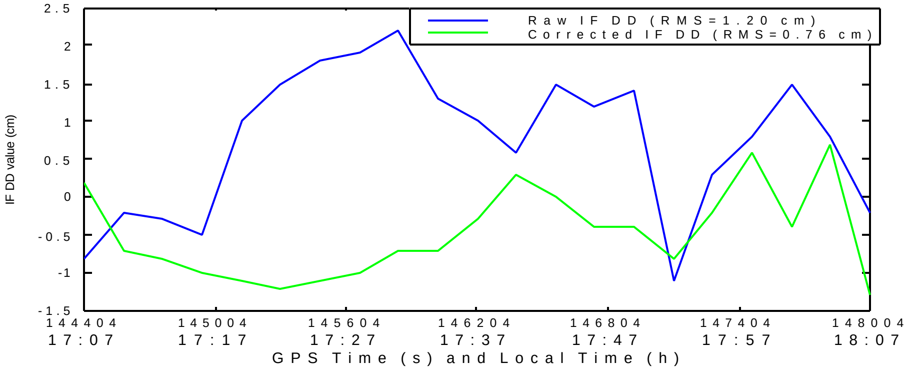

Figure 5.15(b): Tryr-Tron (220km) for PRN 27-10 (RMS improvement = 36%)

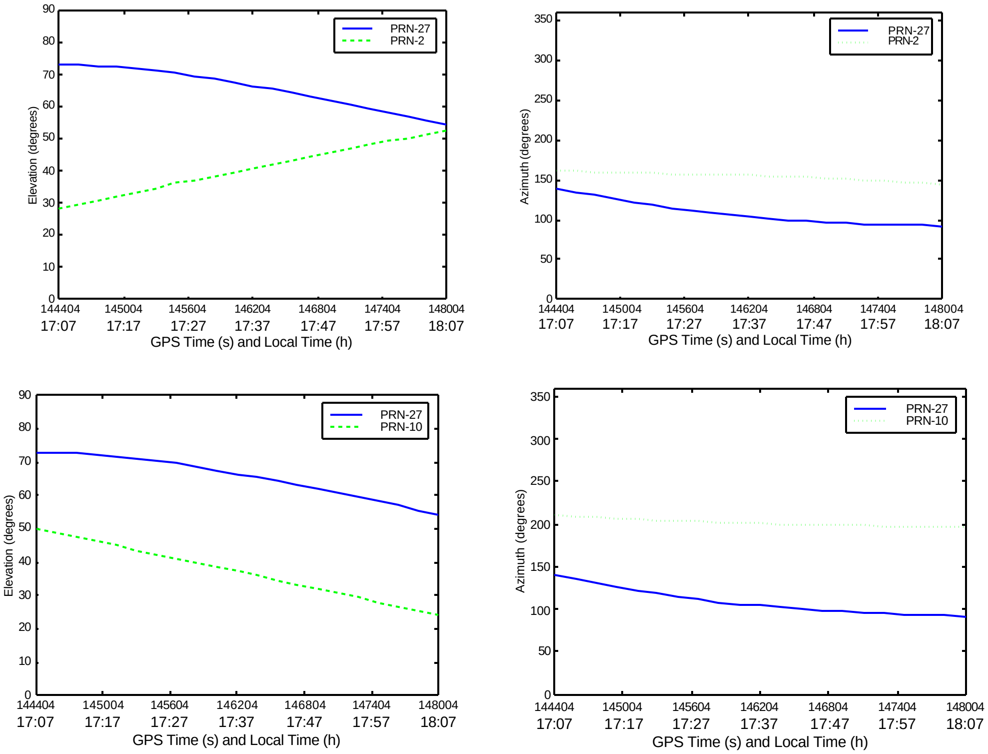

Figure 5.15(c): Elevation and azimuth angles for satellite pairs 27-2 and 27-10

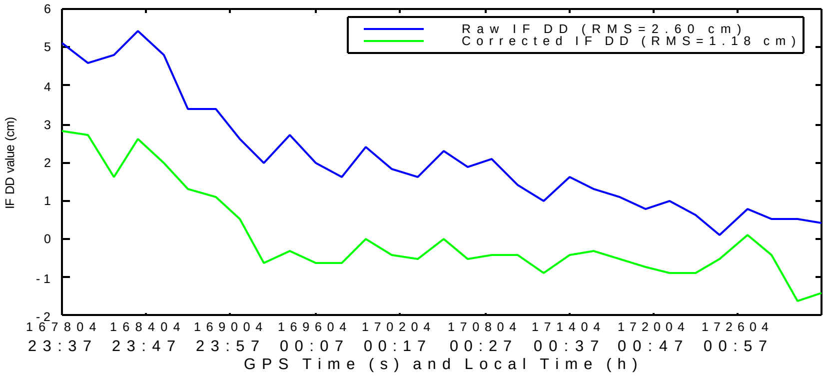

Figure 5.16(a): Tryr-Geim (276km) for PRN 30-6 (RMS improvement = 54%)

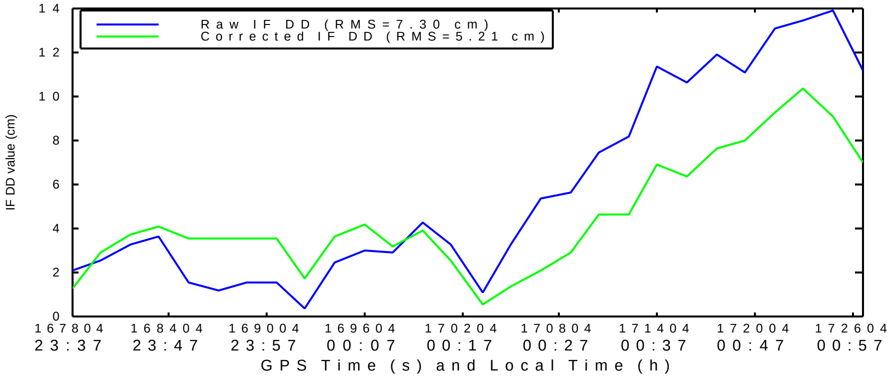

Figure 5.16(b): Tryr-Geim (276km) for PRN 30-4 (RMS improvement = 28%)

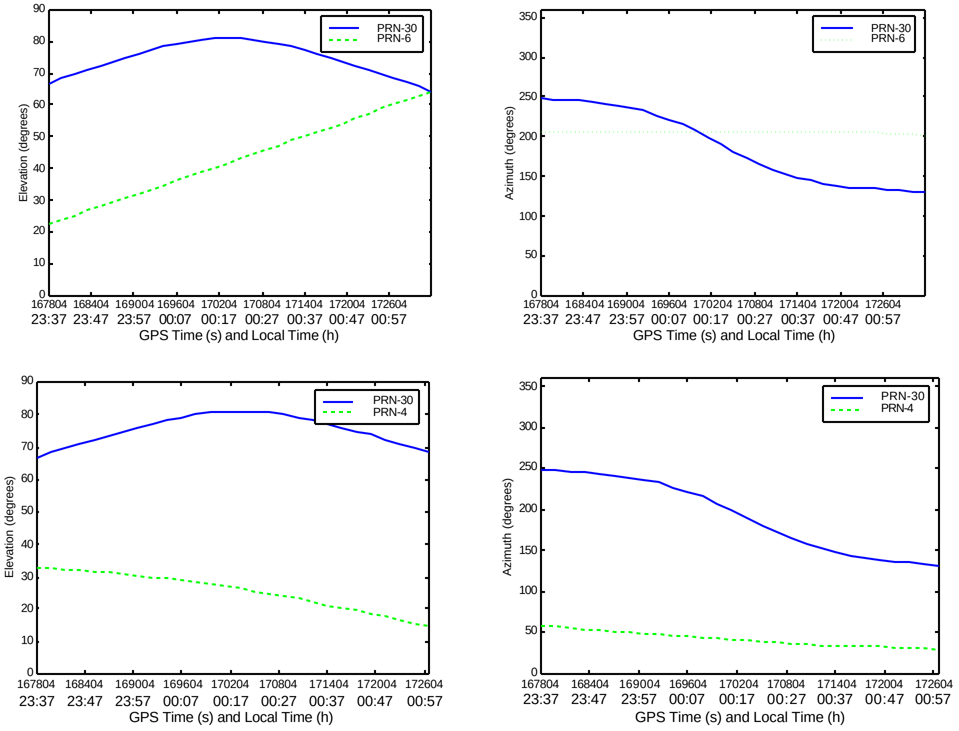

Figure 5.16(c): Elevation and azimuth angles for satellite pair 30-6 and 30-4

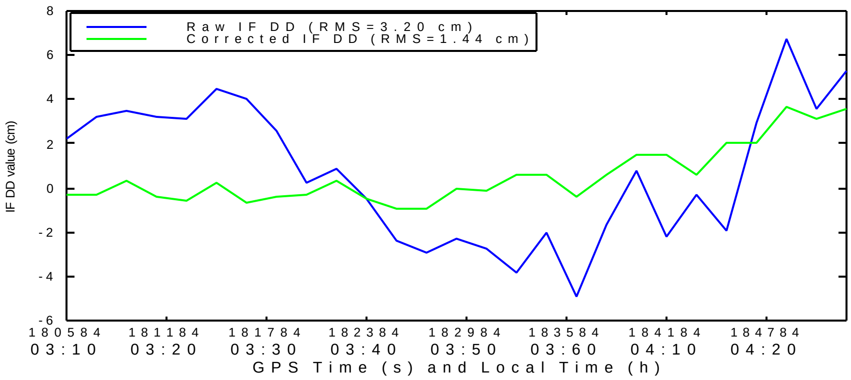

Figure 5.17(a): Tryr-Berg (406km) for PRN 17-6 (RMS improvement = 55%)

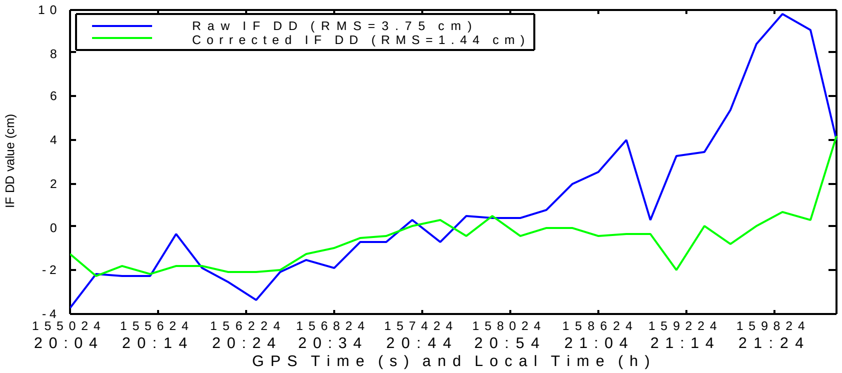

Figure 5.17(b): Tryr-Berg (406km) for PRN 9-26 (RMS improvement = 61%)

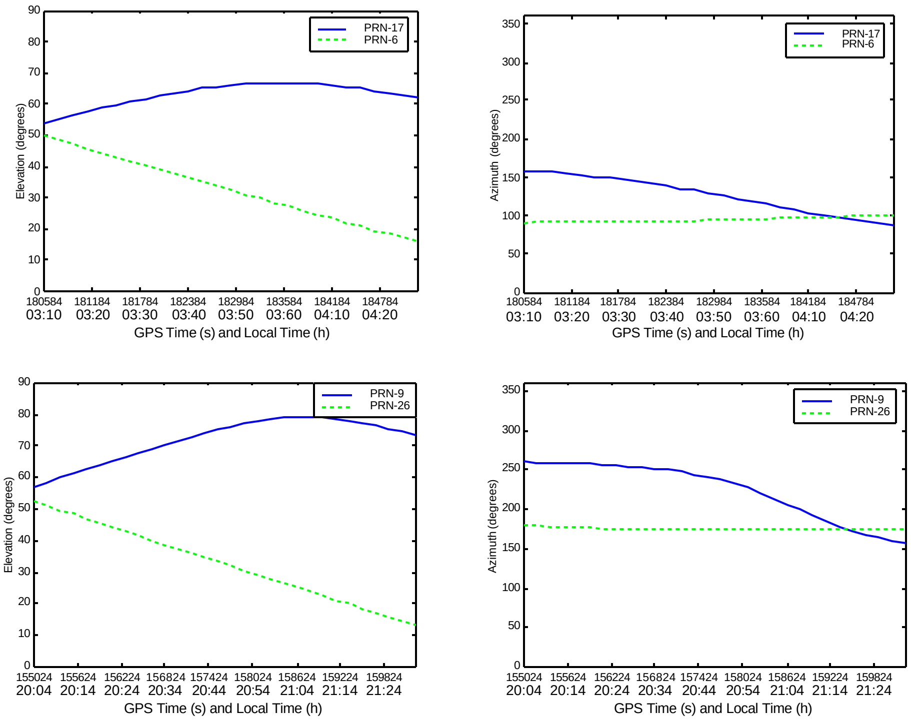

Figure 5.17(c): Elevation and azimuth angles for satellite pairs 17-6 and 9-26

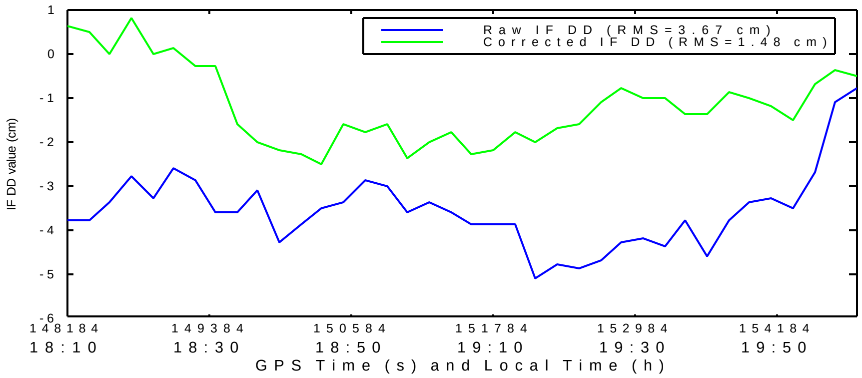

Figure 5.18(a): Tryr-Kris (448km) for PRN 26-2 (RMS improvement = 59%)

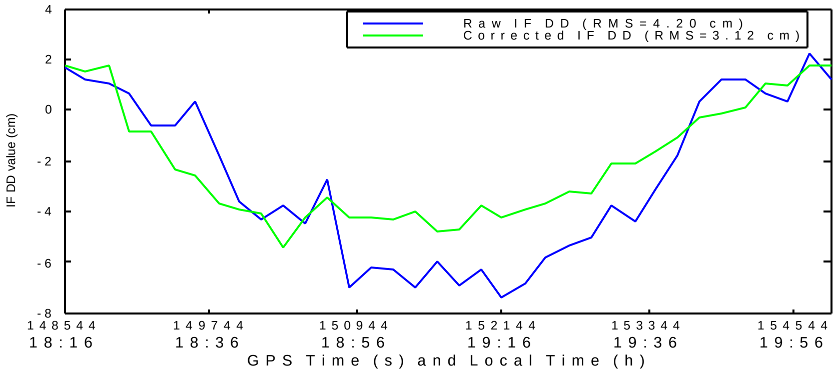

Figure 5.18(b): Tryr-Kris (448km) for PRN 26-23 (RMS improvement = 71%)

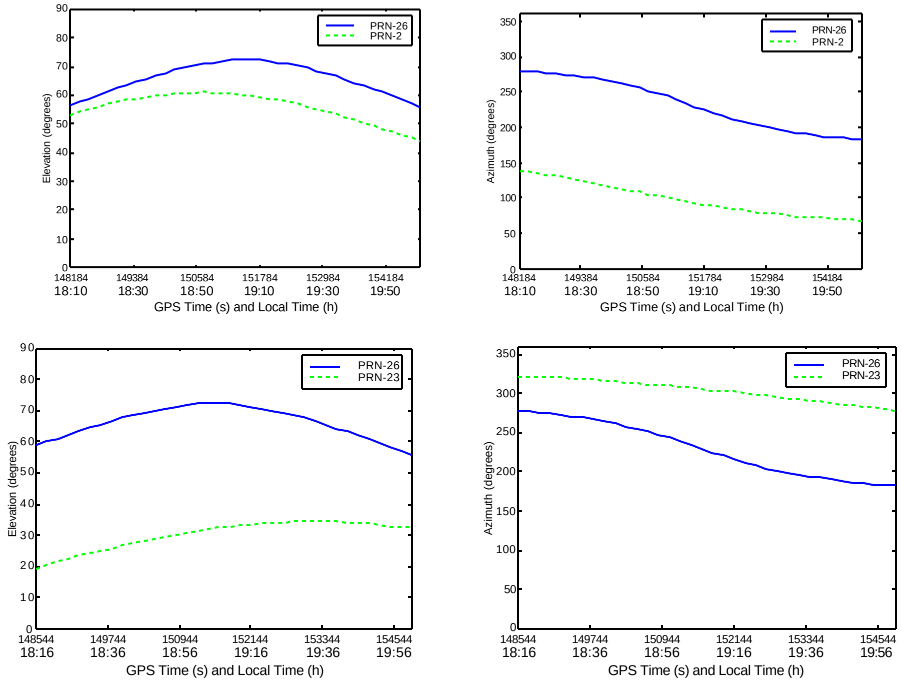

Figure 5.18(c): Elevation and azimuth angles for satellite pairs 26-2 and 26-23

5.2.2.1 Statistical analysis of Trop_NetAdjust performance

The same 15 hours of data at a 3-minute sampling rate were processed for statistical analysis for the Tryr-Net case. To implement this statistical analysis, several steps were followed similar to the analysis for Geim-Net:

1) Choose "Tryr" as the "mobile" receiver (computation point).
2) Choose seven test baselines from Tryr whose direction is different from each other, as shown in figure 5.14.
3) For each baseline, Trop_NetAdjust estimated residual tropospheric delay corrections are calculated as the sum of the estimate at the "mobile" receiver and the estimate at the corresponding reference receiver.
4) For each baseline, apply this Trop_NetAdjust residual tropospheric delay corrections to raw ionospheric-free double difference measurements.
5) For each baseline, calculate the RMS of each double difference (DD) satellite-receiver pair for raw measurements and corrected measurements, respectively.
6) Compare the RMS percentage improvement between raw measurements and corrected measurements.

Figure 5.19 to figure 5.22 show the improvements between the raw and corrected measurements after using Trop_NetAdjust, with respect to the following baselines: Tryr-Tron, Tryr-Geim, Tryr-Berg and Tryr-Kris. For each comparison, all possible satellite pairs are combined together to measure the overall statistical performance.

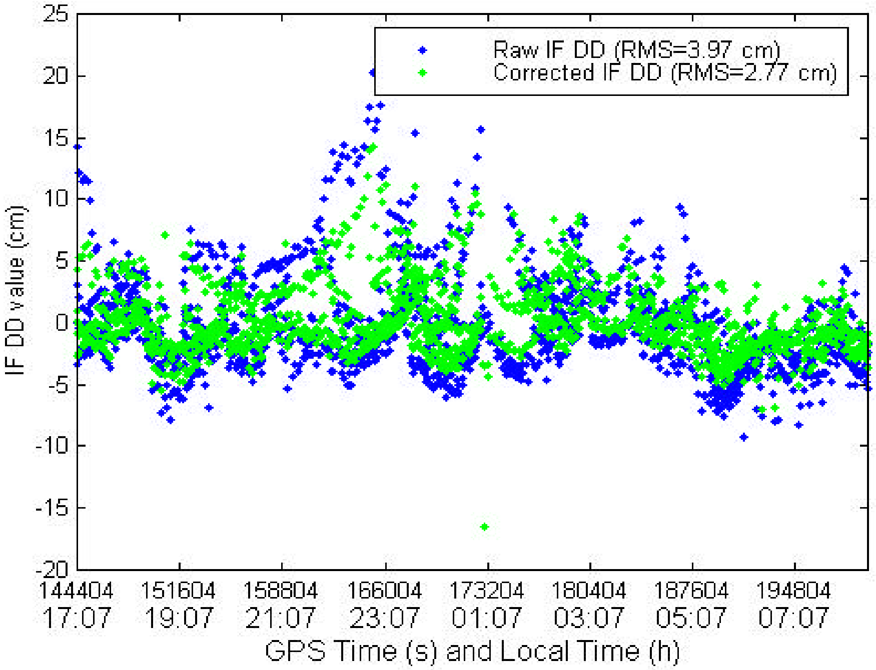

Figure 5.19: Time series of IF double difference measurements for Tryr-Tron baseline (220km)—30% improvement percentage

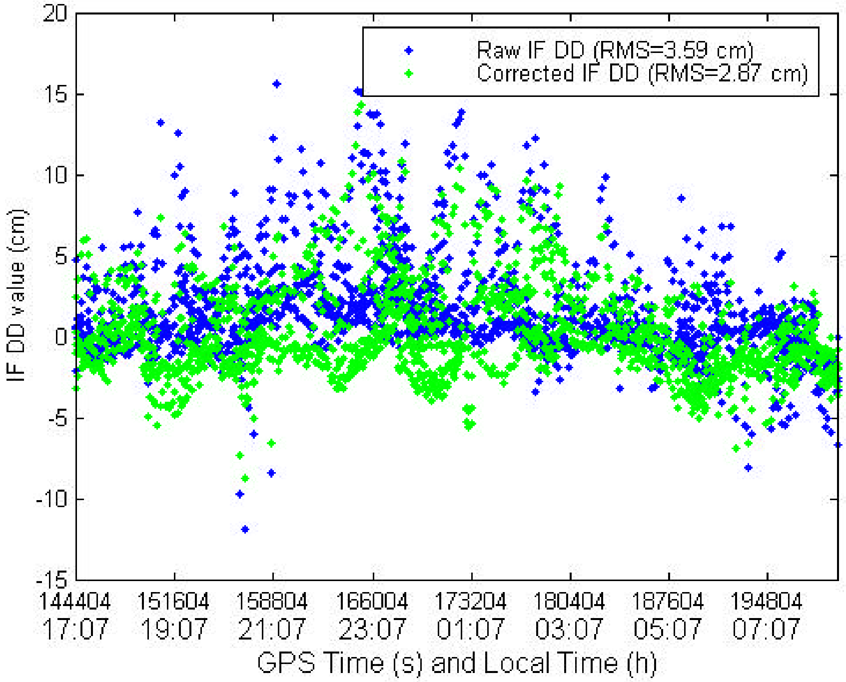

Figure 5.20: Time series of IF double diference measurements for Tryr-Geim baseline (276km)—20% improvement percentage

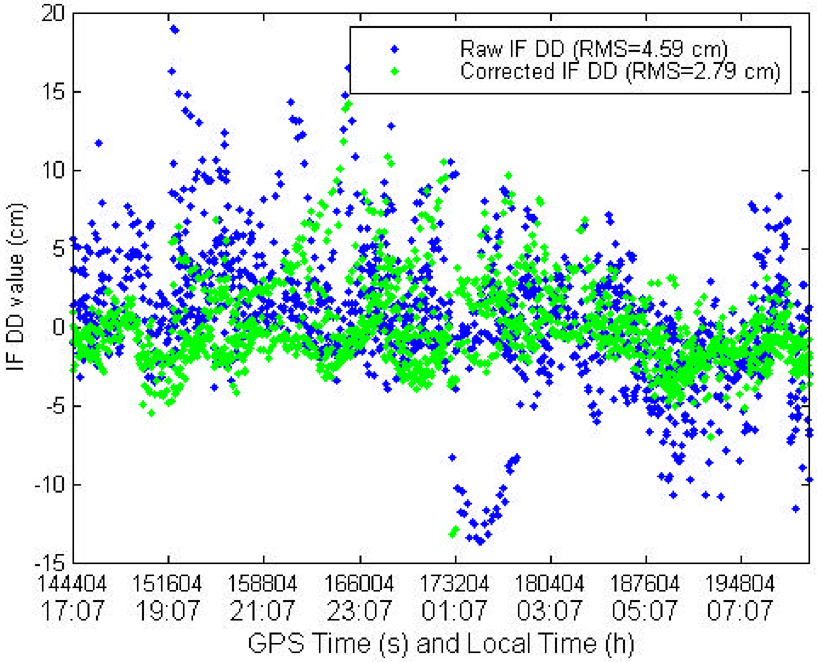

Figure 5.21: Time series of IF double difference measurements for Tryr-Berg baseline (406km)—39% improvement percentage

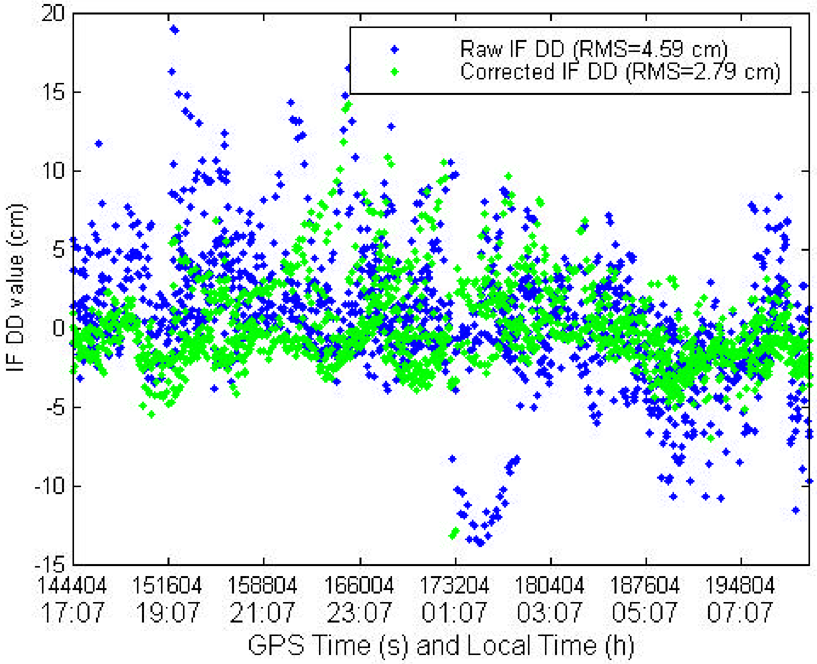

Figure 5.22: Time series of IF double difference measurements for Tryr-Kris baseline (448km)—32% improvement percentage

The test results for the seven baselines shown in figure 5.14 are summarized in figure 5.23 and Table 5.3. The improvement when the residual tropospheric delay corrections are applied is at the range from 20% to 39%. The reason the improvement is lower than in the previous case is that the geometry of the network and the sub-optimal location of Tryr at the eastern edge of the network.

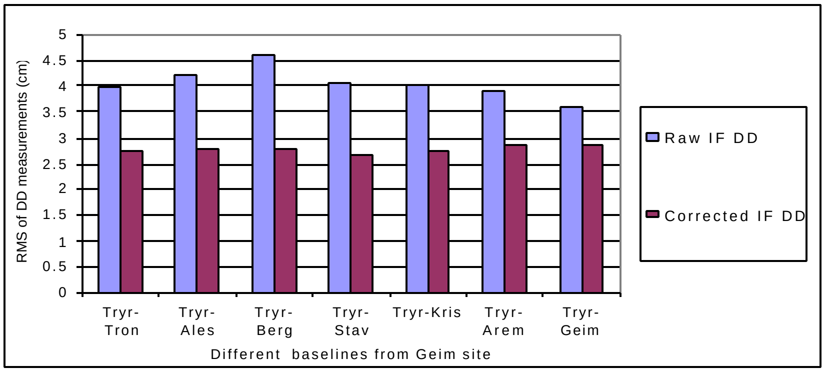

Figure 5.23: Stochastic RMS residual analysis - Tryr-Net (seven baselines), new station case

Table 5.3: RMS residual improvement - Tryr-Net, new station case

Baselines	DD RMS residuals (no residual tropo corr) (cm)	DD RMS residuals (residual tropo corr) (cm)	Percentage improvement (%)
Tryr-Tron (220 km)	3.97	2.77	30%
Tryr-Ales (344 km)	4.20	2.78	34%
Tryr-Berg (406 km)	4.59	2.79	39%
Tryr-Stav (461 km)	4.05	2.69	34%
Tryr-Kris (448 km)	4.02	2.74	32%
Tryr-Arem (384 km)	3.93	2.87	26%
Tryr-Geim (276 km)	3.59	2.87	20%

5.3 Prediction of residual tropospheric delays for a new satellite

Usually the tropospheric effect on a new satellite is very significant because of the relatively low elevation angle as the satellite rises above the horizon. The residual tropospheric delay for a new satellite, whose elevation angle is low (such as 5^{o}) is relatively large. Hence, Trop_NetAdjust provides a good method to deal with this problem and predict the residual tropospheric delay for the new satellite. The RMS of corrected measurements after using Trop_NetAdjust will be significantly smaller compared with raw measurements and it will be very useful to resolve the ambiguities for this new satellite. Trop_NetAdjust was tested using the Geim-Net and Tryr-Net cases described in the previous section (figures 5.2 and 5.3). In order to test the residual tropospheric delay prediction performance for a new satellite, the methodology used is as follows:

- select one existing satellite to be the predicted “new” satellite and remove this satellite from the measurements.
- select one reference station as the computation point (such as Geim or Tryr).
- use all the other visible satellite measurements from all reference stations in Trop_NetAdjust and calculate residual tropospheric delay estimates for the predicted satellite at the computation point.
- apply the residual tropospheric delay estimates to the ionospheric-free (IF) DD raw measurements and calculate the corresponding corrected IF DD measurements. As the selected "new" satellite is from one of the observed satellites, the raw measurements of this satellite can be used for comparison of performance improvement.

5.3.1 Geim-Net test network

The same four baselines are chosen to provide examples of improvement prior to and after Trop_NetAdjust corrections. Figure 5.24 shows the prediction case for the Geim-Tron baseline where the "new" satellites are SV 1 and SV 19, whose changes in elevation and azimuth angles are shown in figure 5.24(c). When double differencing, the total residual tropospheric delay correction for a pair of satellite is the sum of the estimate for the new satellite and the estimate for the base satellite (which is usually the highest elevation satellite) at the computation point-Geim. The DD residual improvement after Trop_NetAdjust corrections are applied is significant, at over 50%. Figures 5.25, 5.26 and 5.27 also show significant improvements for Geim-Kris, Geim-Berg and Geim-Tryr baselines. For Geim-Kris, satellite SV10 and SV 7 are assumed to be the new satellites for the Trop_NetAdjust prediction. For Geim-Berg, the new satellites are SV 17 and SV 30. For Geim-Tryr, SV 22 and SV 26 are calculated as the new satellites. The corresponding elevation and azimuth angles with respect to each satellite pair are shown in the set (c) of each figure.

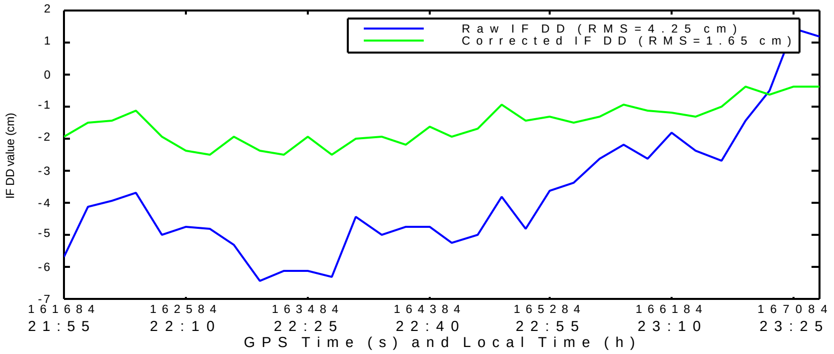

Figure 5.24(a): Geim-Tron (372 km) for PRN 5-1, new PRN 1 (RMS improv.=61%)

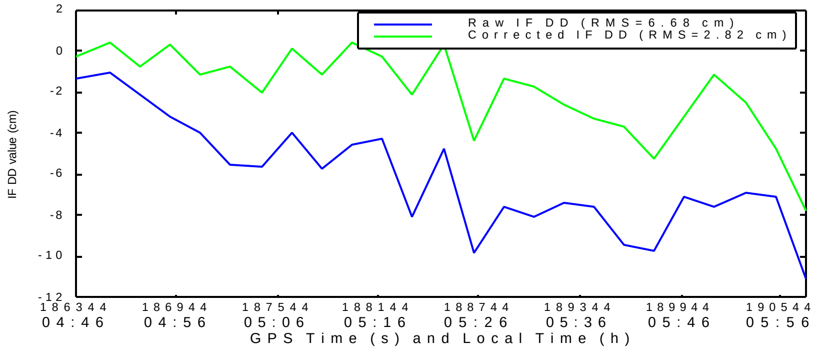

Figure 5.24(b): Geim-Tron (372km) for PRN3-19, new PRN 19(RMS improv.=57%)

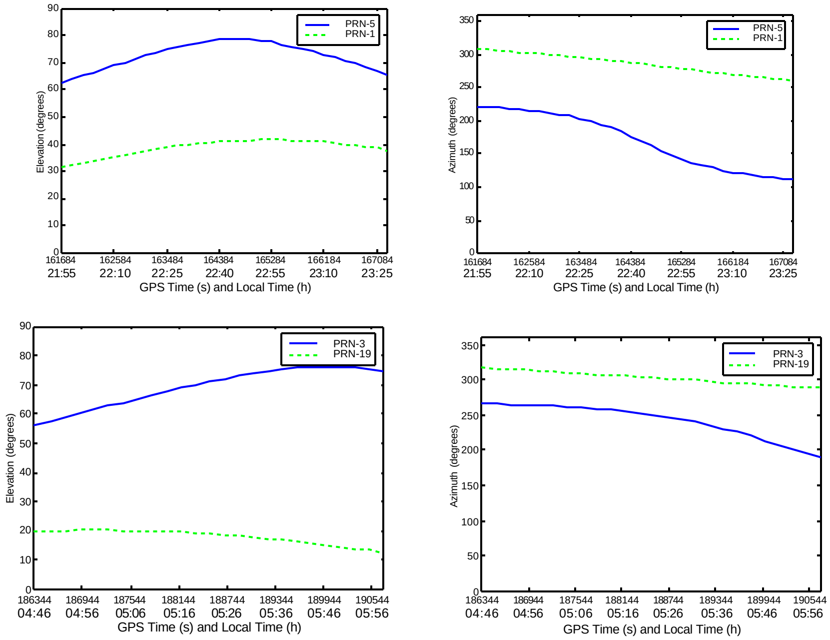

Figure 5.24 (c): Elevation and azimuth angles for satellite pairs PRN 5-1 and PRN3-19

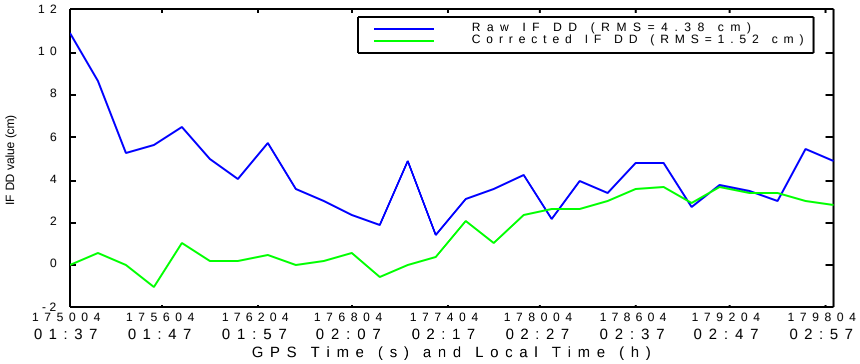

Figure 5.25(a): Geim-Kris (272 km) for PRN 6-10, new PRN 10 (RMS improv. =65%)

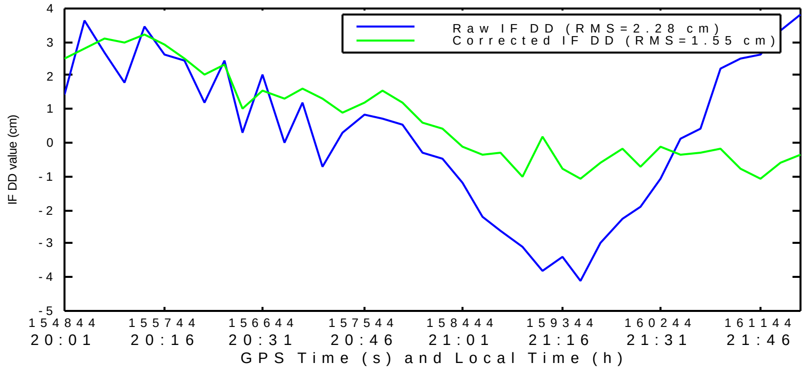

Figure 5.25(b): Geim-Kris (272 km) for PRN 9-7, new PRN 7 (RMS improv. =32%)

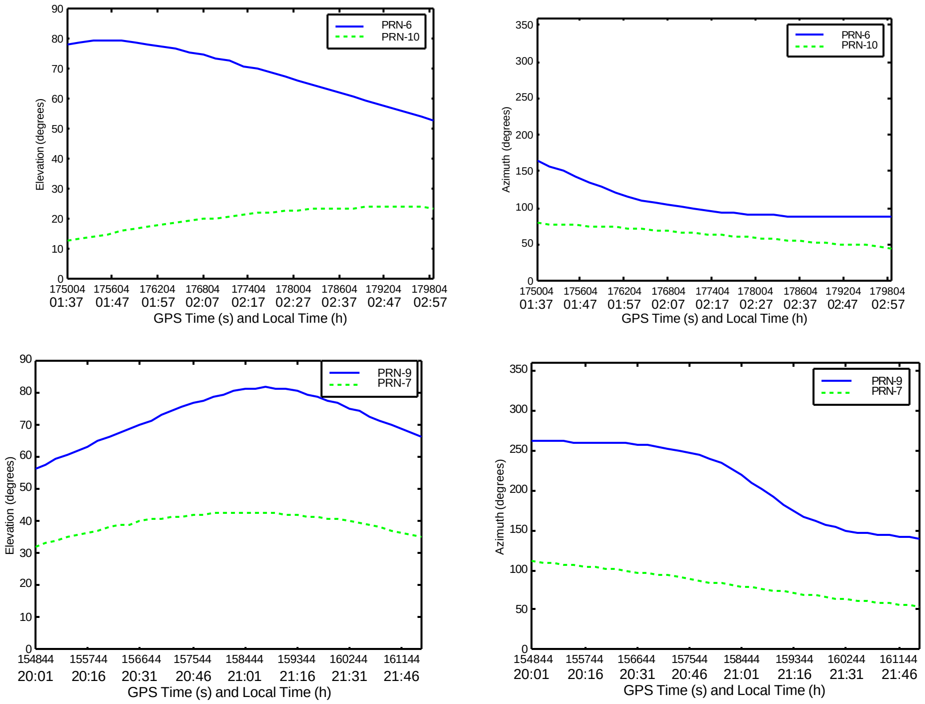

Figure 5.25 (c): Elevation and azimuth angles for satellite pairs PRN 6-10 and PRN 9-7

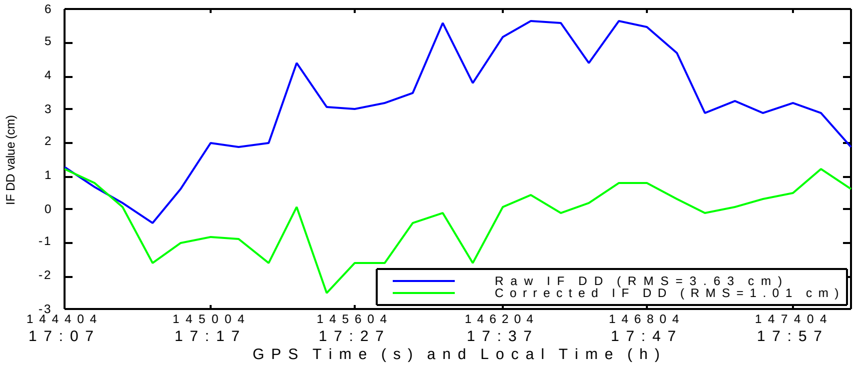

Figure 5.26(a): Geim-Berg(163 km) for PRN 27-17, new PRN 17(RMS improv.=72%)

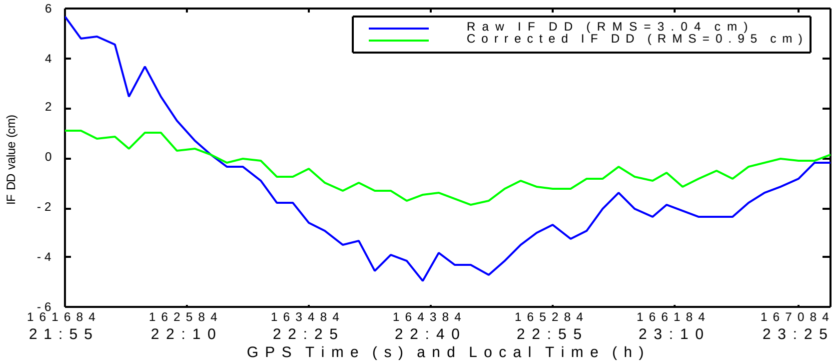

Figure 5.26(b): Geim-Berg(163 km) for PRN 5-30, new PRN 30 (RMS improv.=69%)

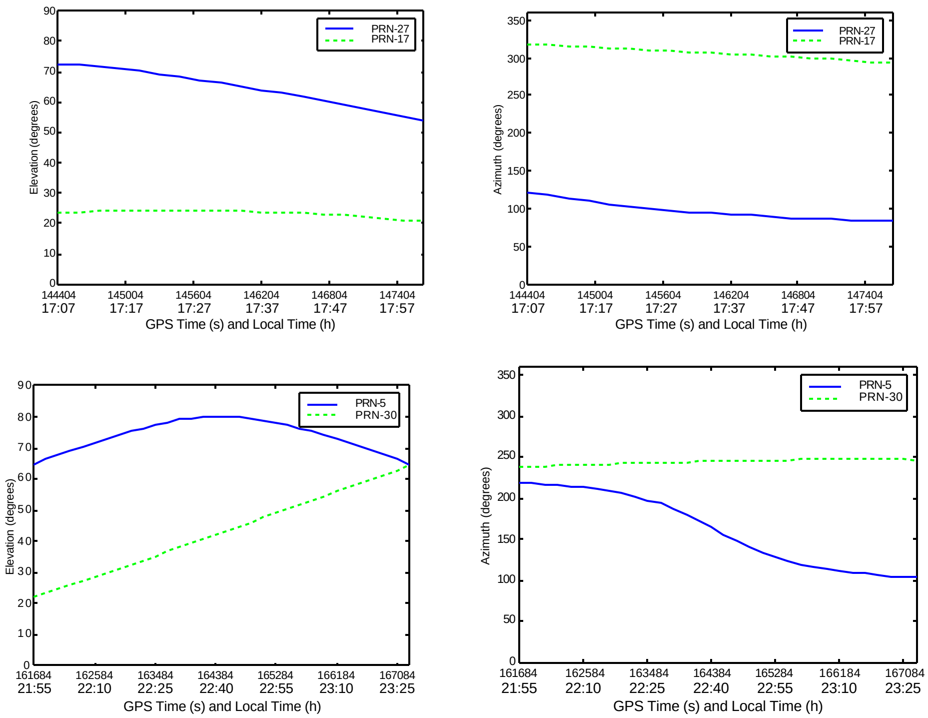

Figure 5.26(c): Elevation and azimuth angles for satellite pairs PRN 27-17 and PRN 5-30

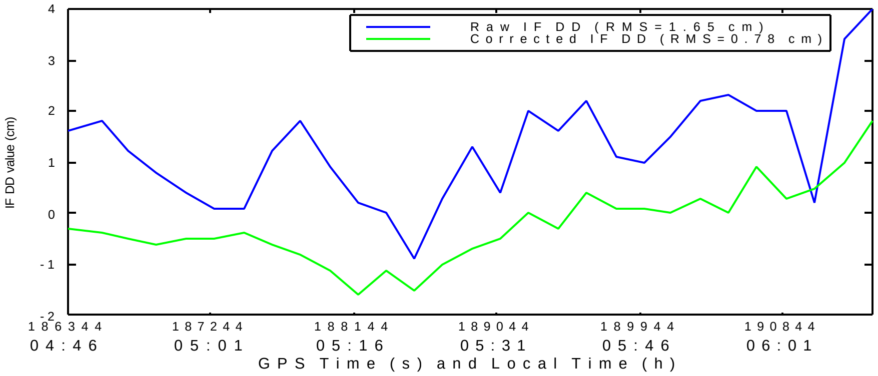

Figure 5.27(a): Geim-Tryr(276 km) for PRN 3-22, new PRN 22(RMS improve.=53%)

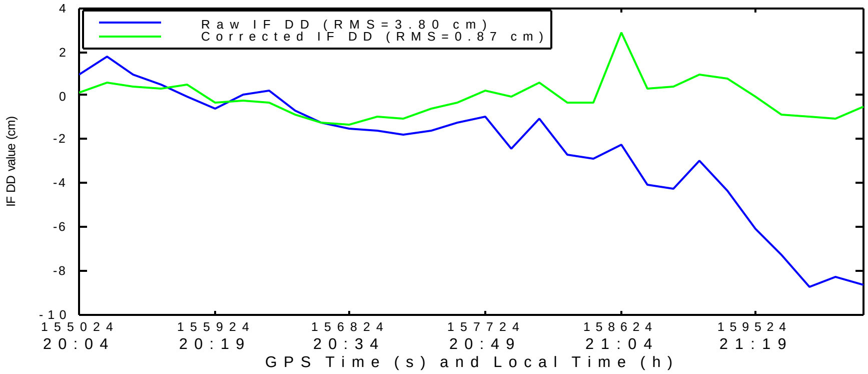

Figure 5.27(b): Geim-Tryr(276 km) for PRN 9-26, new PRN 26(RMS improve.=77%)

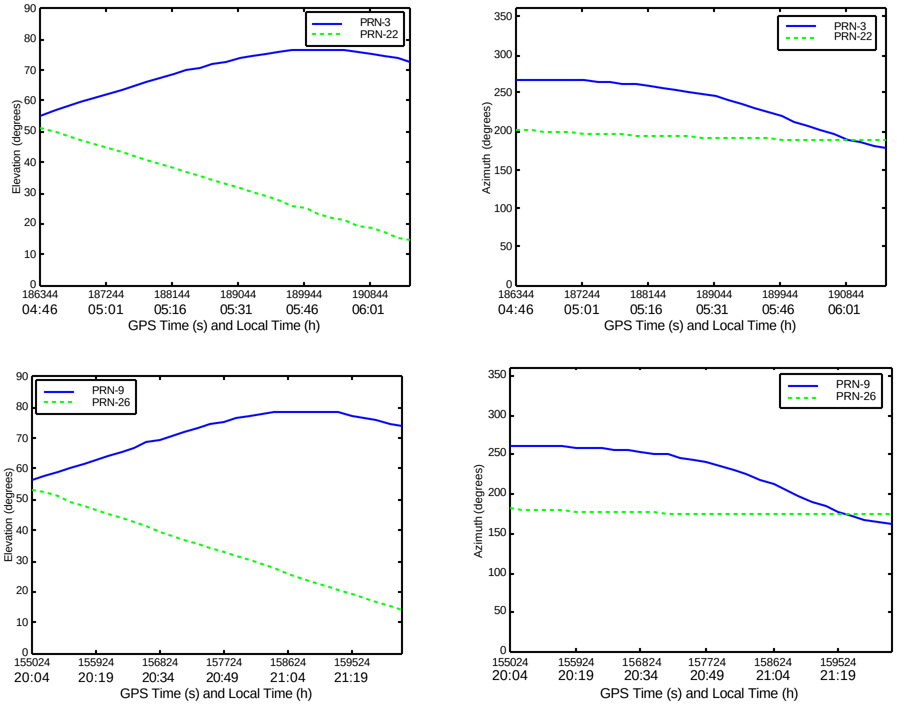

Figure 5.27(c): Elevation and azimuth angles for satellite pairs PRN 3-22 and PRN 9-26

5.3.1.1 Statistical analysis for Trop_NetAdjust performance

In order to analyze the performance improvement of Trop_NetAdjust for the new satellite prediction case, the same 15 hours of data at a 3-minute sampling rate was processed for statistical analysis. For this analysis, the following steps were implemented:

1) Choose "Geim" as the "mobile" receiver (computation point).
2) Each existing satellite is sequentially omitted and used as the new satellite.
3) Choose seven test baselines from Geim which are along different directions to each other, as shown in figure 5.4.
4) For each baseline, Trop_NetAdjust estimated residual tropospheric delay for the "selected" new satellite is calculated using all available measurements from all reference stations to all other visible satellites.
5) For each baseline, Trop_NetAdjust residual tropospheric delay corrections were calculated as the sum of the estimate at the "mobile" receiver for the "selected" new satellite and the estimate at the corresponding reference receiver for the same new satellite.
6) For each baseline, apply this Trop_NetAdjust residual tropospheric delay correction to raw ionospheric-free double difference measurements to obtain the corrected ionospheric-free double difference measurements.
7) For each baseline, calculate the RMS for each double difference (DD) satellite-receiver pairs for raw and corrected measurements, respectively.
8) Compare the RMS percentage improvement between raw and corrected measurements.

In figures 5.28 to 5.31, a comparison between the raw and corrected measurements is shown among Geim-Tron, Geim-Kris, Geim-Berg and Geim-Tryr baselines. The improvement prior to and after, applying Trop_NetAdjust is above 55% in all cases. All of the seven baseline test results are summarized in figure 5.32 and Table 5.4. Since seven satellites were generally available, the Trop_NetAdjust prediction was normally based on six satellites' measurements as one of the seven satellites was selected as the "new" one. Since these predictions were made every three minutes, the rms values for each case over the 15 hour time period are based on approximately 1,500 DD measurements.

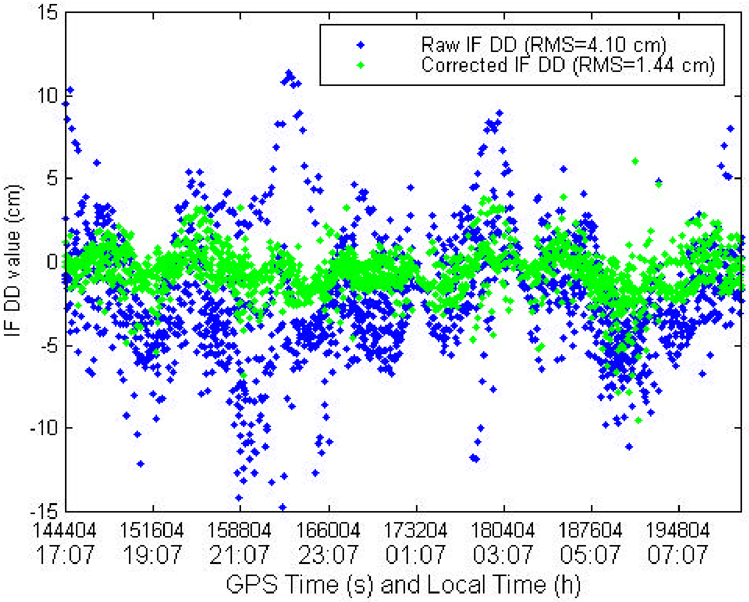

Figure 5.28: Time series of IF double difference measurements for Geim-Tron baseline (372km)—65% improvement percentage

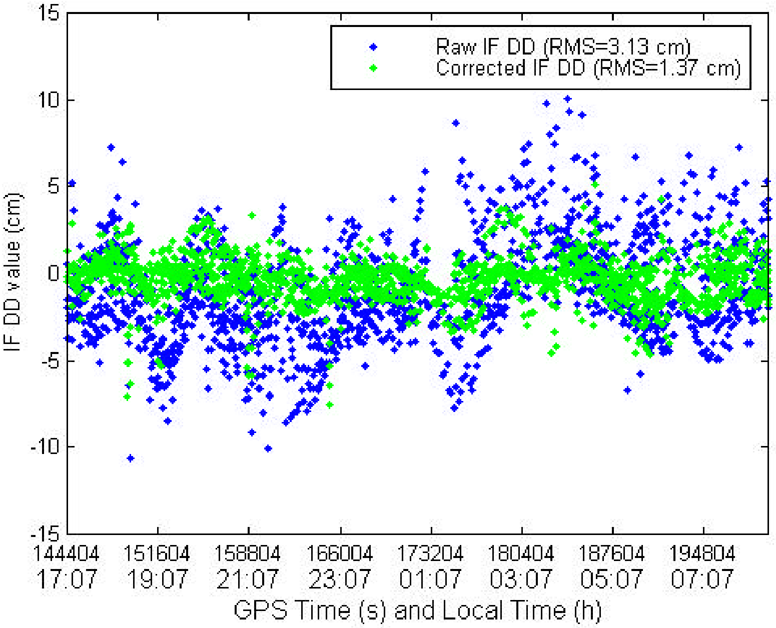

Figure 5.29: Time series of IF double difference measurements for Geim-Kris baseline (272km)—56% improvement percentage

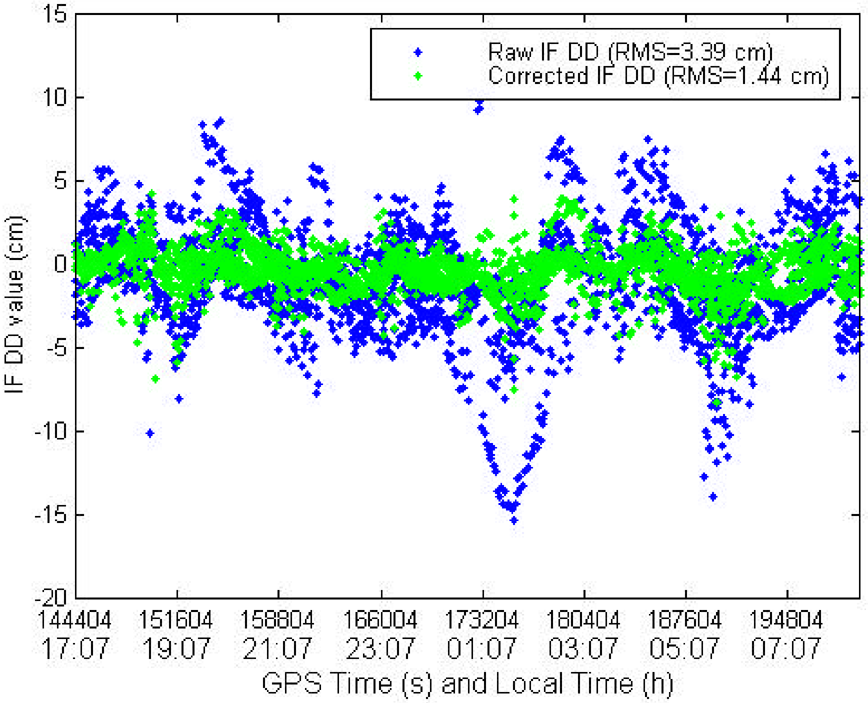

Figure 5.30: Time series of IF double difference measurements for Geim-Berg baseline (163km)—61% improvement percentage

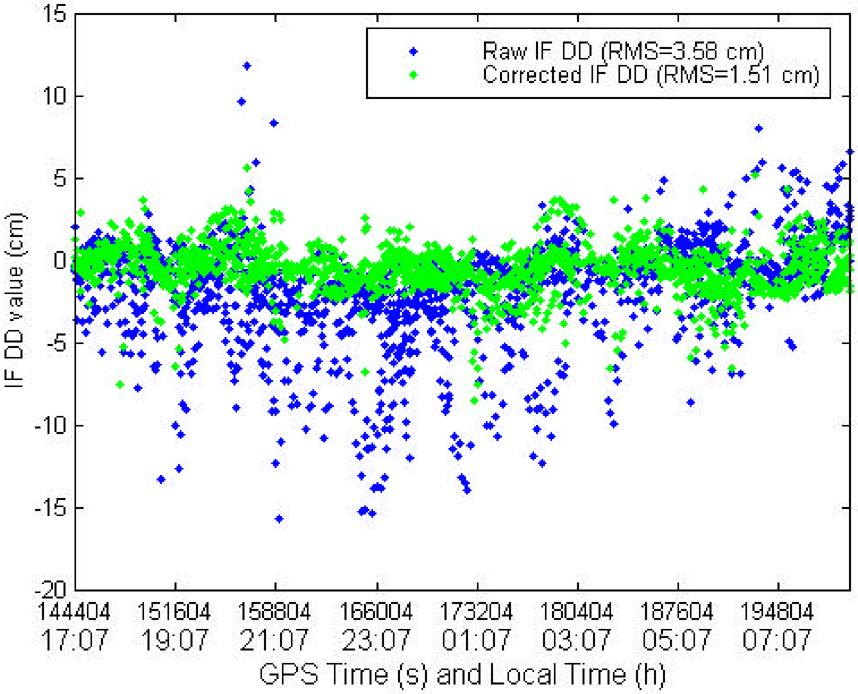

Figure 5.31: Time series of IF double difference measurements for Geim-Tryr baseline (276km)—58% improvement percentage

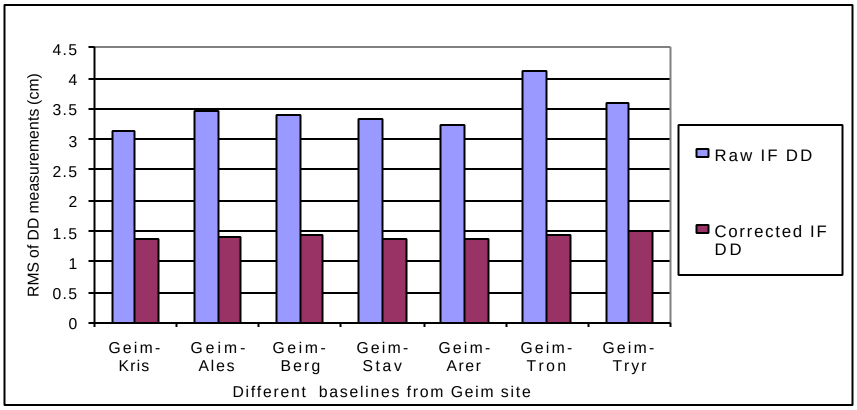

Figure 5.32: Stochastic RMS residual analysis - Geim-Net (seven baselines), new satellite case

Table 5.4: RMS residual improvement - Geim-Net, new satellite case

Baselines	DD RMS residuals (no residual tropo corr) (cm)	DD RMS residuals (residual tropo corr) (cm)	Percentage improvement (%)
Geim - Kris (272 km)	3.13	1.37	56%
Geim- Ales (242 km)	3.46	1.41	59%
Geim-Berg (163 km)	3.39	1.44	61%
Geim –Stav (222 km)	3.33	1.38	58%
Geim –Arer (223 km)	3.24	1.37	58%
Geim Tron (372km)	4.10	1.44	65%
Geim - Tryr (276 km)	3.58	1.51	58%

5.3.2 Tryr-net test network

For the second Tryr test net, the corresponding results are shown in figures 5.33 to 5.36. Different new satellites are chosen in these figures. The computation point is the "Tryr" site. In figure 5.33, satellite SV 17 and SV 5 are processed as the "new" satellites for the baseline Tryr-Tron. The elevations and azimuths of the DD satellite pairs are shown in figure 5.33(c). Figures 5.34, 5.35, and 5.36 present more time series examples for the double difference measurements with the "new" satellites according to Tryr-Kris, Tryr-Geim and Tryr-Berg baselines. The elevation and azimuth angles of each satellite DD pair are shown in the set (c) of each figure.

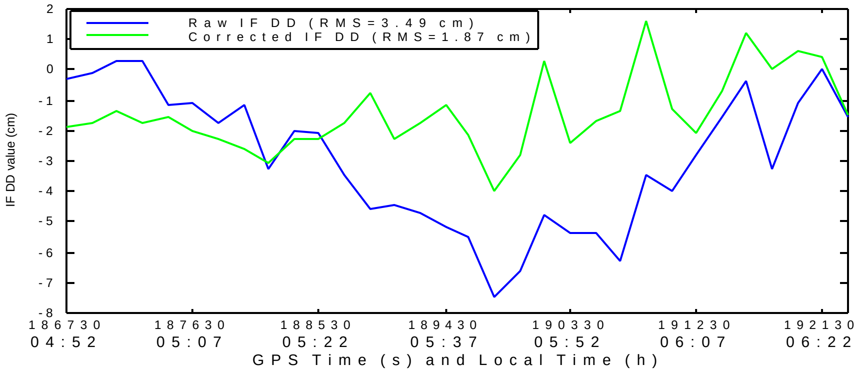

Figure 5.33(a): Tryr-Tron (220 km) for PRN 3-17, new PRN 17 (RMS improv.=46%)

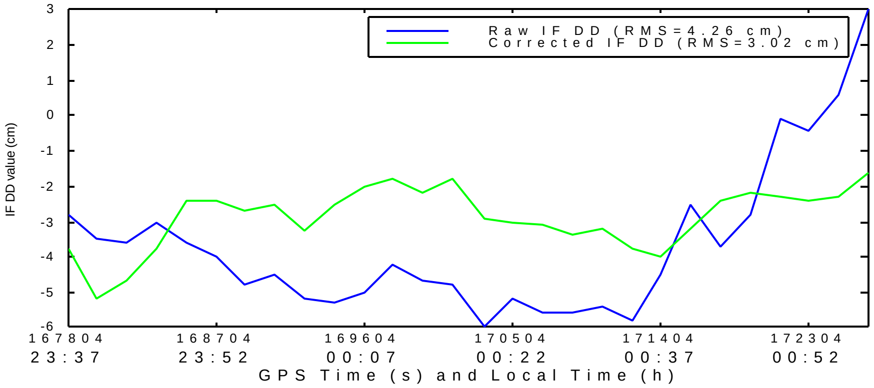

Figure 5.33(b): Tryr-Tron (220 km) for PRN 30-5, new PRN 5 (RMS improv.=29%)

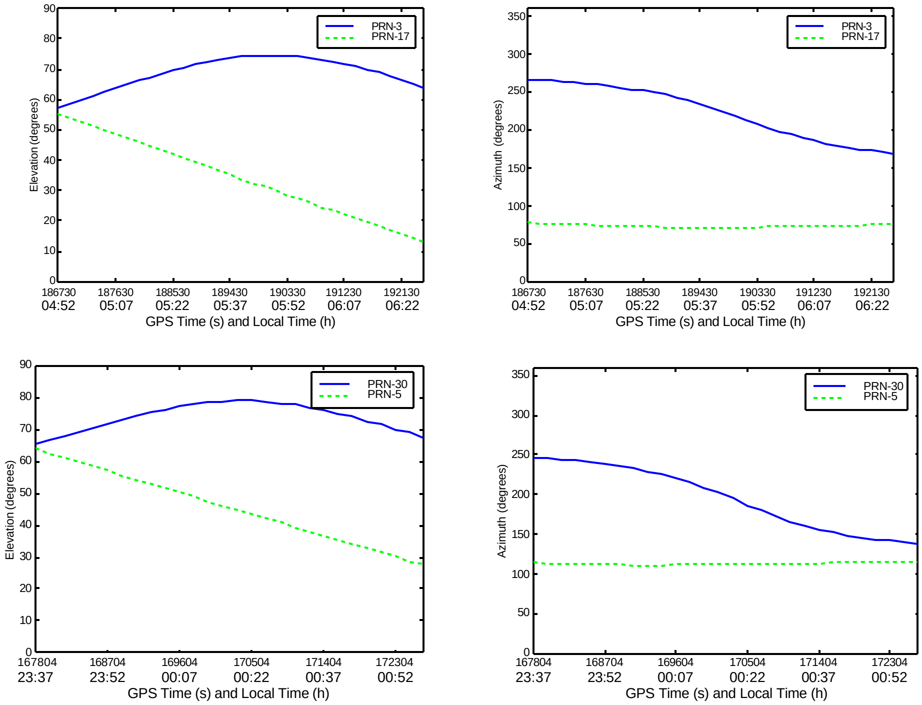

Figure 5.33(c): Elevation and azimuth angles for PRN 3-17 and PRN 30-5

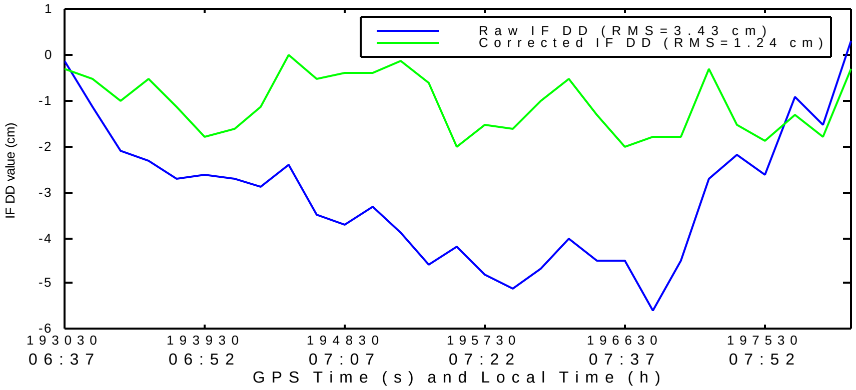

Figure 5.34(a): Tryr-Kris (448km) for PRN 31-3, new PRN 3 (RMS improv.=63%)

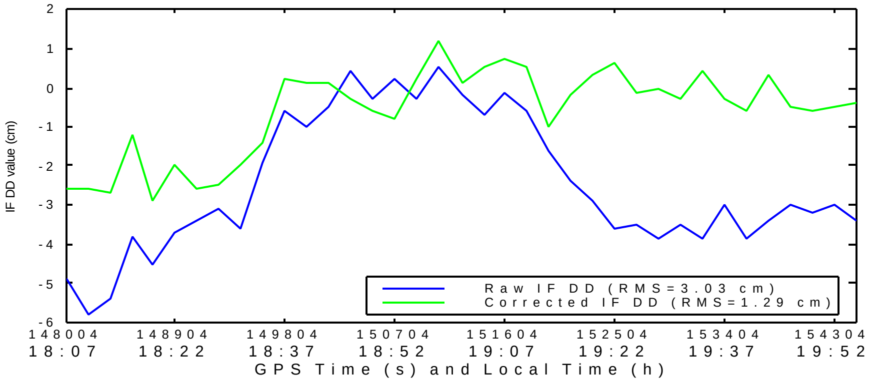

Figure 5.34(b): Tryr-Kris (448km) for PRN 26-2, new PRN 2 (RMS improv.=57%)

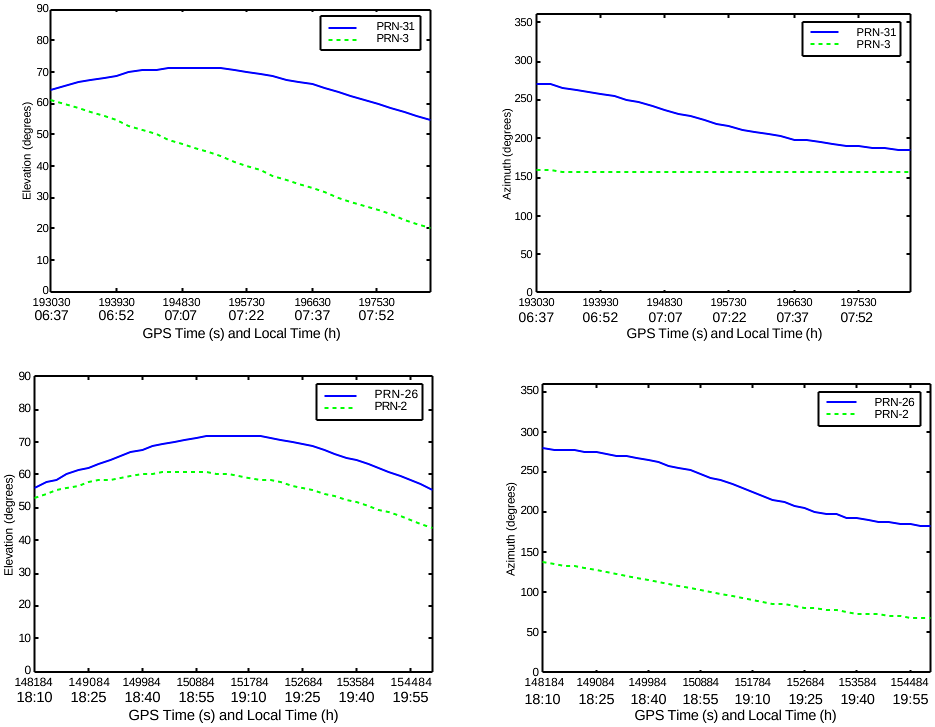

Figure 5.34(c): Elevation and azimuth angle for PRN 31-3 and PRN 26-2

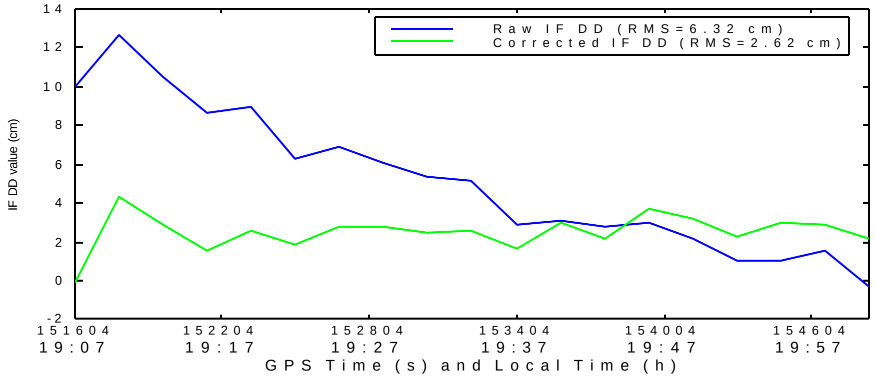

Figure 5.35(a): Tryr-Geim (276km) for PRN 26-7, new PRN 7 (RMS improv.=59%)

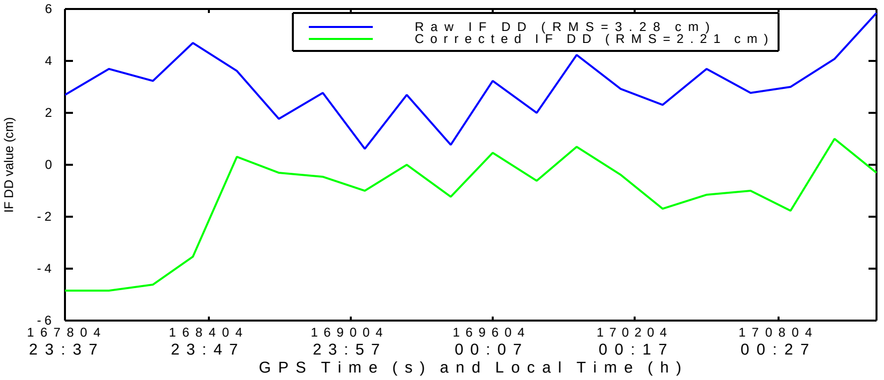

Figure 5.35(b): Tryr-Geim(276km) for PRN 30-29,new PRN 29(RMS improv.=33%)

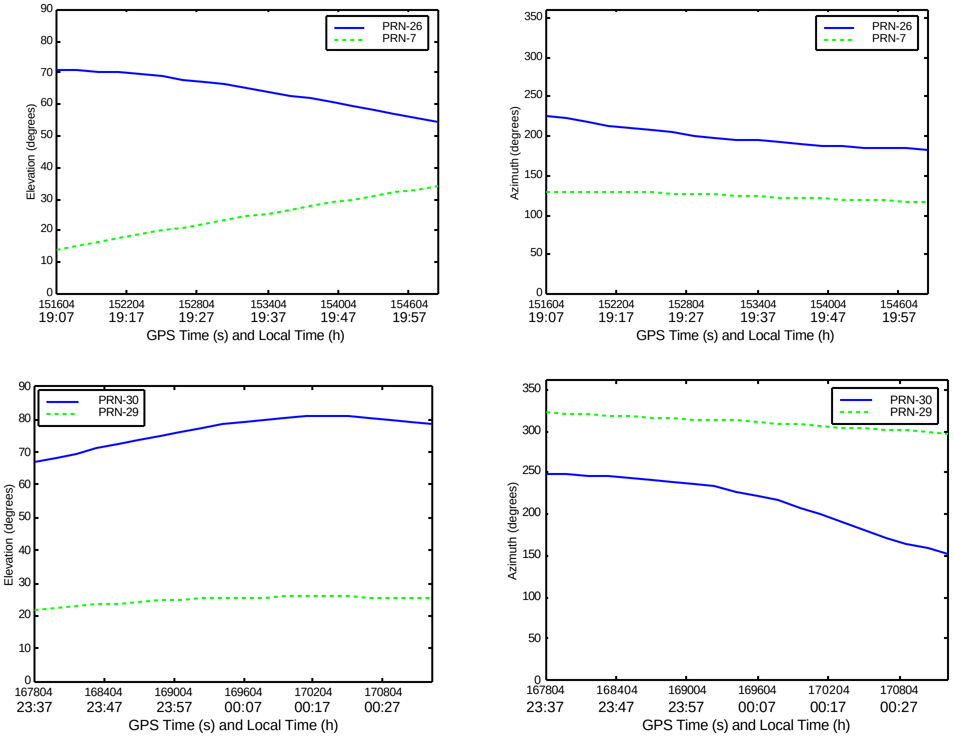

Figure 5.35(c): Elevation and azimuth angles for PRN 26-7 and PRN 30-29

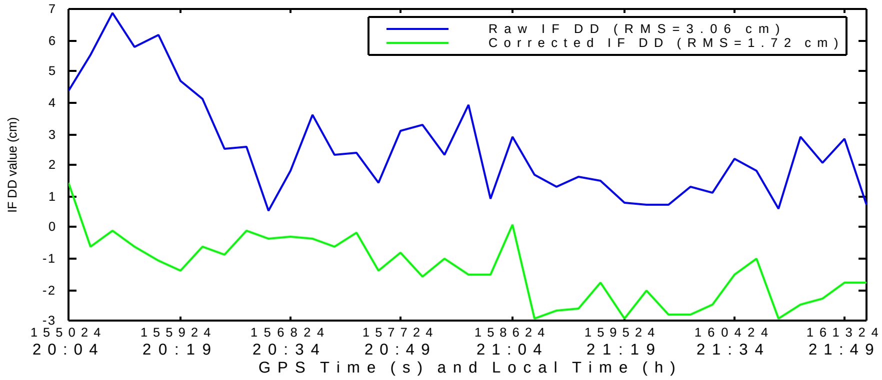

Figure 5.36(a): Tryr-Berg (406km) for PRN 9-7, new PRN 7 (RMS improv.=43%)

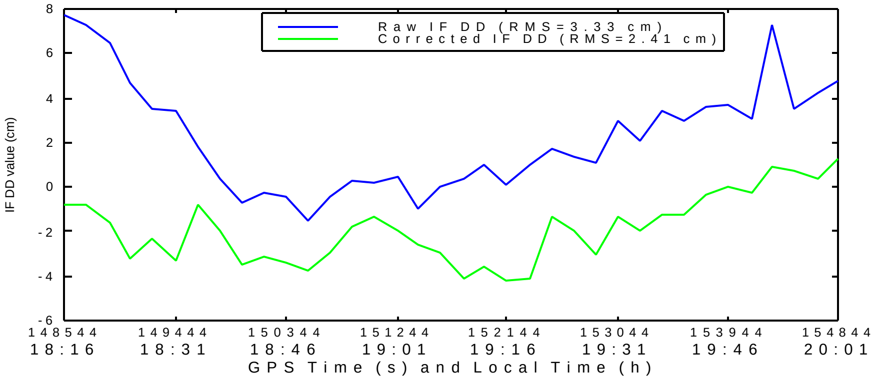

Figure 5.36(b): Tryr-Berg(406km) for PRN 26-23, new PRN 23(RMS improv.=28%)

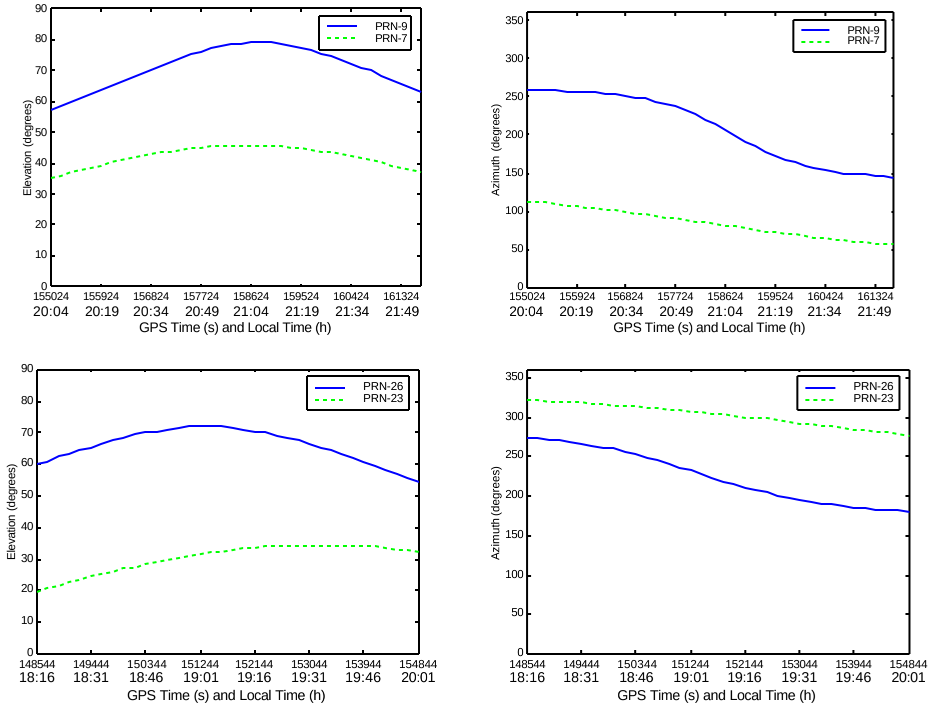

Figure 5.36(c): Elevation and azimuth angles for PRN 9-7 and PRN 26-23

5.3.2.1 Statistical analysis of Trop_NetAdjust performance

To analyze the performance improvement of Trop_NetAdjust, the same 15 hours of data at 3-minute sampling rate was processed. To implement this statistical analysis, the steps followed was:

1) Choose "Tryr" as the "mobile" receiver (computation point).
2) Each existing satellite was sequentially assumed to be missing and used as the new satellite.
3) Choose seven test baselines from Tryr to different directions, as shown in figure 5.14.
4) For each baseline, the Trop_NetAdjust residual tropospheric delay for the "selected" new satellite was calculated by using measurements from all reference stations to all the other visible satellites.
5) For each baseline, Trop_NetAdjust corrections were calculated as the sum of the estimate at "mobile" receiver for this "selected" new satellite and the estimate at the corresponding reference receiver for the same new satellite.
6) For each baseline, apply this Trop_NetAdjust correction to raw ionospheric-free double difference measurements.
7) For each baseline, calculate the RMS of raw measurements for each double difference (DD) satellite-receiver pair and corrected measurement, respectively.
8) Compare RMS improvements between raw and corrected measurements.

Figures 5.37 to 5.40 show a comparison between raw and corrected measurements with respect to the following four baselines: Tryr-Tron, Tryr-Kris, Tryr-Geim and Tryr-Berg. The improvement with Trop_NetAdjust can be clearly seen and range from 23% to 44%. The seven baselines test results are summarized in figure 5.41 and Table 5.5. The improvement when the tropospheric residual corrections are applied is still at the 30% level. The reason that the improvement is lower than in the previous case is the geometry of the network and the sub-optimal location of Tryr at the eastern limit of the network.

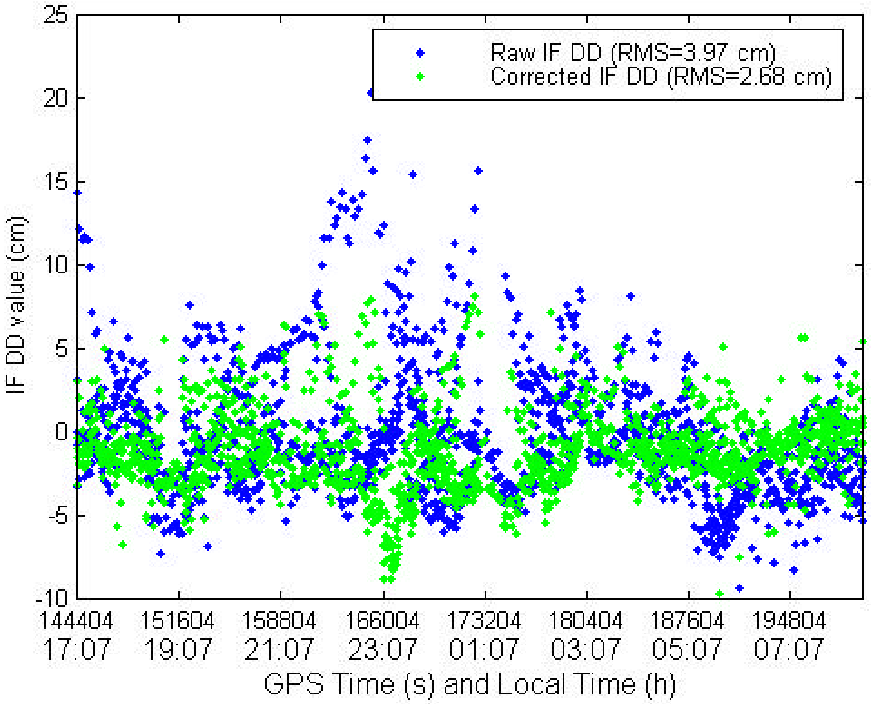

Figure 5.37: Time series of IF double difference measurements for Tryr-Tron baseline (220km)—32% improvement percentage

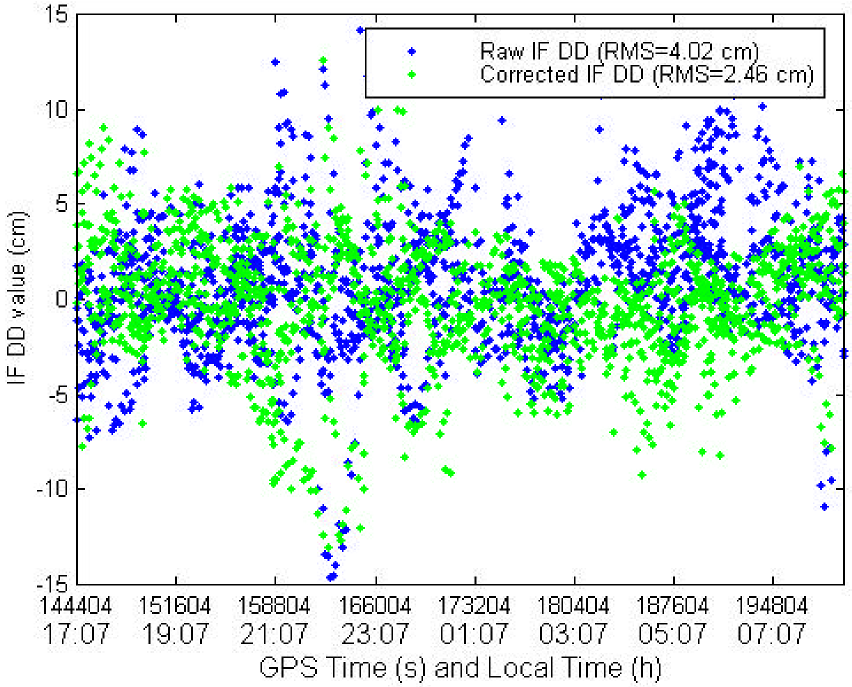

Figure 5.38: Time series of IF double difference measurements for Tryr-Kris baseline (448km)—38% improvement percentage

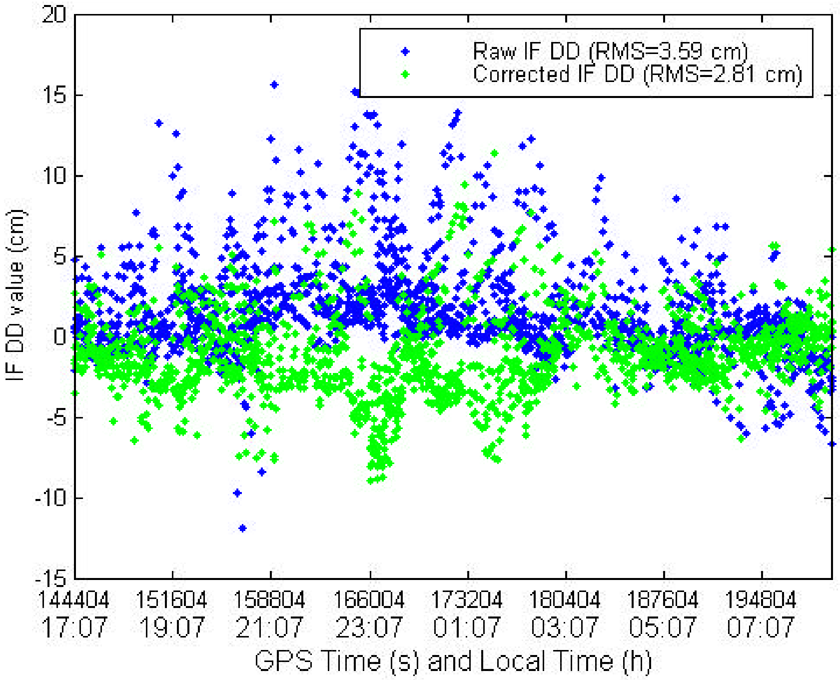

Figure 5.39: Time series of IF double difference measurements for Tryr-Geim baseline (276km)—23% improvement percentage

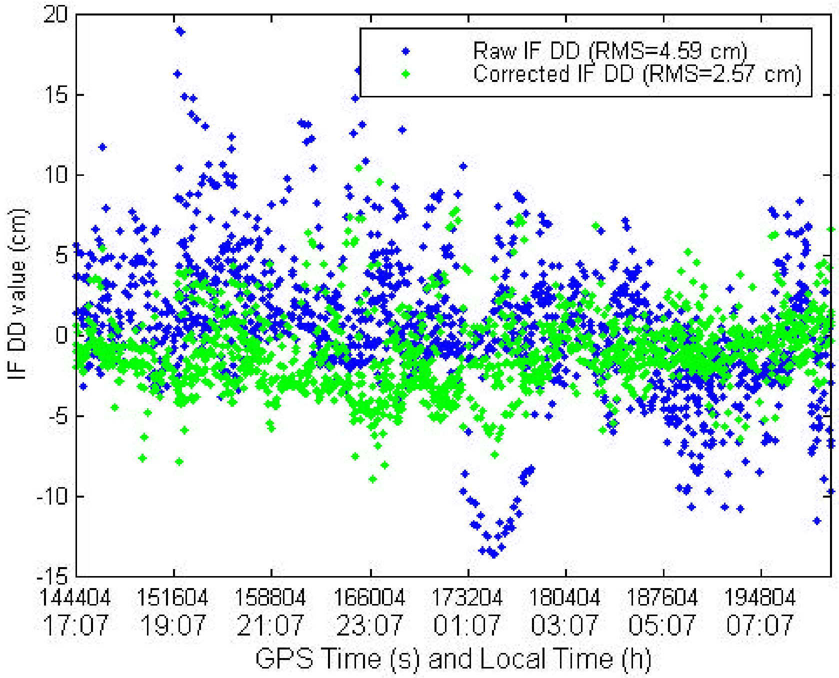

Figure 5.40: Time series of IF double difference measurements for Tryr-Berg baseline (406km)—44% improvement percentage

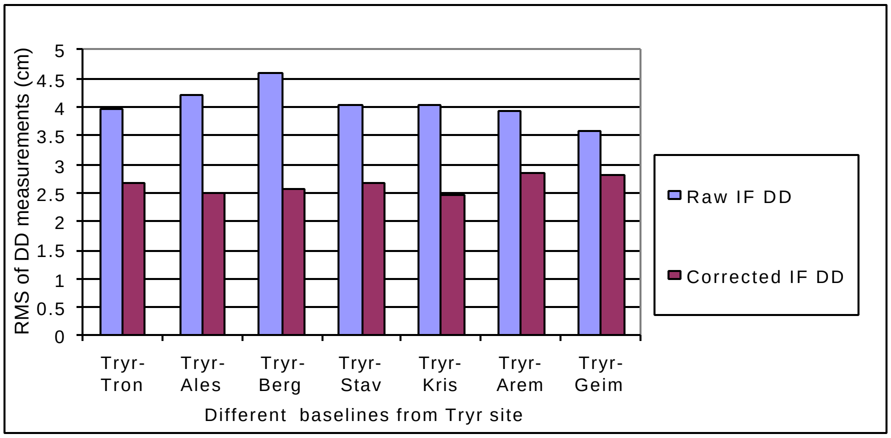

Figure 5.41: Stochastic RMS residual analysis - Tryr-Net (seven baselines), new satellite case

Table 5.5: RMS residual improvement - Tryr-Net, new satellite case

Baselines	DD RMS residuals (no residual tropo corr) (cm)	DD RMS residuals (residual tropo corr) (cm	Percentage improvement (%)
Tryr-Tron (220 km)	3.97	2.68	32%
Tryr-Ales (344 km)	4.20	2.49	40%
Tryr-Berg (406 km)	4.59	2.57	44%
Tryr-Stav (461 km)	4.05	2.68	33%
Tryr-Kris (448 km)	4.02	2.46	38%
Tryr-Arem (384 km)	3.93	2.85	28%
Tryr-Geim (276 km)	3.59	2.81	22%

5.4 Analysis of Trop_NetAdjust performance improvement versus satellite elevation

To analyze the Trop_NetAdjust performance improvement with respect to satellite elevations, the double difference measurements with and without Trop_NetAdjust corrections were compared to obtain the RMS percentage improvement based on the remote satellite elevations. The remote satellite elevations were divided into six groups, namely 10^o-20^o, 20^o-30^o, 30^o-40^o, 40^o-50^o, 50^o-60^o, and 60^o-70^o.

The same test nets were used to compare the differences between the performance improvement with respect to satellite elevations. They are Geim-Net and Tryr-Net, as shown in figures 5.2 and 5.3. For Geim-Net, the "mobile" receiver was located at Geim and for Tryr-Net, the "mobile" receiver was Tryr. Figure 5.42 shows the location of the reference receivers and the triangles represent the "mobile" receivers.

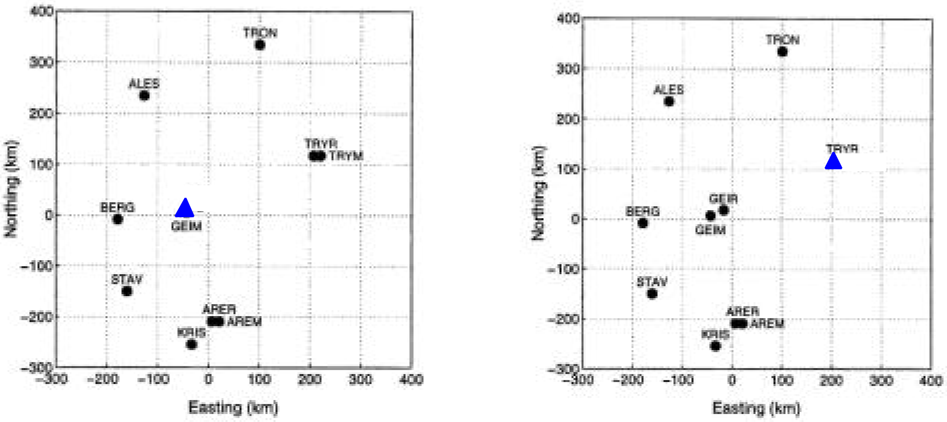

Figure 5.42 Reference and "mobile" receivers

For these tests, Trop_NetAdjust was used to calculate the estimates of residual tropospheric delays at the computation point ("mobile" receiver) and at the reference receiver. Using the sum of these estimates, the residual tropospheric delay corrections for a double difference receiver pair were then calculated. Applying these corrections to the raw IF double difference measurements, a significant decrease was achieved because of the predicted corrections. It should be noted that the following analysis is based on the previous "new station" prediction case discussed in section 5.2.

Geim-Net:

For each elevation range, the RMS percentage improvement between raw and corrected ionospheric-free double difference measurements after applying Trop_NetAdjust estimates are listed in Table 5.6.

Table 5.6: RMS percentage improvement as a function of elevation range

Baselines	Remote Satellite Elevation (degrees)																	
	10^{o}-20^{o}			20^{o}-30^{o}			30^{o}-40^{o}			40^{o}-50^{o}			50^{o}-60^{o}			60^{o}-70^{o}		
	Raw (cm)	Cor. (cm)	%	Raw (cm)	Cor. (cm)	%	Raw (cm)	Cor. (cm)	%	Raw (cm)	Cor. (cm)	%	Raw (cm)	Cor. (cm)	%	Raw (cm)	Cor. (cm)	%
Geim-Tron	5.49	2.18	60%	4.08	1.41	66%	3.52	1.39	61%	3.36	1.42	58%	2.69	1.31	52%	2.06	1.04	49%
Geim-Ales	4.44	2.07	53%	2.50	1.39	45%	2.32	1.14	51%	2.23	1.23	45%	1.90	1.18	38%	1.35	0.72	47%
Geim-Berg	4.22	2.11	50%	2.54	1.40	45%	2.39	1.14	52%	2.12	1.20	43%	2.81	1.22	57%	1.45	0.72	50%
Geim-Stav	3.69	2.27	38%	2.77	1.47	47%	2.75	1.22	55%	3.00	1.33	55%	2.89	1.37	53%	2.74	0.88	68%
Geim-Kris	3.50	2.17	38%	2.56	1.37	46%	3.16	1.15	63%	3.40	1.20	65%	3.00	1.24	59%	2.27	0.82	64%
Geim-Arer	3.89	2.01	48%	2.05	1.44	30%	2.39	1.18	51%	2.90	1.20	59%	2.13	1.20	43%	1.28	0.83	35%
Geim-Tryr	6.02	2.47	59%	3.41	1.66	51%	2.42	1.31	46%	1.61	1.37	15%	0.77	1.24	-59%	0.82	0.89	-8%

*Raw: raw measurements; Cor.: corrected measurements; %: percentage improvement

Tryr-Net:

The RMS percentage improvements between raw and corrected ionospheric-free double difference measurements prior and after applying Trop_NetAdjust are listed in Table 5.7.

Table 5.7 RMS percentage improvement as a function of elevation range

Baselines	Remote Satellite Elevation (degrees)																	
	10^{o}-20^{o}			20^{o}-30^{o}			30^{o}-40^{o}			40^{o}-50^{o}			50^{o}-60^{o}			60^{o}-70^{o}		
	Raw (cm)	Cor. (cm)	%	Raw (cm)	Cor. (cm)	%	Raw (cm)	Cor. (cm)	%	Raw (cm)	Cor. (cm)	%	Raw (cm)	Cor. (cm)	%	Raw (cm)	Cor. (cm)	%
Tryr-Tron	5.51	3.74	32%	3.66	2.59	29%	3.60	2.28	37%	3.25	1.99	39%	2.53	1.62	36%	2.41	1.68	30%
Tryr-Ales	6.99	3.81	45%	4.13	2.60	37%	3.03	2.32	23%	2.27	2.05	10%	1.79	1.69	5%	1.40	1.97	-41%
Tryr-Berg	6.40	3.67	43%	4.13	2.55	38%	3.46	2.28	34%	3.05	2.03	34%	5.76	1.43	75%	3.65	1.49	59%
Tryr-Geim	6.22	4.07	35%	3.17	2.63	17%	2.09	2.32	-11%	1.16	2.00	-73%	0.80	1.71	-113%	0.80	1.77	-121%
Tryr-Stav	5.56	3.63	35%	4.10	2.57	37%	3.32	2.28	31%	3.26	1.98	39%	3.46	1.49	57%	3.28	1.34	59%
Tryr-Kris	6.54	3.70	43%	3.14	2.62	17%	3.01	2.20	27%	2.68	1.94	27%	3.01	1.65	45%	2.42	1.42	41%
Tryr-Arem	6.72	3.82	43%	2.94	2.60	12%	2.36	2.24	5%	2.18	1.96	10%	1.84	1.67	10%	0.99	1.45	-46%

*Raw: raw measurements; Cor.: corrected measurements; %: percentage improvement

Considering Table 5.6 and 5.7, one can see that the performance improvement is high, stable and consistent for low elevation satellites ($10^0 - 20^0$). Mostly the RMS percentage improvement can be as much as 60% for the Geim-Net and 45% for the Tryr-Net with little variations. However, the stochastic performance varies largely in the case of high elevation angles $(50^0 - 70^0)$ and the RMS percentage is negative for some baselines (Geim-Tryr for Geim-Net, Tryr-Geim, Tryr-Ales, and Tryr-Arem for Tryr-Net). In these cases, the Trop_NetAdjust approach yields poorer results than the uncorrected approach. This is due to the fact that the absolute values of the RMS of raw measurements for the negative improvement cases (high elevations) are already small considering the size of the error level typically caused by multipath and receiver noise. The values prior to the correction are in the order of 1 cm level. Therefore, even though having a negative improvement as much as -59% for Geim-Net and –121% for Tryr-Net, it does not usually increase the absolute value of RMS much and does not cause a problem in modeling the errors in the network.

In practice the largest effect of the tropospheric delay on GPS signal mostly results from the satellites with low elevations due to the limitation of the standard tropospheric model on low elevation satellites. Therefore, the stable performance of Trop_NetAdjust for satellites with low elevations is significant because there is still room for improvement.

It should be noted that accuracy estimates are also obtained when applying the prediction equations. The estimated covariance matrix of the predicted quantities is given by equation 4.43. The estimated standard deviations were compared to the RMS values obtained by comparing the predicted and ionospheric-free double differences. The agreement was consistently better than 30%, which is considered satisfactory. In this chapter, RMS values were used because they are considered more statistic since "true" double differences were used to generate them.

CHAPTER 6

ANALYSIS OF TROP_NETADJUST PERFORMANCE USING SWEDISH GPS NETWORK AND WVR

6.1 Description of Swedish GPS network

A permanent GPS network was designed for continuous measurements of the vertical and horizontal crustal deformations in Sweden and was built in cooperation with the Swedish National Land Survey (NLS). It currently consists of 21 continuously operating GPS stations, as shown in figure 6.1 (Onsala Space Observatory 1998). Some of the sites are situated in rather remote areas in order to meet the most important requirements, that is access to solid rock, low horizon mask, and no known construction plans that could cause interference problems in the future. The complete permanent GPS network spans 400 km x 1200 km in the east-west and north-south directions, respectively. The average separation between the sites is about 200 km but baselines as short as 100 km also exist. The coordinates of these 21 GPS stations are listed in Table 6.1 (Emardson, 1998).

Table 6.1 GPS sites in Swedish network

GPS site (Acronym)	Latitude (^{o}N)	Longitude (^{o}E)	Ellipsoidal Height (m)
Kiru	67.8775731694	21.0602357889	497.971
Over	66.3178559833	22.7733696333	222.863
Arje	66.3180157556	18.1248613444	489.138
Skel	64.8791947806	21.0482860333	81.161
Vilh	64.6978448944	16.5599274667	449.925
Umea	63.5781365000	19.5095933444	54.463
Oste	63.4427912833	14.8580652667	490.011
Sund	62.2324726806	17.6598842861	31.753
Sveg	62.0174110417	14.7000094778	491.168
Leks	60.7221427556	14.8770045972	478.080
Mart	60.5951411833	17.2585225583	75.359
Karl	59.4440186694	13.5056223667	114.268
Lovo	59.3378002361	17.8289125694	79.597
Vane	58.6931248972	12.0350002278	169.674
Norr	58.5902290806	16.2463792417	40.907
Jonk	57.7454712583	14.0596060222	260.362
Bora	57.7149560028	12.8913456806	219.919
Visb	57.6538673278	18.3673131306	79.766
Onsa	57.3952962361	11.9255139861	45.570
Oska	57.0656366972	15.9968067000	149.769
Hass	56.0922150222	13.7180735528	114.045

In order to achieve similar operating conditions at all sites, a careful design was done. The network uses 14 SNR-8000 TurboRogue and 28 Ashtech-Z12 GPS receivers. At several permanent GPS sites located in areas with periodically severe environmental conditions, such as snow or heavy rain, radomes have been employed. In order to maintain network homogeneity, all sites have been equipped with radomes since the start of the network in 1993. All receivers provide code and carrier phase observables on both frequencies, even when Anti-Spoofing (AS) is enabled, utilizing the cross correlation technique.

Figure 6.1: Swedish GPS network

6.2 Water vapor radiometer at Onsala

One of the tasks of the Onsala Space Observatory is to monitor the wet delay using a microwave water vapor radiometer (WVR). The radiometer measures the radiation from the atmosphere at two different frequencies, 21.0 and 31.4 GHz. This data can be used to infer the total amount of water vapor and cloud liquid water in the atmosphere along the direction of the observation. With this instrument we can study variation in the wet delay.

The radiometer is mounted on a foundation some ten metres from, and at approximately the same height as, the GPS antenna where the radome of a 20m radio-telescope results in a relatively small sky blockage. The installed microwave radiometer is shown in figure 6.2 (Onsala Space Observatory 1998).

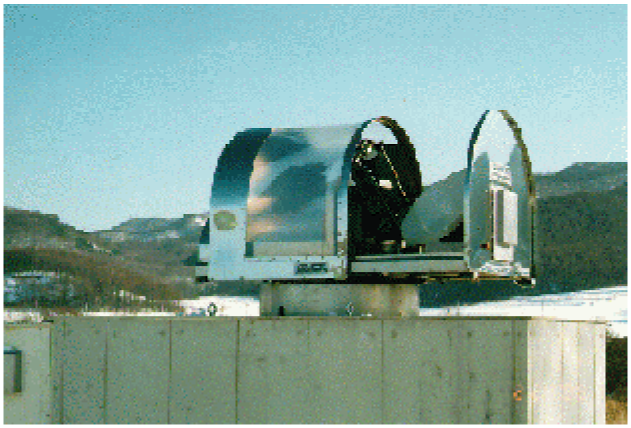

Figure 6.2: Water vapor radiometer at Onsala

Elgered (1993) gives the wet delay estimate from a WVR, measuring the emission at two different frequencies v_1 and v_2, as

$$l_w = c_b X_b \tag{6.1}$$

where X_b is formed from the observables as

$$X_b = (\frac{v_2}{v_1})^2 T'_{v_1} - T'_{v_2} - T_{bg,ox} \tag{6.2}$$

where $T_{bg,ox}$ is the equivalent temperature of the cosmic background and the atmospheric oxygen. T'_{v_1} and T'_{v_2} are the linearized brightness temperatures and can be determined from the measured brightness temperature T_{v_1} and T_{v_2} as (Jarlemark 1994)

$$T'_v = T_{bg} - (T'_{eff} - T_{bg}) \ln(1 - \frac{T_v - T_{bg}}{T_{eff} - T_{bg}}) \tag{6.3}$$

where T_{bg} is the cosmic background radiation, T_{eff} and T'_{eff} are the effective temperature and linearized effective temperature of the atmosphere respectively. The two latter temperatures are determined by the temperature profile of the atmosphere and the height profile of the atmospheric absorption in the microwave range due to water vapor. The coefficients c_b in equation 6.1 can be modeled using meteorological surface data. Elgered (1993) suggests three different models, where the simplest is a constant and the most sophisticated is

$$c = c_{eff}(1 + a_1 P_\Delta + a_2 T_\Delta + a_3 X_\Delta) \tag{6.4}$$

where the coefficients c_{eff} and a_n can be estimated using radiosonde profiles. P_Δ, T_Δ and X_Δ are the deviations from the mean for the pressure, the temperature at the ground and the observable X_b from equation 6.1 respectively.

6.3 Analysis of Trop_NetAdjust prediction of residual tropospheric delays in the double difference measurement domain

As shown in figure 6.3, a sub-network with five stations in the southern part of Sweden is used for this test. The acronyms of these five stations are Jonk (Jönköping), Vane (Vänersborg), Karl (Karlstad), Bora (Borås) and Hass (Hässleholm). The GPS measurements were made on April 30, 1998. The GPS sampling data rate was five seconds and the mask angle was 10^o. The Bora reference receiver is selected as the "mobile" receiver for residual tropospheric delay prediction because the actual GPS measurements at the reference station Bora can be used to externally assess the accuracy of the predicted values. The measurements at the Bora station are excluded from the data set used in the Trop_NetAdjust prediction.

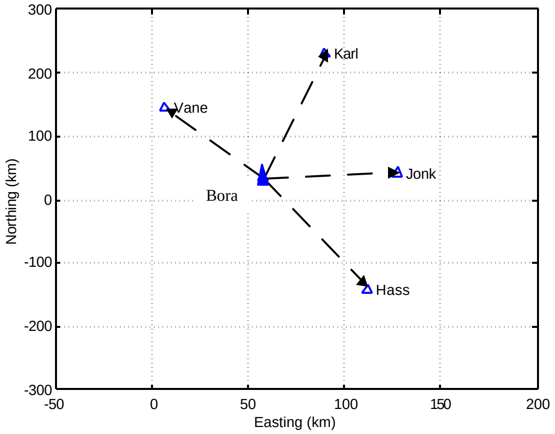

Figure 6.3: Four baselines from Bora to other reference stations

In order to present the results of the Trop_NetAdjust method, the residual tropospheric delay is estimated at the Bora site using Trop_NetAdjust. To test the improvement, the estimated residual tropospheric delay is applied to the ionospheric-free double difference measurements based on the predicting station location and other reference stations. Analysing the reduction in the double difference errors provides us a good method to test how well the residual tropospheric delay is estimated at the Bora site. The basic approach was illustrated in Chapter 5.

To relax the computational burden, 21 hours of the data at a two-minute rate was processed for statistical analysis. During the test, five or more satellites were typically visible at any time at each receiver site. The number of observed satellites is shown in figure 6.4. The number of observed satellites shown here is the average value of the number of observed satellites from all of the reference stations in the test network.

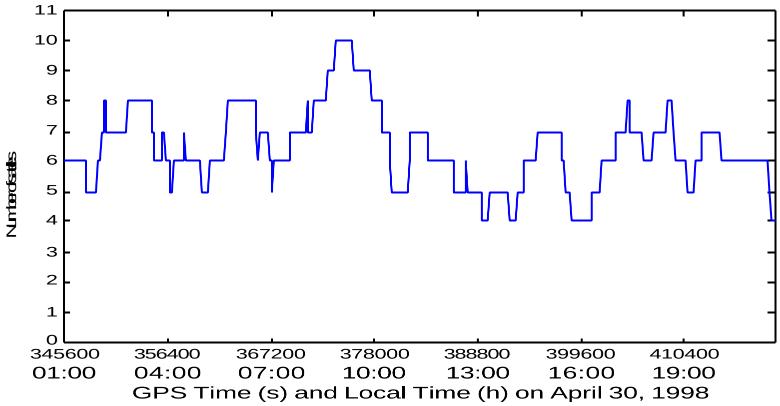

Figure 6.4: Average number of visible satellites from four stations on 30/04/1998

Four different baselines starts from the Bora site, as shown in figure 6.3, namely Bora-Vane, Bora-Karl, Bora-Jonh, and Bora-Hass. For each baseline, all of the possible double difference satellite pairs are used for the comparison between raw and corrected ionospheric-free double difference measurements. A significant improvement is achieved for the residual tropospheric delay estimation using the Trop_NetAdjust. Because residual tropospheric delays are mostly due to the tropospheric wet delay, it follows that Trop_NetAdjust gives us a good approach to estimate the tropospheric wet delay. However, the correct percentage of ambiguity resolution is not 100% but above 90%, and the measurements with wrong ambiguities were removed from Trop_NetAdjust calculations. All the results are based on the assumption that the corrected ambiguities are used for Trop_NetAdjust estimation. As an example, the measurements with wrong ambiguities for baseline Bora-Hass (188km) on 30/04/1998 are shown in figure 6.5. In this figure, all of the measurements with different satellite pairs are combined together using a two-minute sampling data rate.

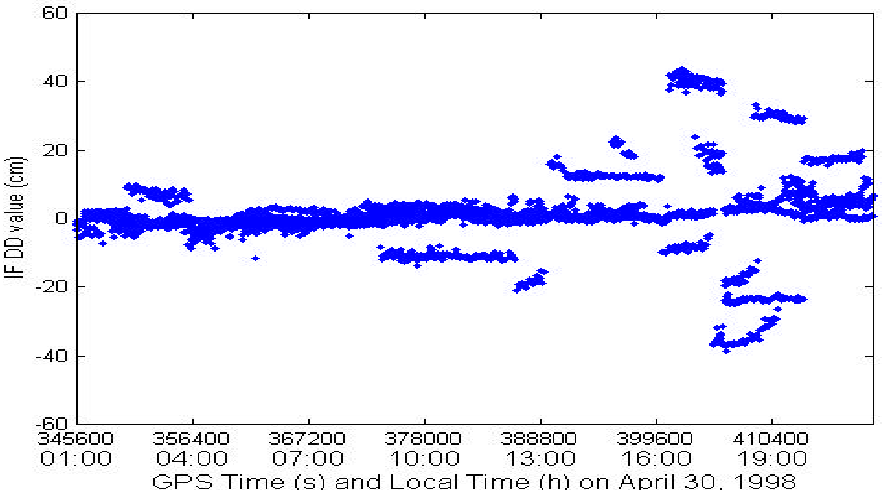

Figure 6.5: 22-hour raw ionospheric-free double difference measurements for Bora-Hass (188km)

Figure 6.6 shows the number of satellites available during the observation period. It is obvious that there are some very short time periods during which the number of satellites is down to three, such as from GPS time 398640 (seconds) to 400560 (seconds) which is about 32 minutes. For this short time period, the satellite geometry is not good for positioning.

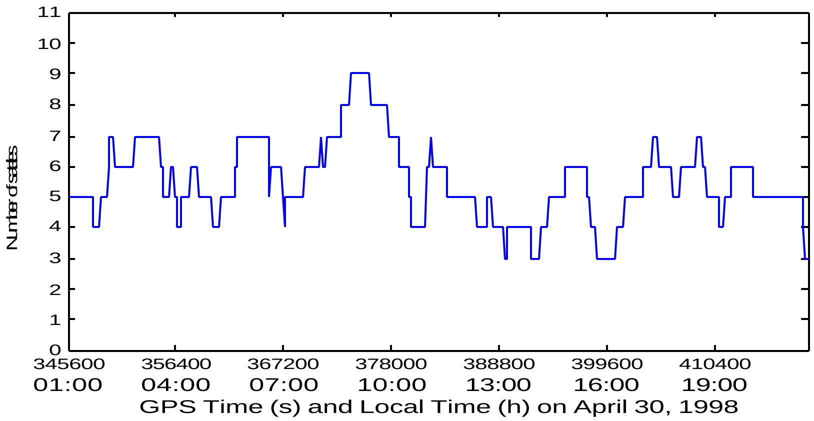

Figure 6.6: Observed number of satellites for Bora-Hass (188km)

In figure 6.5, the ionospheric-free double difference measurements include some large values, which are like biases and their amplitudes are close to one or two times the L1 wavelength (L1: 19.03cm). This is caused by the fact that the ionospheric-free double difference measurement is the combination of L1 and L2 carrier phase measurements:

$$f_{IF} = f_1 - \frac{f_2}{f_1} f_2 \tag{6.5}$$

If there is a cycle error in the L1 ambiguity, the ionospheric-free double difference measurement becomes biased by this amount bias. Similarly, if there is a cycle error in the L2 ambiguity, the ionospheric-free double difference measurement is biased by $\frac{f_2}{f_1}$ times this error. Picking a satellite pair from figure 6.5, figure 6.7 presents us with a good example of a case with a wrong ambiguity for satellite pair PRN 15-31, thus causing a large bias error to exist in the double difference measurements. Figure 6.8 presents the elevation angles of the two satellites.

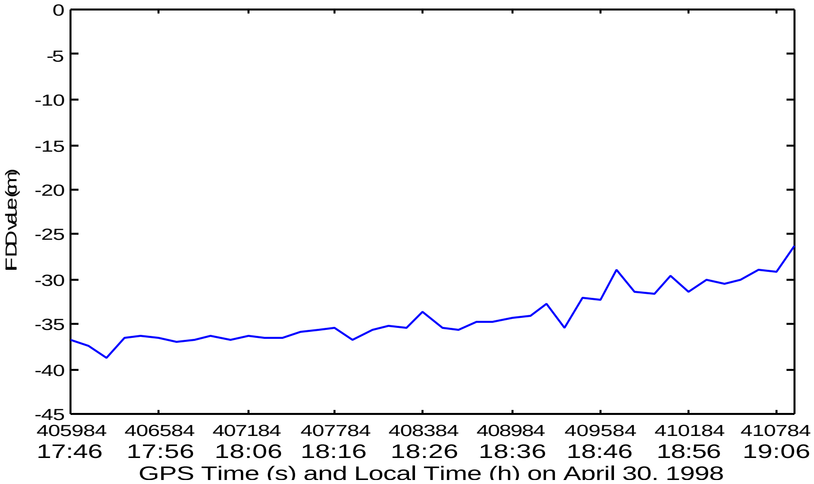

Figure 6.7: Satellite pair PRN 15-31 for Bora-Hass (188km)

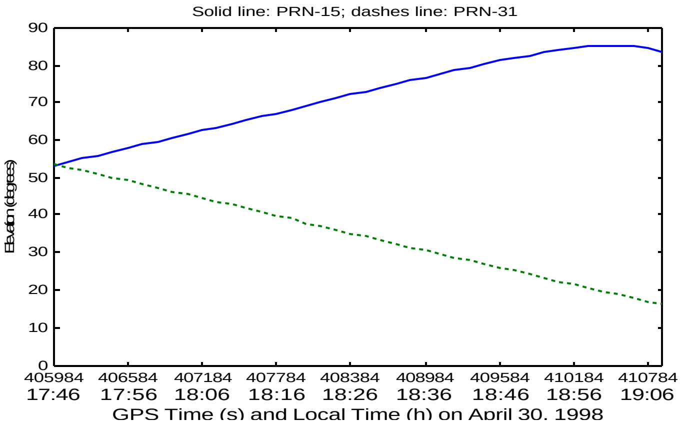

Figure 6.8: Elevation angles for satellite pair PRN15-31 (Bora-Hass baseline)

A similar example of wrong ambiguities is shown in figure 6.9 for satellite pair PRN 3-26. Figure 6.10 shows the satellite elevations for the two satellites.

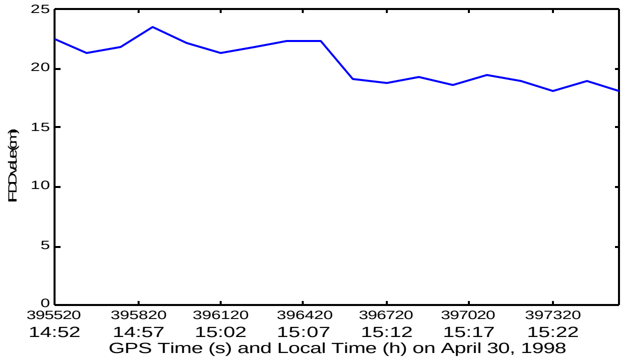

Figure 6.9: Satellite pair PRN 3-26 for baseline Bora-Hass (188km)

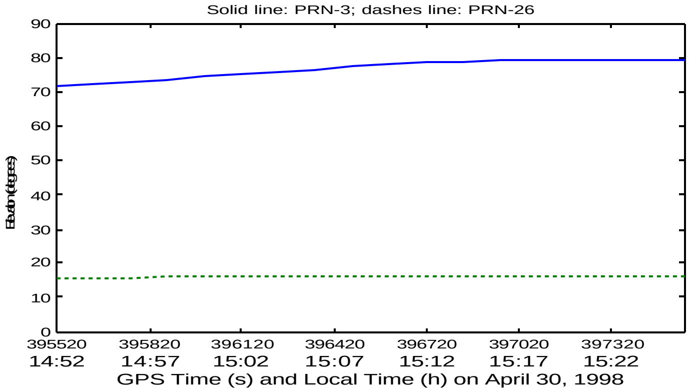

Figure 6.10: Elevation angles for satellite pair PRN3-26 (Bora-Hass baseline)

In order to remove the effect of incorrect ambiguities, an ionosphere free double difference measurement between network reference receivers was rejected if the measurement exceeded a $4s$ value based on *a priori* double difference error covariance matrix $B_n C_{l_n} B_n^T$. In this case, the measurement was not a part of any usable double difference measurements between network reference receivers, so its errors were unobservable, and no correction could be generated. Only the measurements that were corrected were included in the output corrected measurement file.

While analyzing the error reduction brought about by Trop_NetAdjust, it is desirable to compare various results generated from corrected reference receiver measurements with results generated from the raw reference receiver measurements. Recall that

Trop_NetAdjust generates residual tropospheric delay estimates for both the reference receiver measurements and for the unknown measurements at the "mobile" receiver, or computation point (Bora site in this case). The total corrections were calculated as the sum of the estimated residual tropospheric delay at reference receivers and computation point. These corrections were applied to the raw measurements to generate corrected measurements. A cut-off angle of 10^0 is chosen for this analysis.

In figures 6.11 to 6.14, the comparison between the raw IF double difference measurements and corrected IF double difference measurements are shown in time series. The measurements with wrong ambiguities have been rejected from the Trop_NetAdjust estimation. The data period is about 21 hours and the data rate is two-minutes.

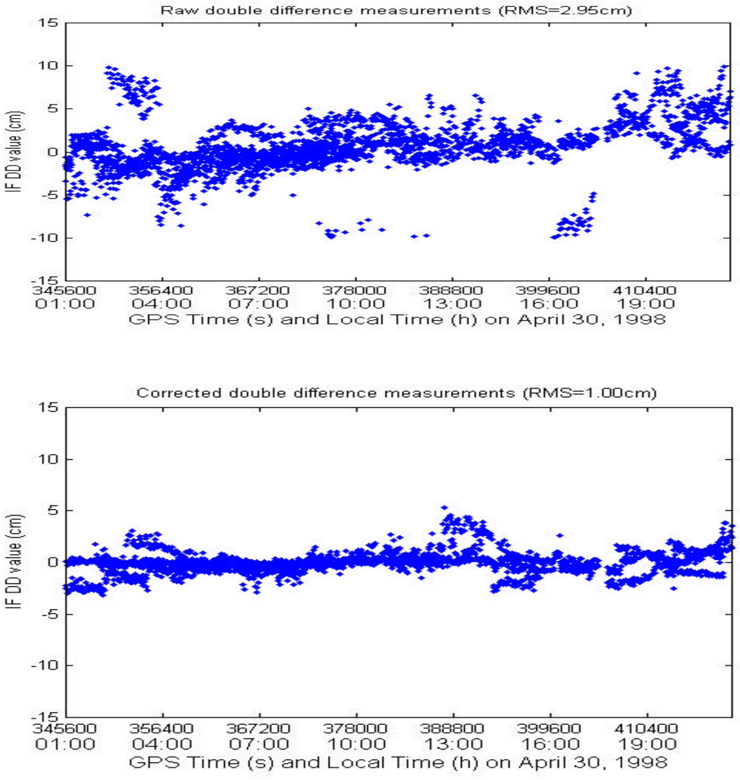

Figure 6.11: IF double difference measurements for Bora-Hass (188km)

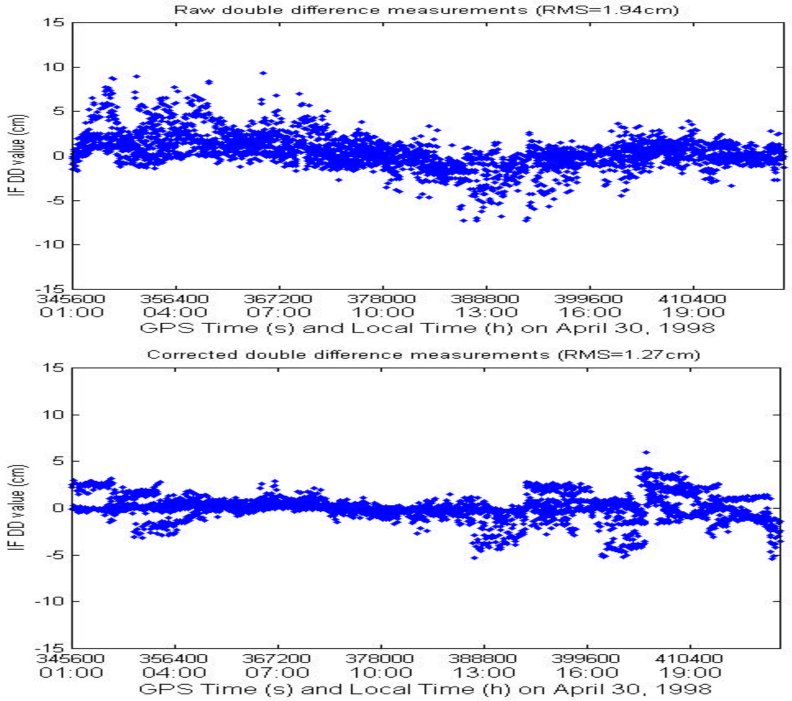

Figure 6.12: IF double difference measurements for Bora-Vane (159km)

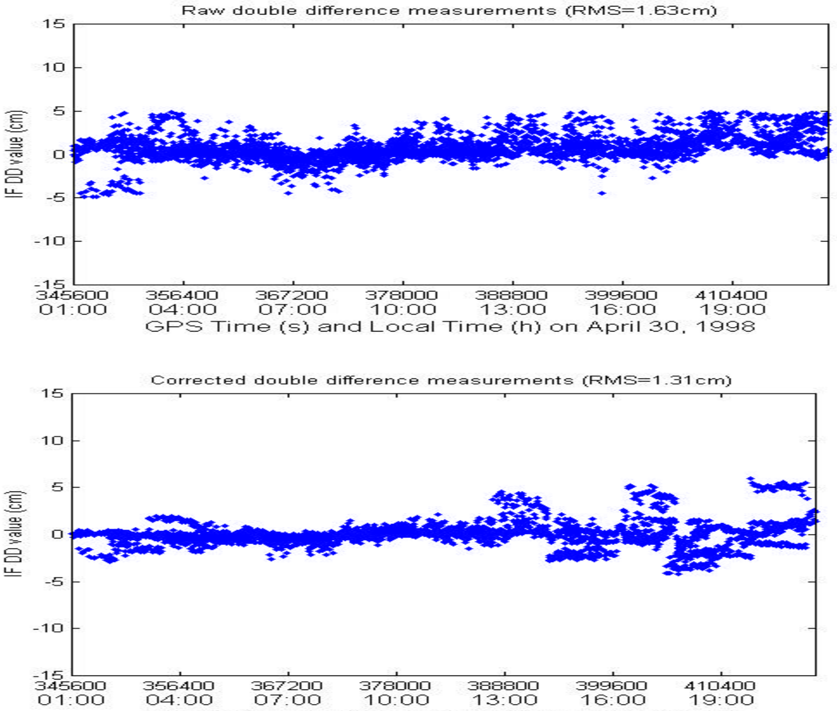

Figure 6.13: IF double difference measurements for Bora-Jonk (70km)

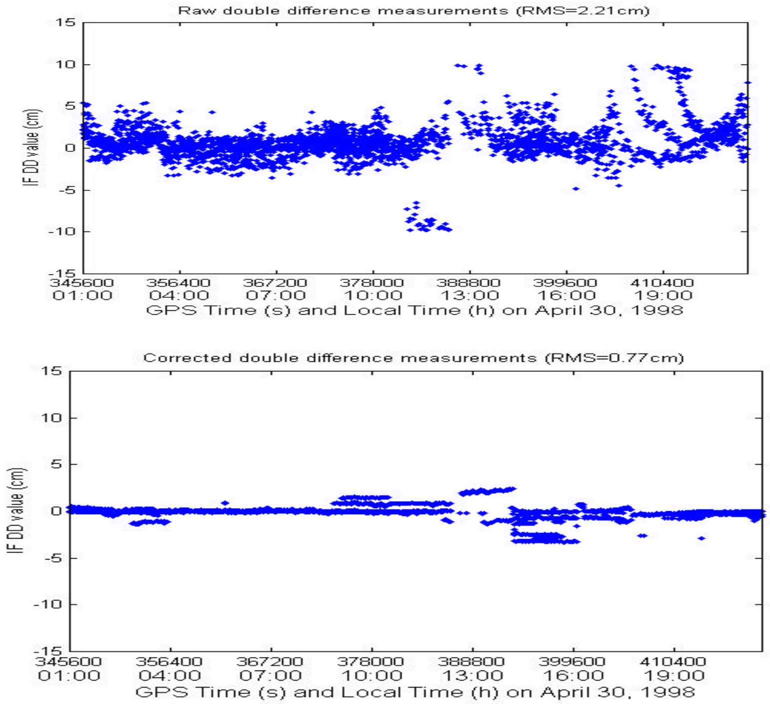

Figure 6.14: IF double difference measurements for Bora-Karl (196km)

The stochastic RMS analysis results based on these selected four baselines are summarized in figure 6.15 and Table 6.2. For each baseline, the rms of residuals prior to and after applying Trop_NetAdjust corrections were calculated for each double difference pair at an interval of two minutes. Since typically six satellites were available above 10^0 from figure 6.6, the rms values for each baseline are based on approximately 3,000 DD measurements.

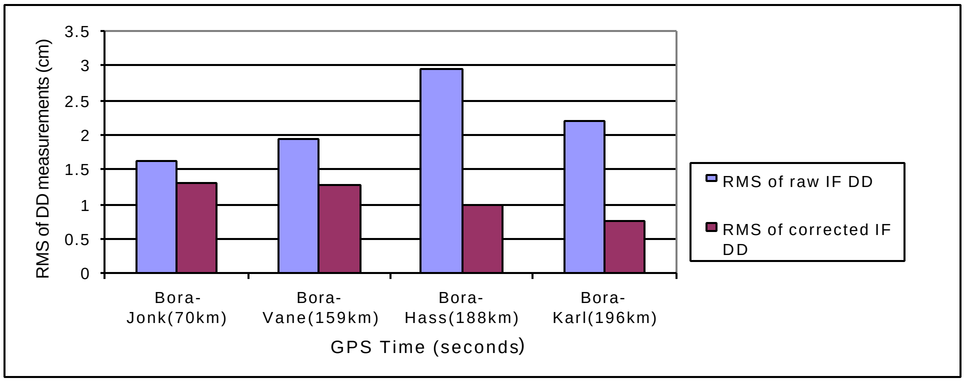

Figure 6.15: Stochastic RMS residual analysis

Table 6.2: RMS residual improvement

Baselines	DD RMS residuals (no residual tropo corr) (cm)	DD RMS residuals (residual tropo corr) (cm)	Percentage improvement (%)
Bora- Jonk (70 km)	1.63	1.31	20%
Bora-Vane (159 km)	1.94	1.27	35%
Bora-Hass (188 km)	2.95	1.00	66%
Bora-Karl (196 km)	2.21	0.77	65%

The RMS percentage improvement of the ionospheric-free double difference measurements increases as the baseline length increases. For short baselines (such as Bora-Jonk 70km), the differential errors are already low, and the additional network reference receivers do not provide much useful information. As the baseline length increases, the residual tropospheric delay errors grow, and the network reference receivers become more useful. Figure 6.16 shows that the raw ionospheric-free double difference measurements increased with an increase in the baseline length. In addition, figure 6.17 presents the RMS percentage improvement between raw and corrected measurements as a function of the baseline length. A clear trend is evident with larger improvements occurring at longer baseline lengths. Therefore, the double difference errors can be decreased much for a long baseline because of the significant RMS percentage improvement. The remaining errors after Trop_NetAdjust become small enough for precise GPS positioning applications.

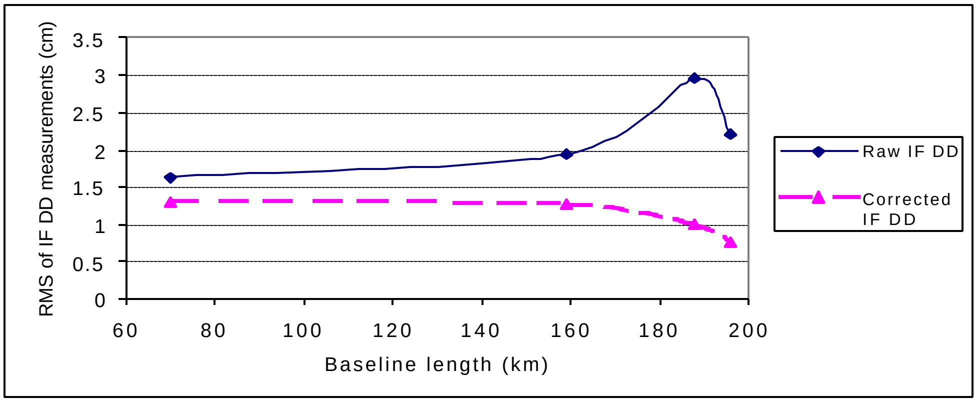

Figure 6.16: RMS of ionospheric-free double difference for raw and corrected measurements

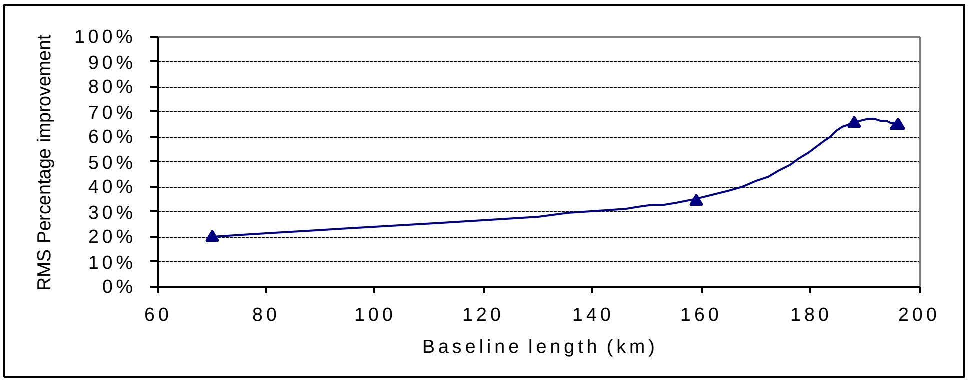

Figure 6.17: RMS percentage improvements of ionosphere free double difference for raw and corrected measurements

6.4 Performance comparison between Trop_NetAdjust estimates and WVR measurements

In this section, the residual tropospheric delay estimated from Trop_NetAdjust is compared with the water vapor radiometer (WVR) measurements. As mentioned in the previous sections, ground-based, upward-looking water vapor radiometers (WVRs) are instruments that measure the background microwave radiation produced by atmospheric water vapor and can estimate the corresponding wet delay along a given line of sight. WVRs actually measure the sky brightness temperature at two or more frequencies. The algorithm that is used to retrieve wet delay from observation of sky brightness temperature contains parameters which show seasonal and geographic variation. Because of the limited scope of this thesis, the details for retrieving the wet delay from sky brightness temperature is not presented here.

For this analysis, 3-days of WVR measurements were provided by the Onsala observation lab. from UTC 1998/4/29: 23(h):02(m):35(s) to 1998/5/2: 23(h):58(m):39(s)., which have been converted to GPS time. In figure 6.18, the equivalent zenith wet delay from WVR is plotted as the solid curve. The dotted curve shows the zenith wet delay calculated from modified Saastamonien model, which is provided with WVR data by Onsala observation lab. The unit of zenith delay is cm. The sampling data interval is not consistent but averaged over 10 seconds.

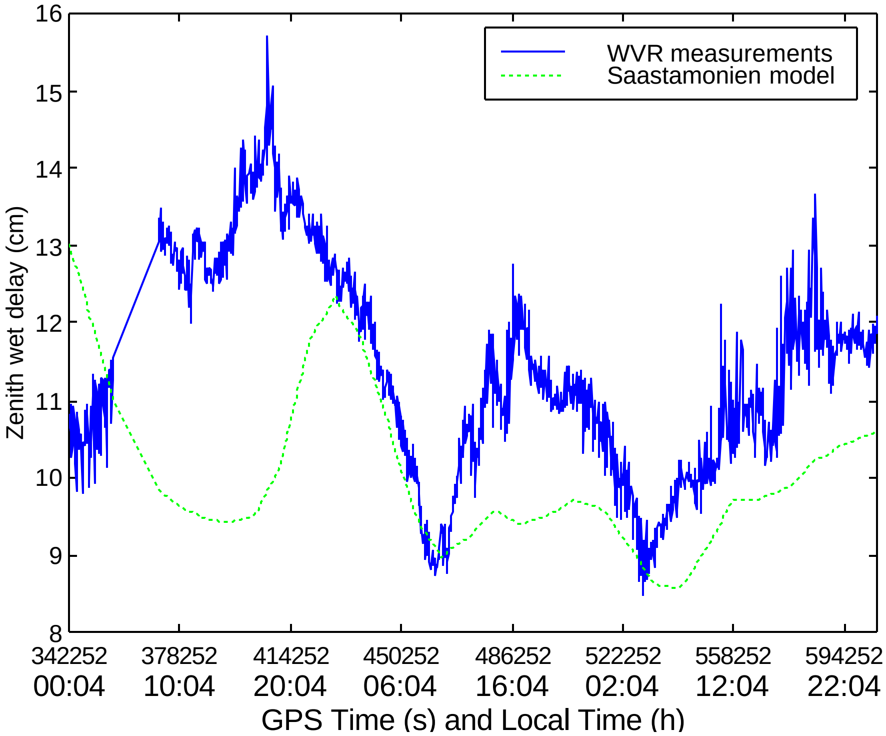

Figure 6.18: Zenith wet delay from WVR

These WVR measurements are used for comparison with the results of residual tropospheric delay derived from Trop_NetAdjust using the network reference GPS stations. The retrieved wet delay at the Onsala station from the water vapor radiometer is used as the calibration term because most of the residual tropospheric delay is due to unmodeled wet delay. The WVR measurements have the accuracy for retrieving wet delay better than 1cm. It is a good calibration for our estimated wet delays (most part of residual tropospheric delays) from Trop_NetAdjust.

For this comparison, two different days of water vapor radiometer measurements at Onsala are used in order to present the change of the wet delay. The measurement comparison periods are chosen from UTC 1998/4/30: 01(h): 18(m): 00(s) to UTC 1998/4/30: 17(h):18(m):00(s) and from UTC 1998/5/1: 01(h):53(m):00(s) to UTC 1998/5/1: 19(h):53(m):00(s). As shown in figure 6.19, the five stations in the southern part of Swedish GPS network around the Onsala site are used to estimate the residual tropospheric delay at Onsala using the Trop_NetAdjust method. The GPS data at the same measurement period have been processed with a sampling data rate of five seconds. Onsala is selected as the prediction point based on the redundant GPS measurements from five other stations: Hass, Jonk, Karl, Bora and Vane. Then Trop_NetAdjust is used to estimate the residual tropospheric delays at the prediction point Onsala. Here the mask angle of GPS observation is chosen as 10^{o}. Figure 6.20 shows the flow chart of the approach used to obtain the Trop_NetAdjust estimated wet delay and the comparison with the wet delay from WVR.

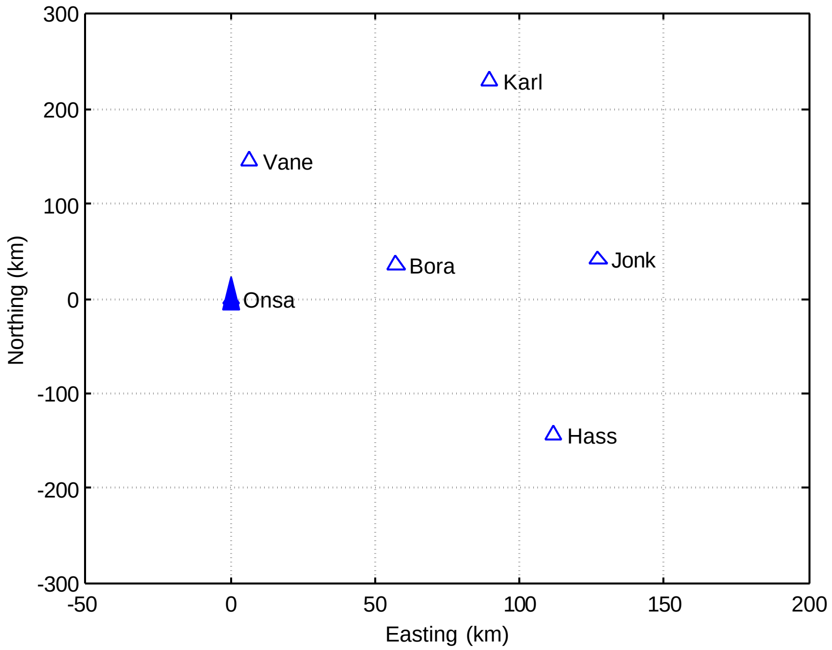

Figure 6.19: Five GPS reference sites around Onsala

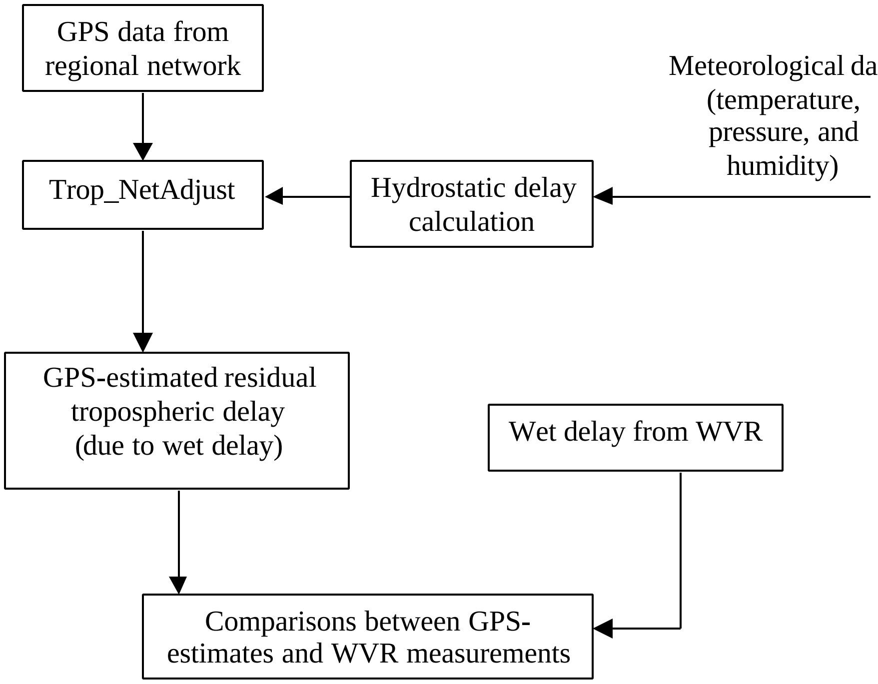

Figure 6.20: Flow chart of the data processing algorithm

In the test network, the separation between receivers is less than 200 km. With the use of double difference GPS measurements to estimate the residual tropospheric delays in the Trop_NetAdjust, the differencing of the GPS data may be more sensitive to relative than to absolute tropospheric changes. This is because a GPS satellite observed by two or more receivers is viewed at almost identical elevation angles for a relatively short baseline, causing the delay estimates to be highly correlated. The tropospheric delay at one station is called the absolute delay, which is the measurement by the WVR, while the relative delay is the differential tropospheric delay between two stations. For Trop_NetAdjust, the estimate of residual tropospheric delay is relative in nature.

Figures 6.21 shows the absolute and relative wet delays from WVR and Trop_NetAdjust over a 16 hour data period on April 30, 1998. Note that, in figure 6.21, WVR measurement data are not available over a period of about 4 hours. Figure 6.22 shows the absolute and relative wet delays from WVR and Trop_NetAdjust of 18 hours data on May 1, 1998.

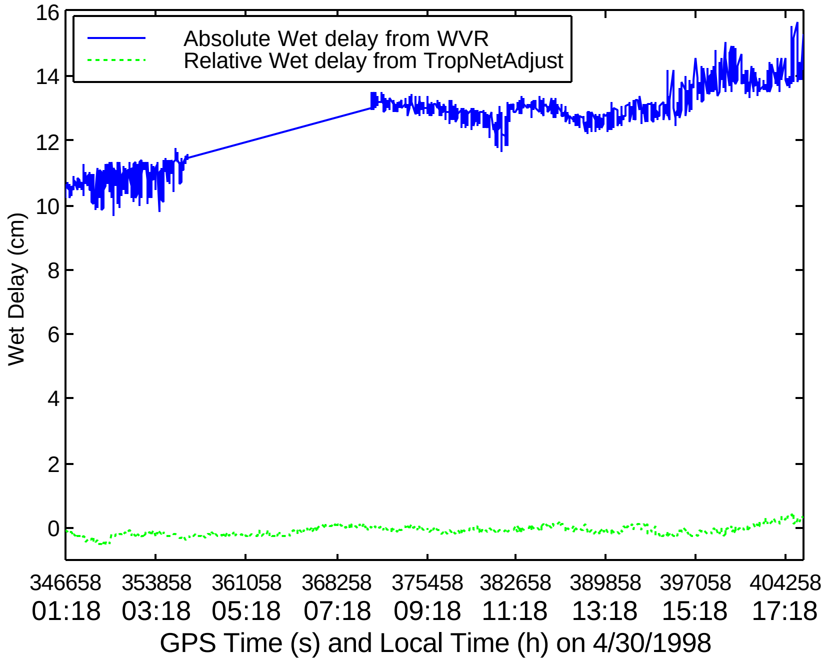

Figure 6.21: Absolute and relative wet delays from WVR and Trop_NetAdjust at Onsala (30/4/1998)

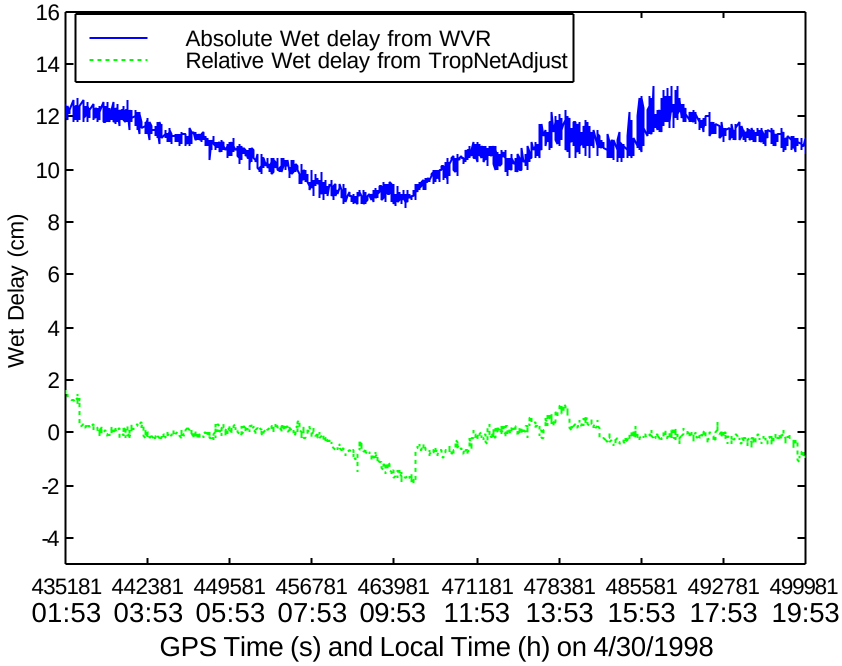

Figure 6.22: Absolute and relative wet delays from WVR and Trop_NetAdjust at Onsala (01/05/1998)

It is obvious that there are large differences between wet delay estimated from Trop_NetAdjust and wet delay from WVR measurements. This difference makes them difficult to compare. Using Trop_NetAdjust method, the relative tropospheric delay between two reference stations can be obtained. If the distribution of the tropospheric delay is assumed to be homogeneneous in this region, the relative tropospheric delay from Trop_NetAdjust should be flat or close to zero given that the absolute values of the two sides are quite the same. If WVR measurements are available in more than one station, the relative tropospheric delay from WVR and from Trop_NetAdjust can then be compared.

On the other hand, if the absolute wet delay has been measured at one reference station, for example at Onsala site, the estimates of relative wet delay from Trop_NetAdjust can be used to calculate the absolute wet delays for surrounding stations, such as Jonk, Bora, Karl, Hass and Vane. Therefore, even though the Trop_NetAdjust method cannot give the absolute estimates of wet delay, it provides a good approach to map the absolute wet delay available at one reference station from WVR measurements to surrounding stations. Based on this approach, a regional wet delay distribution map can be easily achieved in real-time using GPS network information plus one station's WVR measurements.

CHAPTER 7

CONCLUSIONS AND RECOMMENDATIONS

Trop_NetAdjust predicts the residual tropospheric delay on the GPS carrier phase observables using redundant measurements from a network of GPS reference stations. The Trop_NetAdjust method is based on least squares prediction and effectively estimates the effects of residual tropospheric delays on GPS signals using a network of reference stations. Based on the ionospheric-free double difference GPS measurements, this prediction approach enables one to predict the residual tropospheric delays remaining after a standard tropospheric model has been applied to the GPS data. As in any prediction method, the covariance function of the residual tropospheric delays must be calculated.

Two Trop_NetAdjust prediction cases were analyzed, namely a first case when the tropospheric delay is required for an existing satellite at a new location within the network using optimally all available satellite measurements from the network. A second case was to predict the residual tropospheric delays for a new satellite being observed by the network stations and user alike, using other satellite measurements available from the network. This implies that the tropospheric delays between satellites and observation points are spatially correlated, which is indeed the case.

Trop_NetAdjust method was tested using an 11-receiver network covering a 400km x 600km region in southern Norway. Two different test networks, Geim-Net and Tryr-Net, of different network geometry and varying baseline lengths and directions, were used to evaluate the Trop_NetAdjust performance. All of the evaluation results were based on the RMS percentage improvement of ionospheric-free double difference measurements prior to and after applying the Trop_NetAdjust residual tropospheric delay estimates. For the new station prediction case, Trop_NetAdjust yielded consistent improvements in the double difference domain at the 55% level for Geim-Net and at 30% level for Tryr-Net. For the new satellite prediction case, Trop_NetAdjust yielded improvements in the double difference domain at 60% level for Geim-Net and 30% level for Tryr-Net. Based on the analysis of the relationship between the RMS improvements and the satellite elevations, the improvements using Trop_NetAdjust are high, stable and consistent for low elevation satellites (10^{o}-20^{o}). The improvements vary largely in the case of high elevation satellites (50^{o}-70^{o}). But the RMS of raw measurements of the satellites with high elevations usually is small. Therefore, it does not result in a problem for Trop_NetAdjust even if the RMS improvements are not stable. The results demonstrate that Trop_NetAdjust significantly improves the tropospheric modeling overall

The performance of Trop_NetAdjust was tested using the permanent Swedish network of GPS stations. This test was conducted on a small network, comprised of five stations in the southern part of Sweden. Improvements in the ionospheric-free double difference residuals ranged from 20% to 66% in this case. For the short baselines, Trop_NetAdjust yielded less significant improvements; however, for the longer baselines the improvement from Trop_NetAdjust was most significant. At 196 km the RMS of IF DD measurements was reduced from 2.21 cm down to 0.77 cm. The associated RMS percentage improvement is at 65% level.

The Trop_NetAdjust method provides relative wet delays based on estimates of the residual tropospheric delays. By combining the wet delay measurements from a water vapor radiometer at one reference station with the estimates from Trop_NetAdjust, the absolute wet delays can be extended for any locations near the WVR station. Therefore, even if the Trop_NetAdjust method cannot provide absolute estimates of wet delays, it can provide a good method of mapping the absolute wet delay from one reference station equipped with a WVR to surrounding locations. With this approach, a regional wet delay distribution map can be generated in real-time using a GPS network of reference stations and WVR.

Some recommendations following are presented for the consideration:

1) Analyze the sensitivity of the Trop_NetAdjust prediction results to the choice of covariance functions.
2) Develop a method to generate selected covariance function parameters adaptively in order to track the real-time changes in the tropospheric delays.
3) Test the prediction performance of the Trop_NetAdjust method with different data sets collected from different GPS networks, and under a wide variety of weather conditions.
4) Develop and test an effective method to map the absolute wet delay from one reference station to others, and compare the results with raw WVR measurements.
5) Test the prediction performance of the Trop_NetAdjust method for the case of low satellite elevations (such as 5^{o}).

REFERENCES

Axelrad, P., C. Comp and P. MacDoran (1994), "Use of Signal-To-Noise Ratio for Multipath Error Correction in GPS Differential Phase Measurements: Methodology and Experimental Results", *Proceedings of ION GPS-94*, Salt Lake City, September 20-23, pp. 655-666

Baby, H.B., P. Golé, and J. Lavergnat (1988), " A model for the tropospheric excess path length of radio waves from surface meteorological measurements", *Radio Science*, Vol. 23, No. 6, pp. 1023-1038

Bevis, M., S. Businger, T.A. Herring, C. Rocken, R.A. Anthes, and R.H. Ware (1992), " GPS meteorology: remote sensing of atmospheric water vapor using the Global Positioning System", *Journal of Geophysical Research*, Vol.97, No.D14, pp. 15,787-15,801

Biermen, G.J. (1977), *Factorization Methods for Discrete Sequential Estimation*, Academic Press, Orlando, Florida

Black, H.D. (1978), "An easily implemented algorithm for the tropospheric range correction", *Journal of Geophysical Research*, Vol. 83, No. B4, pp. 1825-1828

Blewitt, G. (1993), "Advances in Global Positioning System technology for geodynamics investigation: 1978-1992", *Contributions of Space Geodesy to Geodynamics: Technology*, D.E. Smith and D.L. Turcotte (Eds.), American Geophysical Union, Washington, D.C., Geodynamics Series, Vol. 25, pp.195-213

Boudouris, G. (1963), "On the index of refraction of air, the absorption and dispersion of centimeter waves by gases", *Journal of Research of the National Bureau of Standards – D. Radio Propagation*, Vol. 67D, No. 6, pp. 631-684

Brunner, F.K. (Ed.) (1984), *Geodetic refraction: effects on electromagnetic wave propagation through the atmosphere*, Springer-Verlag, New York, N.Y.

Brunner F.K., and W.M. Welsch (1993), "Effect of the troposphere on GPS measurements", *GPS World*, Vol. 4, No. 1, pp. 42-51

Businger S., S.R. Chiswell, M. Bevis, J. Duan, R.A. Anthes, C.Rocken, R.H. Ware, M. Exner, T. VanHove, and F.S. Solheim (1996), “The promise of GPS in atmospheric monitoring”, *Bulletin of American Meteorology Society*, Vol. 77, No.1, pp. 5-18

Champion, K.S., A.E. Cole, and A.J. Cantor (1985), "Standard and reference atmospheres", Chapter 14 of the Handbook of Geophysics and the Space Environment, A.S. Jursa (Ed.), Air Force Geophysics Laboratory, Air Force Systems Command, United State Air Force, pp. 14-1 to 14-43

Chao, C.C. (1972), "A model for tropospheric calibration from daily surface and radiosonde balloon measurement", Technical Memorandum 391-350, Jet Propulsion Laboratory, Pasadena Calif.

Darin F., J. Johansson, R. Carlsson, G. Elgered, P. Jaelemark, and B. Ronnang (1997), “Continuous monitoring of the atmosphere using GPS”, *Proceedings of ION-GPS 97*, Kansas City, Missouri, U.S.A. September 16-19, The Institute of Navigation, pp.199-205

Davis, J.L., T.A.Herring, I.I., Shapiro,, A.E.E. Rogers, and G. Elgered (1985), "Geodesy by radio interferometry: Effects of atmospheric modeling errors on estimates of baseline length", *Radio Science*, Vol.20 , No. 6, pp. 1593-1607

Davis, J.L. (1986), " Atmospheric propagation effects on radio interferometry" AFGL technical report 86-0243, US Air Force Geophysics Laboratory, Hanscomm AFB, Mass.

Dixon, T.H. (1991), "An introduction to the Global Positioning System and some geological application", *Reviews of Geophysics*, Vol. 29, No.2, pp. 249-276

Dixon, T.H., and S. Kornreich Wolf (1990), " Some tests of wet tropospheric calibration for the CASA Uno Global Positioning System experiment", *Geophysics Research Letters*, Vol. 17, No. 3, pp. 203-206

Dodson A.H., P.J. Shardlow, L.C.M. Hubbard, G. Elegered, and P.O.J. Jarlemark (1996), “Wet Tropospheric effects on precise relative GPS height determination”, *Journal of Geodesy*, No. 70, No. 4, pp. 188-202

Dodson A.H. and Baker H.C. (1998), “ The accuracy of GPS water vapour estimation”, *Proceedings of ION-NTM 98*, January, The Institute of Navigation, pp. 649-657

Duan J.P., et al (1996), “ GPS meteorology: direct estimation of the abolute value of perceptiable water”, *Journal of Applied Meteorology*, Vol.35, No. 6, pp. 830-838

Elgered, G., J.L.Davis, T. A. Herring, and I.I. Shapiro (1991), " Geodesy by radio interferometry: Water vapor radiometry for estimation of the wet delay", *Journal of Geophysical Research*, Vol. 96, No. B4, pp. 6541-6555

Elgered, G. (1992), "Refraction in the troposphere", *Proceedings of the Symposium on Refraction of Transatmospheric Signals in Geodesy*, J.C. de Munck and T.A. Spoelstra (Eds.), Netherlands Geodetic Commission, Publications in Geodesy, New Series No. 36, The Hague, Netherlands, 19-22 May, pp. 13-19

Elgered, G. (1993), "Tropospheric radio path delay from ground-based microwave radiometry", *Atmospheric Remote Sensing by Microwave Radiometry*, John Wiley, New York, pp. 215-258

Emardson T.R. (1998), "Studies of atmospheric water vapor using the Global Positioning System", Technical report No. 339, Chalmers University of Technology

Fenton, P., B. Falkenberg, T. Ford, K. Ng, A.J. van Dierendonck (1991), "Novatel's GPS Receiver: The High Performance OEM Sensor of the Future", *Proceedings of ION GPS-91*, Albuquerque, September 9-13, pp. 49-58

Gelb, A. (1974), *Applied Optimal Estimation*, The MIT Press, Massachusetts Institute of Technology, Cambridge, Mass.

Goad C.C., and L. Goodman, (1974), " A modified Hopfield tropospheric refraction correction model", Paper presented at the American Geophysical Union Fall Annual Meeting, 12-17 December, San Francisco, Ca., pp. 28

Herring, T.A (1992), "Modeling atmospheric delays in the analysis of space geodetic data", *Proceedings of the Symposium on Refraction of Transatmospheric Signals in Geodesy*, J.C. de Munck and T.A. Spoelstra (Eds.), Netherlands Geodetic Commission, Publications in Geodesy, New Series No. 36, The Hague, Netherlands, 19-22 May, pp. 157-164

Herring, T.A., J.L. Davis, and I.I Shapiro (1990), " Geodesy by radio interferometry: the application of Kalman filtering to the analysis of very long baseline interferometry data", *Journal of Geophysical Research*, Vol. 95, No. B8, pp. 12561-12581

Hofmann-Welllenhof, B., H. Lichtenegger, and J. Collions (1993), *GPS Theory and Practice*, 2nd ed., Springer-Verlag, Wien, Austria

Hopfield, H.S. (1969), " Two-quartic tropospheric refractivity profile for correcting satellite data", *Journal of Geophysical Research*, Vol. 74, No. 18, pp. 4487-4499

Ifadis, I.I. (1986), " The atmospheric delay of radio waves: modeling the elevation angle dependence on a global scale", Technical report 38L, Chalmers University of Technology, Göteborg, Sweden

Janes, H.W., R.B. Langley, and S.P. Newby (1991), "Analysis of tropospheric delay prediction models: comparisons with ray tracing and implications for GPS relative positioing", *Bulletin Géodésique*, Vol. 65, No.3, pp. 151-161

Jarlemark, P.O.J. (1994), "Studies of wet delay algorithms for three European sites utilizing new attenuation models", Research report No. 171, Department of Radio and Space Science, Onsala Space Observatory, Chalmers University of Technology, Sweden

Klobuchar, J.A. (1996), "Ionospheric Effects on GPS", in *Global Positioning System: Theory and Applications,* Vol. I, ed. B.W. Parkinson and J.J. Spilker, American Institute of Aeronautics and Astronautics, Inc., Washington, D.C.

Kroger, P.M., J.M. Davidson, and E.C. Gardner (1986), "Mobile very long baseline interferometry and Global Positioning System measurement of vertical crustal motion", *Journal of Geophysical Research*, Vol. 91, No. B9, pp. 9169-9176

Lachapelle, G. (1994), "High Accuracy GPS Positioning", Navtech Seminars Course 330 Lecture Notes

Lachapelle, G., H. Sun, M.E. Cannon, and G. Lu (1994), " Precise Aircraft-to-Aircraft Positioning Using a Multiple Receiver Configuration", *Proceedings of the National Technical Meeting*, The Institute of Navigation, San Diego, California, pp.793-799

Lachapelle, G. (1997), "GPS Theory and Applications", ENGO 625 Course Lecture Notes

Langley, R.B., (1992), " The effect on the ionosphere and troposphere on satellite positioning systems", *Proceedings of the Symposium on Refraction of Transatmospheric Signals in Geodesy*, J.C. de Munck and T.A. Spoelstra (Eds.), Netherlands Geodetic Commission, Publications in Geodesy, New Series No. 36, The Hague, Netherlands, 19-22 May, p.97 (abstract only).

Lanyi, G. (1984), "Tropospheric delay effects in radio interferometry", Telecommunications and Data Acquisition Progress, JPL Technical Report 42-78, Jet Propulsion Laboratory, Pasadena, California, pp. 152-159

Leick, A. (1995), *GPS Satellite Surveying*, John Wiley and Sons, Inc., 2nd edition

Lichten, S.M. and J.S. Border (1987), "Strategies for high-precision Global Positioning System orbit determination", *Journal of Geophysical Research*, Vol. 92, No. B12, pp. 12751-12762

Lichten, S.M. (1990), "Estimation and filtering for tropospheric path delays with GPS techniques", *Manuscripta Geodaetica*, Vol. 15, pp. 159-176

Lutgens, F.K., and E.J. Tarbuck (1979*), The Atmosphere – An Introduction to Meteorology*, Prentice-Hall, Englewood Cliffs, New Jersey

Marini, J.W. (1972), "Correction of satellite tracking data for an arbitrary tropospheric profile", *Radio Science*, Vol. 7, No.2, pp. 223-231

McCorkle, D. (1998), "The Earth's atmosphere ", Astronomy 161 "The Solar System" Course Lecture Notes, Department of Physics and Astronomy, University of Tennessee, http://csep10.phys.utk.edu/astr161/lect/earth/atmosphere.html

Mendes, V.B., and R.B. Langley (1994), " A comprehensive analysis of mapping functions used in modeling tropospheric propagation delay in space geodetic data", In *Proceedings of KIS94*, International Symposium on Kinematic Systems in Geodesy, Geomatics and Navigation, Banff, Canada, 30 August – 2 September, pp. 87-98

Mendes V.B. (1999), "Modeling the neutral-atmosphere propagation delay in radiometric space techniques", Technical reports of Department of Geodesy and Geomatics Engineering, University of New Brunswick, Fredericton

Moritz, H. (1972), "Advanced Least Squares Methods", Reports of the Department of Geodetic Science, No. 75, The Ohio State University, Columbus

Neill, A.E. (1993), " A new approach for the hydrostatic mapping function", *Proceedings of the International Workshop for Reference Frame Establishment an Technical development in Space Geodesy*, Communications Research Laboratory, Koganei, Tokyo, Japan, 18-21 January, pp. 61-68

Neill, A.E. (1996), " Global mapping functions for the atmosphere delay at radio wavelengths", *Journal of Geophysical Research*, Vol. 101, No. B2, pp. 3227-3246

Onsala Space Observatory (1998), Chalmers University of Technology, "Microwave Radiometer", http://www.oso.chalmers.se/geo/radio.html

Onsala Space Observatory (1998), Chalmers University of Technology, "Global Positioning System", http://www.oso.chalmers.se/geo/gps.html#Meteorology

Raquet J.F., and G. Lachapelle (1996), " Determination and Reduction of GPS Reference Station Multipath using Multiple Receivers", *Proceedings of ION GPS-96*, September 17-20, Kansas City, pp. 673-681

Raquet J.F. (1998), "Development of a method for kinematic GPS carrier-phase ambiguity resolution using multiple reference receivers", UCGE report 20116, University of Calgary

Raquet J.F., G. Lachapelle, T.E. Melgård (1998), “ Test of a 400km X 600km network of reference receivers for precise kinematic carrier-phase positioning in Norway”, *Proceedings of ION-GPS 98*, Nashville, Tennessee, U.S.A. September 15-18, The Institute of Navigation, pp. 407-416

Ray J.K, M.E. Cannon, and P. Fenton (1998), " Mitigation of Static Carrier Phase Multipath Effects using Multiple Closely-Spaced Antennas", *Proceeding of ION GPS-98*, Nashville, Tennessee, U.S.A. September 15-18, The Institute of Navigation, pp. 1025-1034

Rothacher, M. (1997), "Geodetic Applications of GPS: Lecture Notes for Nordic Autumn School", Chapter GPS Satellite Orbits, Orbit Determination, and the IGS, pp. 55-108, National Land Survey of Sweden

Saastamonien, J. (1972), “Atmospheric correction for the troposphere and stratosphere in radio ranging of satellites”, The Use of Artificial Satellites for Geodesy, *Geophysics Monograph. Series*, Vol. 15

Saastamonien, J. (1973), "Contribution to the theory of atmospheric refraction", *Bulletin Géodésique*, No. 105, pp. 279-298; No. 106, pp. 383-397; No. 107, pp. 13-34

Schmid, H.H., and E. Schmid (1965), "A Generalized Least Squares Solution for a Hybrid Measuring System", *The Canadian Surveyor*, XIXm No.1, Ottawa

Smith, E.K., and S. Weintraub (1953), " The constants in the equation for atmospheric refractive index at radio frequencies", *Proceedings of the Institute of Radio Engineers*, Vol. 4, pp. 1035-1037

Sun, H., T. Melgård and M.E. Cannon (1999), "Real-time GPS Reference Network Carrier Phase Ambiguity Resolution", *Proceedings of the ION National Technical Meeting*, San Diego, January 25-27, pp.193-199

Thayer, G.D. (1974), "An improved equation for the radio refractive index of air", *Radio Science*, Vol. 9, No. 10, pp. 803-807

Tralli, D.M., and S.M. Lichten (1990), “ Stochastic estimation of tropospheric path delays in Global Positioning System geodetic measurements”, *Bulletin Géodésique,* Vol 64, No. 2, pp. 127-159

Trehauft, R.N. (1992), " Tropospheric and charged particle propagation errors in very long baseline interferometry", *Proceedings of the Symposium on Refraction of Transatmospheric Signals in Geodesy*, J.C. de Munck and T.A. Spoelstra (Eds.), Netherlands Geodetic Commission, Publications in Geodesy, New Series No. 36, The Hague, Netherlands, May 19-22, pp. 45-53

van Dierendonck, A.J., P. Fenton, and T. Ford (1992), "Theory and Performance of Narrow Correlator Technology in GPS Receiver", *Navigation: Journal of The Institute of Navigation*, Vol. 39, No. 3, pp. 265-283

Wallace, J.M., and P.V. Hobbs (1977), *Atmospheric Science: An introductory Survey*, Academic Press, New York

Wells, D.E., N. Beck, D. Delikaraoglou, A. Kleusberg, E.J. Krakiswsky, G. Lachapelle, R. B. Langley, M.Nakiboglou, K.P. Schwarz, J. Tranquilla, and P. Vanicek (1986), *Guide to GPS positioning*, Canadian GPS Associates, Fredericton, N.B., Canada

Wells, D.E. and E.J. Krakiwsky (1971), " The Method of Least Squares", Department of Surveying Engineering Lecture Notes No.18, University of New Brunswick, Fredericton

Wolf. H (1968), *Ausgleichungsrechnung nach der Methode der Kleinsten Quadrate*, Dummler, Bonn

APPENDIX A

DESCRIPTION OF NORWAY TEST NETWORK AND LOCAL ATMOSPHERIC CONDITIONS

The Norway test network is located in the southern portion of Norway, indicated in figure A.1.

Figure A.1: Test network spaced throughout the southern portion of Norway

This test network consists of 11 reference receivers as shown in figure A.2. The coordinates of these 11 reference sites are shown in Table A.1 and these are expressed in WGS-84 ellipsoidal coordinates (Raquet, 1998). Five of the receivers (KRIS, STAV, BERG, ALES, and TRON) were part of the existing Norwegian SATREF system used for code differential GPS inland and in the waterways around Norway. The receivers at these stations are Trimble 4000 SSi dual-frequency receivers using ground plane antennas. The other six receivers (AREM, ARER, GEIM, GEIR, TRYM, TRYR) are dual-frequency Ashtech Z-12 receivers which were temporarily set up for this test. The GEIM, GEIR, TRYM, and TRYR receivers used Dorne-Margolin ground plane antennas while the AREM, ARER receivers used standard Ashtech dual-frequency ground plane antennas.

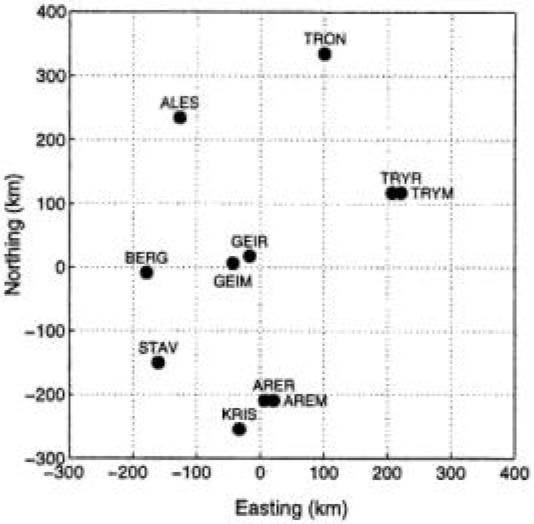

Figure A.2: Relative location of 11 reference receivers in test network

Table A.1 WGS-84 ellipsoidal coordinates for 11 reference sites

Reference Receiver	Longitude (degrees)	Latitude (degrees)	Height (metres)
Ales	6.198539697	62.476380742	194.982
Arem	8.759850207	58.489055592	104.511
Arer	8.759862588	58.489156739	104.123
Berg	5.266541503	60.288741923	98.916
Geim	7.722183907	60.422093600	1247.947
Geir	8.200342981	60.525564727	814.324
Kris	7.907414342	58.082691975	152.801
Stav	5.598620273	59.017709092	110.059
Tron	10.319152630	63.371380847	322.810
Trym	12.381637217	61.422832771	723.940
Tryr	12.381577927	61.423212395	724.795

A 24-hour GPS data set was collected at 1-Hz from 16:00 UTC (17:00 local) on September 29, 1997 to 16:00 UTC (17:00 local) the following day, and later thinned to 0.5 Hz. This data will be used for all of the tests discussed in this thesis. The cut-off elevation angle for all of the analysis was 10^o.

The Norwegian Meteorological Institute provided approximate 24-hour average surface weather statistics for most of the reference stations (there is no data for Kris site). The measurement terms include temperature (mean temperature, maximum temperature, and minimum temperature), precipitation/rainfall (24 hours period), mean relative humidity, air-pressure at sea level, as well as mean wind value, maximum 10 minutes mean wind value, and maximum gust of wind. The statistical value are based on measurements done at 06 (07:00 local), 12 (13:00 local) and 18 (19:00 local) UTC.

Temperature, relative humidity and air pressure at sea level are the major terms under all standard tropospheric models. The distribution maps of mean temperature, mean relative humidity and atmospheric pressure at sea level are shown in figures A.3, A.4 and A.5. Considering figure A.3, it is obvious that the atmospheric temperature increased from east to west. The similar trend for the relative humidity is shown in figure A.4.

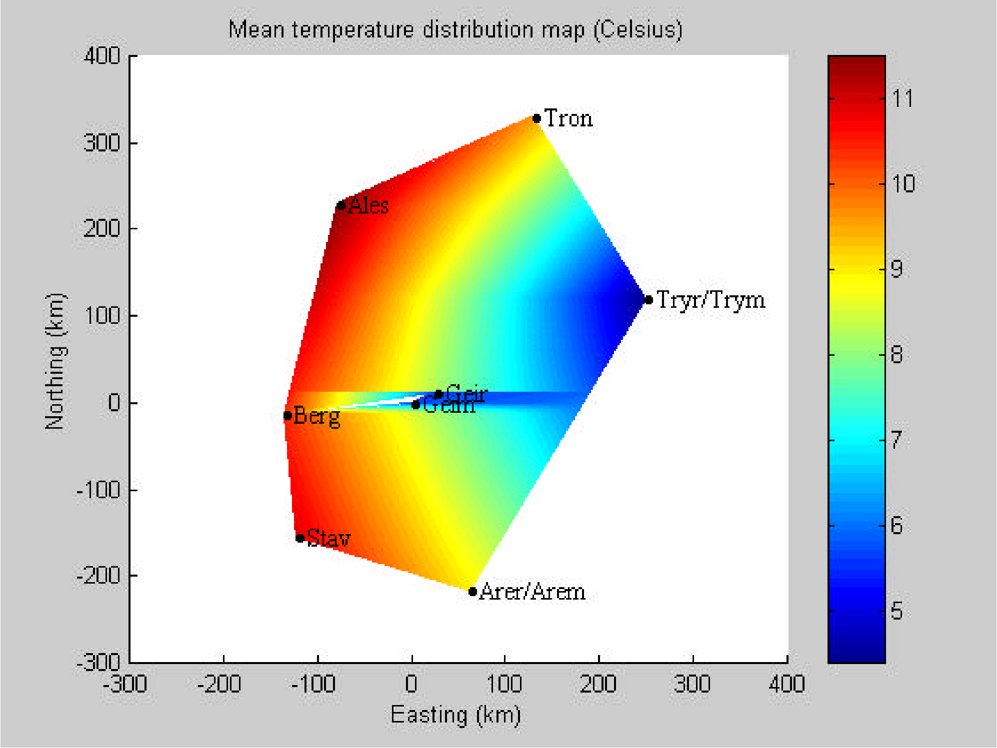

Figure A.3: Mean temperature distribution map

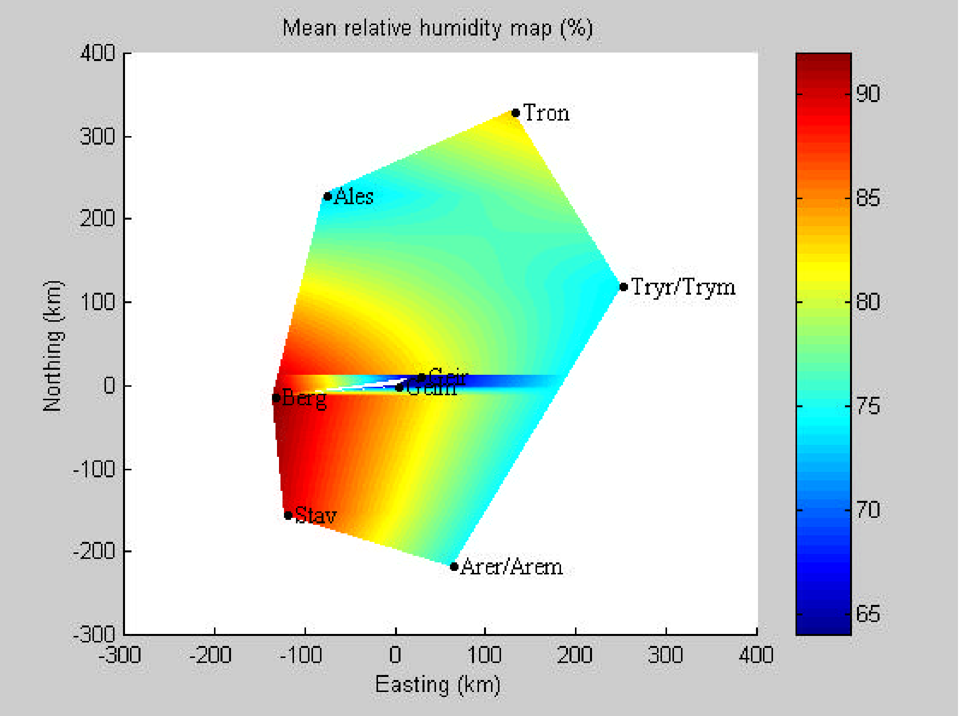

Figure A.4: Mean relative humidity distribution map

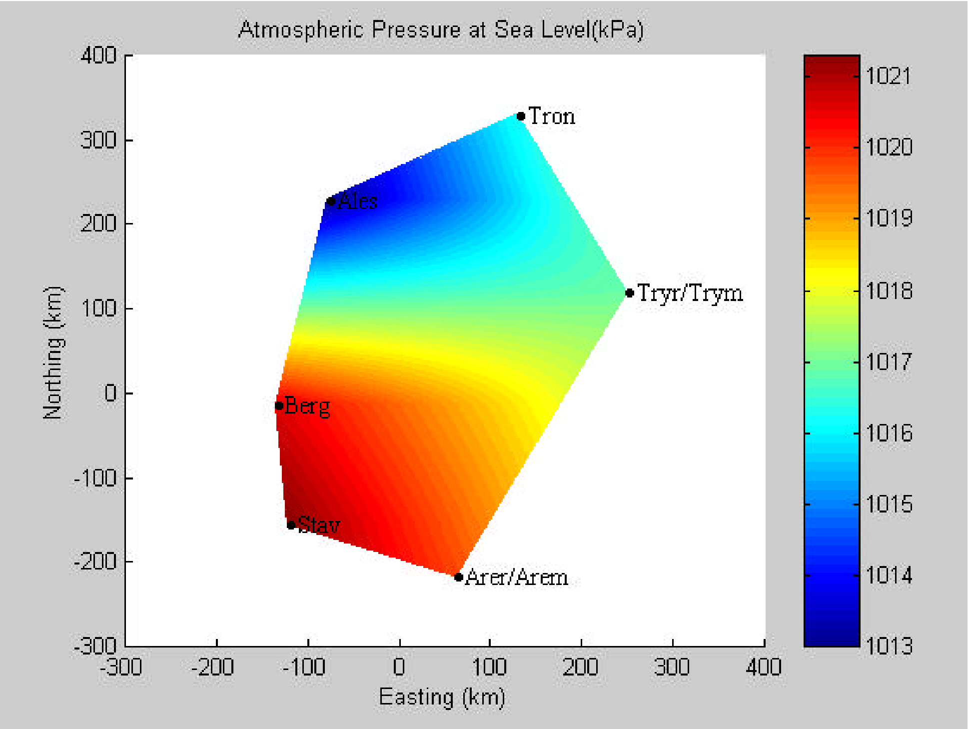

Figure A.5: Atmospheric pressure at sea level (kPa)

Table A.2 shows the 24-hour average surface weather statistical values of measurement data. The weather over the test period varied from cloudy to clear. No major storm fronts existed during this time.

Table A.2 Approximate surface weather data for reference sites

Reference sites	Temperature (°C)			Precipitation(mm)	Mean Relative Humidity (%)	Air Pressure at Sea Level (kPa)
	Mean	Max	Min			
Ales	11.5	12.6	9.3	1.6	73%	1013.0
Arem/Arer	9.0	15.9	2.3	0.1	75%	1019.8
Berg	10.4	13.1	8.0	0.8	92%	1020.6
Geim/Geir	5.7	9.5	2.0	*	64%	*
Stav	10.9	14.3	8.7	0.3	90%	1021.3
Tron	9.6	14.0	6.2	*	83%	1016.2
Trym/Tryr	4.4	10.3	0.8	*	74%	1016.9

Note: *: not available